AFRL-RX-WP-TM-2010-4087

COLLABORATIVE RESEARCH AND DEVELOPMENT CONTRACT

Delivery Order 0047: Mesocscale Modeling of the Thermal Mechanical Processing (TMP) of Superalloys

J. P. Thomas

Universal Technology Corporation

AUGUST 2008
Final Report

Approved for public release; distribution unlimited.

See additional restrictions described on inside pages

STINFO COPY

AIR FORCE RESEARCH LABORATORY
MATERIALS AND MANUFACTURING DIRECTORATE
WRIGHT-PATTERSON AIR FORCE BASE, OH 45433-7750
AIR FORCE MATERIEL COMMAND
UNITED STATES AIR FORCE

NOTICE AND SIGNATURE PAGE

AFRL-RX-WP-TM-2010-4087 HAS BEEN REVIEWED AND IS APPROVED FOR PUBLICATION IN ACCORDANCE WITH ASSIGNED DISTRIBUTION STATEMENT.

*//Signature//

RITA SCHOLES
Project Engineer
Integration and Operations Division

//Signature//

ROBERT ENGHAUSER
Acting Chief
Integration and Operations Division

*Disseminated copies will show "//Signature//" stamped or typed above the signature blocks.

REPORT DOCUMENTATION PAGE

Form Approved
OMB No. 0704-0188

1. REPORT DATE ***(DD-MM-YY)***
August 2008

2. REPORT TYPE
Final

3. DATES COVERED ***(From - To)***
01 April 2006 – 01 February 2008

4. TITLE AND SUBTITLE
COLLABORATIVE RESEARCH AND DEVELOPMENT CONTRACT
Delivery Order 0047: Mesocscale Modeling of the Thermal Mechanical Processing (TMP) of Superalloys

5a. CONTRACT NUMBER
F33615-03-D-5801-0047

5b. GRANT NUMBER

5c. PROGRAM ELEMENT NUMBER
62102F

6. AUTHOR(S)
J. P. Thomas

5d. PROJECT NUMBER
4349

5e. TASK NUMBER
L0

5f. WORK UNIT NUMBER
4349L0VT

7. PERFORMING ORGANIZATION NAME(S) AND ADDRESS(ES)
Universal Technology Corporation
1270 North Fairfield Road
Dayton, OH 45432-2600

8. PERFORMING ORGANIZATION REPORT NUMBER

9. SPONSORING/MONITORING AGENCY NAME(S) AND ADDRESS(ES)
Air Force Research Laboratory
Materials and Manufacturing Directorate
Wright-Patterson Air Force Base, OH 45433-7750
Air Force Materiel Command
United States Air Force

10. SPONSORING/MONITORING AGENCY ACRONYM(S)
AFRL/RXOB

11. SPONSORING/MONITORING AGENCY REPORT NUMBER(S)
AFRL-RX-WP-TM-2010-4087

12. DISTRIBUTION/AVAILABILITY STATEMENT
Approved for public release; distribution unlimited.

13. SUPPLEMENTARY NOTES
PAO case number 88ABW-2009-0045, cleared 01 February 2009. Report contains color.

14. ABSTRACT
This research in support of the Air Force Research Laboratory Materials and Manufacturing Directorate was conducted at Wright-Patterson AFB, Ohio from 1 March 2006 through 1 February 2008. The work done under this contract belongs to two main types of activities, which decides of the overall outline of this report. First, activities regarding the mesoscale model of microstructure evolution of Waspaloy will be presented. They consist in few experiments for the validation of hypothesis used to design the model. And they regard its finalization and industrial application. The knowledge gained during this work on Waspaloy provided the basis for a more fundamental type of work which aims at preparing the extension of the modeling tools used for Waspaloy to other alloys as well as to encompass other types of microstructure-evolution models. It is the topic of the second part of this report. It will introduce the prototypical software modules that were designed to demonstrate the feasibility of a next-generation modeling software for microstructure evolution and assess the difficulty of such development.

15. SUBJECT TERMS
Waspaloy

16. SECURITY CLASSIFICATION OF:			17. LIMITATION OF ABSTRACT:	18. NUMBER OF PAGES	19a. NAME OF RESPONSIBLE PERSON (Monitor)
a. REPORT	**b. ABSTRACT**	**c. THIS PAGE**			Rita Scholes
Unclassified	Unclassified	Unclassified	SAR	76	**19b. TELEPHONE NUMBER** *(Include Area Code)* N/A

Standard Form 298 (Rev. 8-98)
Prescribed by ANSI Std. Z39-18

Foreword

This document describes the work done and results obtained during contract F33615-03-D-5800, 0047 awarded to Universal Technology Corporation (U.T.C.). This contract aims at 1) the application of a mesoscale physics-based model of the microstructure evolution of Waspaloy in the context of the industrial primary processing of ingots into billets and 2) the development of tools that would allow the use of such models on a routine basis as well as the extension of this work to other Nickel-base superalloys and complementary modeling techniques. It follows a previous contract during which most of the development of the above-mentioned mesoscale physcis-based model of microstructure evolution was carried out.

The work done under this contract belongs to two main types of activities, which decides of the overall outline of this report. First, activities regarding the mesoscale model of microstructure evolution of Waspaloy will be presented. They consist in few experiments for the validation of hypothesis used to design the model. And they regard its finalization and industrial application. The knowledge gained during this work on Waspaloy provided the basis for a more fundamental type of work which aims at preparing the extension of the modeling tools used for Waspaloy to other alloys as well as to encompass other types of microstructure-evolution models. It is the topic of the second part of this report. It will introduce the prototypical software modules that were designed to demonstrate the feasibility of a next-generation modeling software for microstructure evolution and assess the difficulty of such development.

Introduction

The hot working of metals, and specifically of Nickel-base superalloys, triggers a variety of local, microstructural phenomena whose combination at higher scales and over time takes the appearance of the nucleation and growth of new grains that replace progressively the grains initially present. Such behavior has been described under the generic name of recrystallization. The local phenomena involved are for instance dislocation accumulation, recovery, sub-boundary generation and disorientation, the formation of new high angle boundaries, grain-boundary migration, the formation and disorientation of twin boundaries, etc.

Despite the extremely complex ways in which its underlying mechanisms combine, recrystallization can be mathematically described in a broad, almost macroscopic fashion using so-called Avrami or JMAK models. Although these models of microstructural evolution are able to capture the overall material behavior during hot working, they exhibit limitations inherent to the over-simplification on which they are based. As they were successfully implemented and used for more and more complex hot working processes, they evolved into sets of equations only remotely connected to the reality they are to describe, which inevitably questions their reliability and the possibility of further improvement of such models.

Some researchers in the academic arena developed models of recrystallization and grain growth that take the opposite approach. Their models, called Cellular Automata (CA) and Monte-Carlo (MC), describe the locality of microstructure-evolution mechanisms at the level of microscopic cells. As these cells are assembled into grids, these models reproduce the evolution of microstructures in a natural and graphic manner. However, due to their resource-intensive character, their application in conjunction with industrial FEM-simulation tools appears limited to few tracking points instead of all mesh nodes. Nevertheless, CA and MC models provide a central teaching: a rather limited set of equations that express the potentials/forces that drive microstructure evolution is sufficient to reproduce the whole recrystallization process, provided the ability to represent the geometric behavior of boundaries, or of their dual, grains.

An intermediate approach was therefore to be investigated which could combine the advantages of both forms of models, namely the lightweight and versatility of the first and the physical foundation of the second. To do so, it had to tackle the main issue at hand, i.e. the way through which local, microscopic phenomena tally up to become a larger-scale phenomenon that impacts and renews the whole grain structure. Research conducted since the end of the 1990s lead to the development of a geometric framework during the previous contract. It is able to capture the variety of configurations observed in Nickel-base superalloys with not only necklace topologies but with coarse, elongated ingot-grains exhibiting PSN-related topologies as well. The latter had been extensively characterized on Waspaloy ingot-structures [1-3]. This geometric framework receives its input from appropriate driving-force equations, the coefficients of which have been adjusted to match the experimental data available on Waspaloy [2-4].

A number of challenges remained at the end of the previous contract. First, the model had only been used on FEM data in 2D for single stroke-and-holding-time thermomechanical sequences. To be applicable in the industry to the primary processing of ingots, namely cogging and rotary forging, the model had to be applicable on 3D FEM data characterized by numerous deformations interspersed with holding times of various durations and exhibiting non-isothermal history. Furthermore industrial applicability is conditioned by the ability to use such model on a routine basis. Appropriate software is thus needed. The software previously developed by the contractor during his PhD, called RX-MOD, and which he used to perform the tasks required to serve the Air Force Research Laboratory, provided an advantageous start. By using it, the applicability of the model was demonstrated, as shown by the results reported in the first part of this document.

However the initial architecture of the software would require modifications and improvements to fully achieve the above-enunciated goals. To identify clearly the modifications needed, significant research was carried out to better understand the overlap between areas that are usually considered separately, such as microstructure-evolution modeling, mesh-representation structures, data management, programming languages and paradigms, and software development. Some prototypical modules were designed and tested to assess the feasibility and applicability of a number of modeling/software concepts. The results of this more exploratory type of work are presented in the second part of this report.

Industrial application of a mesoscale physics-based model of the microstructure evolution of Waspaloy

This first part begins with a brief presentation of the mesoscale physics-based model for Waspaloy. Experimental work is then presented. Additions and modifications to the RX-MOD software that allow 3D FEM application are described afterwards. The subscale validation performed with AFRL industrial partner follows. And it leads finally to the full-scale industrial application of this model.

Mesoscale physics-based model of the microstructure evolution of Waspaloy

The so-called mesoscale modeling technique relies on the association of a geometric framework and a set of driving-force equations. These equations describe the local, microscale mechanisms whose combined effects result in the recrystallization observed at mesoscale. These mechanisms are, to cite a few, dislocation generation, recovery, the formation and disorientation of sub-boundaries, their transition into new high angle boundaries, grain-boundary migration, twin-boundary generation, etc. Through appropriate integration algorithms, they are combined to provide the input of the geometric framework, which triggers recrystallization. Therefore, the central role of the geometric framework is to operate the transition from micro- to meso- scale. In other words, a geometric framework is to mesoscale models what the grids and associated cell-switch laws are to CA and MC models.

Since one of the goals is to maintain a moderate footprint on the computer resources, the geometric framework aims at describing microstructures with far less details than a CA or MC model would. The geometric framework is therefore formed by a rather limited number of grain aggregates whose properties can be seen as averages over the grain populations they encompass. For physical meaning purposes, they have to be composed of grains that exhibit similar properties such that they can be safely assumed to evolve in a similar fashion. Such grain aggregates are the base element of MesoStructure Units, or MSUs. To represent discontinuous dynamic recrystallization, at least two MSUs are necessary: one for the initial grains and another for the recrystallized ones. The implementation of the geometric framework actually allows several grain aggregates per MSU. If an initial grain-size distribution were to be represented, or a distribution of Taylor factors, the MSU that contains the initial grains could comprise several grain aggregates initialized with varying grain sizes or Taylor factors and the grain densities required to match the distribution. Such feature has however not been leveraged in the Waspaloy model. As a result, in the present work, an MSU and the single grain aggregate it contains are interchangeable entities.

When the process to simulate comprises several deformations, (e.g. the cogging of billets), at least two MSUs are necessary – in addition to the MSU of initial grains – to represent the recrystallized grains: one for the grains that appeared during the current or latest deformation, and one for those that appeared earlier in the process, which may have coarsen through static grain growth and then stored some energy again during following deformations. In such a configuration, each new deformation implies a reduction of the fraction of initial grains; and a new wave of recrystallization within recrystallized areas can be represented for each new hit as well as its subsequent static evolution. Ultimately, all initial grains disappear and each new wave of recrystallization triggered by a new deformation is accounted for by the evolution of the two MSUs of recrystallized grains. The geometric description of microstructures is also able to account for coarse elongated grains, e.g. as observed in cast structures. In the latter case, the geometric framework accounts for the impact of nucleation location, specifically at grain boundaries or inside initial grains through particle stimulated nucleation (PSN).

Despite the versatility of the framework, the geometric characteristics of grains and of their aggregates are fully defined by only five primary variables: grain volume, volume contained in the outer grain envelope, grain-aggregate volume, and two anisotropy coefficients. These variables allow the calculation of all other secondary geometric variables, such as grain sizes, grain densities, recrystallized fraction, etc. Additional variables describe the intrinsic properties and internal state of grains, such as Taylor factor, dislocation density, sub-boundary density, sub-boundary disorientations, etc. The evolution of these variables arises from the integration over time or strain of driving-force equations, from which is finally obtained the input that the geometric framework is to translate at mesoscale. These values are 1) the velocity of boundaries between each pair of grain aggregates, 2) the average nucleus volume and 3) the nucleation rates in the grains of each aggregate. Grain-boundary velocities result from the multiplication of grain-boundary mobility by the difference of stored energy between grains. The evaluation of nucleation rates is more complex and will not be detailed here.

The core of the ability of the geometric framework to translate micro-mechanisms input into mesoscale evolution lies in its innovative management of grain interactions. They derive primarily from the careful evaluation of statistical expectancies of surface of contact between grains for each pair of grain aggregates. The multiplication of each of those surfaces by the grain-boundary velocity input gives the volume variation of each grain and of its aggregate. With regard to nucleation input, the volume of nuclei is subtracted from that of the grains in which they appear and it is added to the aggregate of the newest grains. Overall, the microscale input suffices for the geometric framework to calculate in an autonomous and internally consistent fashion the evolution of the various grain populations at mesoscale. All details on the geometric framework are available in the paper written at the beginning of this contract and published in Materials and Metallurgical Transactions A in September 2007 [5]. This article is in Appendix A.

In practice, the Waspaloy model relies on five MSUs. The two first ones are for initial grains, with a variation in the Taylor factor. The two following ones are for previously recrystallized grains, with the same Taylor factor distinction. And the fifth MSU receives all nuclei as it contains the newly recrystallized grains. The Taylor factor distinction may not be really necessary. However, the model would require re-adjustment if Taylor-factor dependence were removed. The input of the model consists in the initial grain size with which the two MSUs of initial grains are to be initialized. In the case of coarser ingot grains, it requires the orientation of grains, from which Taylor factors are derived. It also needs the density of PSN sites, which can actually be seen either as an input of the model or as a non-modifiable model coefficient.

Provided with an integration path in the form of a file of thermomechanical data [time, temperature, strain], RX-MOD carries out the numerical integration of the model in a regular forward-Euler fashion, although with an automated control of time steps to guarantee precision and stability. The thermomechanical data can be either provided internally by the thermomechanical module of RX-MOD, or coming from an external FEM simulation software such as Deform 2D or 3D.

After this summarized description of the model, experimental work and results are presented and discussed in the following section.

Experimental results

Some experiments were needed to further enhance the model or validate some hypothesis used to design it. First, uniaxial compression tests were performed on double-cone samples (Figure 1) with an emphasis on temperatures below the γ' solvus (~1900°F) The goal was to investigate the impact of precipitation on recrystallization kinetics during deformation as well as during holding times.

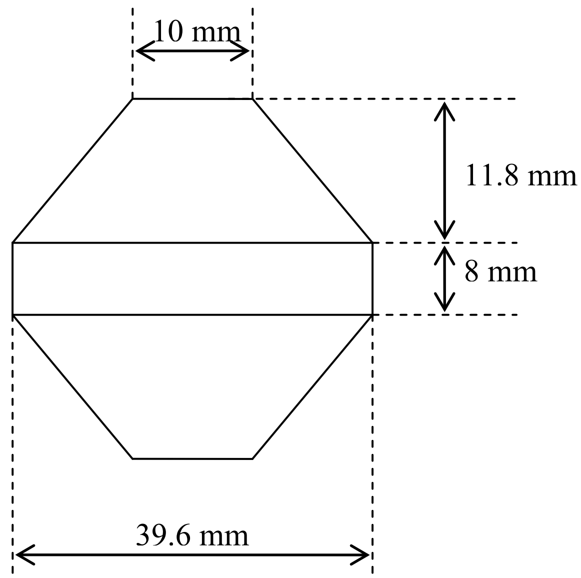

Figure 1: Double-cone geometry

Samples were taken from the same Waspaloy ∅3” rolled bar as during the first contract. They were heat treated for 1 hour at 2050°F to eliminate all precipitation and insure a consistent initial grain size (200 µm) for all samples, independently of test temperature (Figure 2).

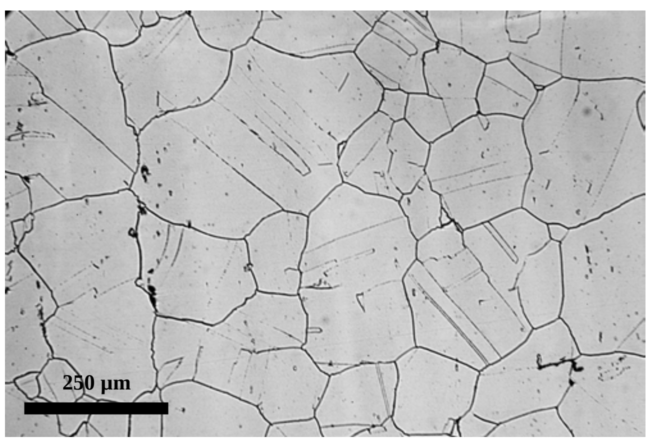

Figure 2: Initial microstructure

Target strain rate ($0.05 s^{-1}$) and strain are calculated as if it were a cylinder sample of the same height as those double-cones. The simulation of a uniaxial compression in isothermal environment (at 1900°F) was performed in Deform-2D to evaluate the strain distribution in double-cones with target strains of 1.0 and 1.2 (Figure 3).

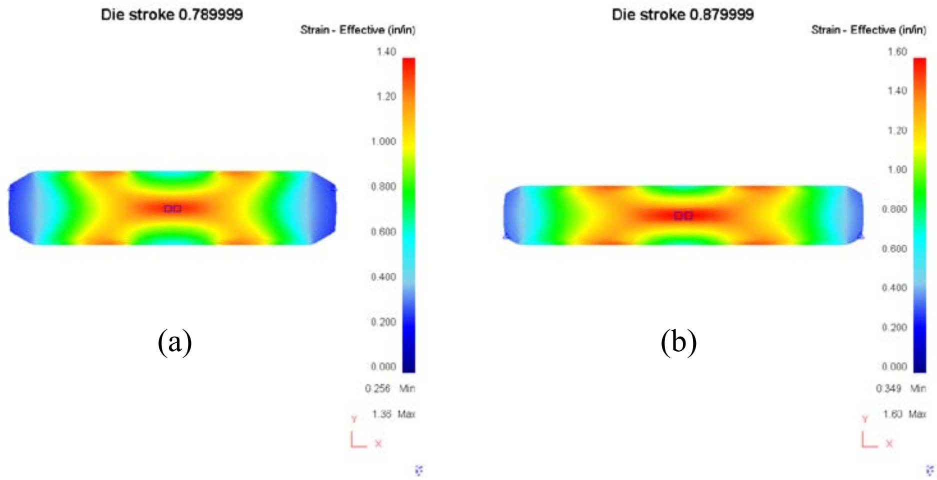

Figure 3: Strain maps for double-cones with nominal strains of 1.0 (a) and 1.2 (b)

Sample #	Deformation temperature (°F)	Strain	Holding time prior to WQ (s)	30-minute reheat temperature (°F)	Follows test #
1	1950	1	10		
2	1830	1.2	30		
5	1830	1.2	30	1900	2
6	1830	1.2	30	1850	2
3	1900	1.2	15		
7	1900	1.2	15	1900	3
9	1900	1.2	15	1850	3
4	1800	1.07	60		
8	1800	1.07	60	1900	4
10	1800	1.07	60	1850	4

Table 1: list of double-cone tests

The list of double-cone tests performed is summarized in Table 1.

Of all these samples, #1 exhibits the highest recrystallization as it was forged 50°F above the γ' solvus. It is fully recrystallized at the center and the recrystallized fraction decreases progressively down to about 40% at the outer radius. The microstructure-evolution model suggests values of 90% at the center and 45% at the surface, which is fairly close to the measurements.

As deformation temperature was lowered to 1900°F, i.e. roughly the γ' solvus, recrystallization is less extensive for samples 3, 7 and 9. All three samples exhibit the same microstructures, showing that reheats were unable to promote metadynamic or static recrystallization, even though precipitate fractions are quite low. For all three samples, at the center, the recrystallized fraction is about 60%; it decreases to 40% at mid-radius and then down to 20% near the outer-radius (Figure 4). In all those cases, the model predicts that dynamic recrystallization is followed by very little metadynamic evolution. It ends up with fractions of 55%, 40% and 7% respectively at the center, mid-radius and outer-radius. These values are quite close to those measured, which is very satisfying considering that no experimental data were available to adjust the model in the specific range of temperatures near the solvus. To further increase model precision, improvements would have to comprise a full γ'-precipitation model so as to better capture the specific temperature range where precipitation starts and where slight chemical variations such as segregations can impact the solvus temperature and precipitate fractions.

At even lower deformation temperatures, i.e. for all remaining samples, generally no recrystallization is visible (Figure 5); only a slight necklace of very fine grains can be observed in some cases at the center (Figure 6). Reheats, even at the solvus temperature, do not release grain boundaries. These results are a bit discordant with model predictions which suggest a 20% recrystallized fraction at the center, decreasing to 0 when moving towards the outer regions. The recrystallized grain size is in good agreement however with a very fine 2.5 to 3 µm. It is worth noticing that at such low temperatures, the model was adjusted on experimental data for which there had not been a γ'-dissolution heat-treatment prior to the tests. It means that the samples exhibited pre-exiting γ'-precipitates that were probably coarser and less numerous than those that appear dynamically during deformation. The latter have a far more detrimental impact on the progress of recrystallization, hence the very limited, almost non-existent necklace. Additionally, the model is used here with a combination of temperature and initial grain size (coarse grains at low temperatures) that is not represented in the experimental data-set on which it was adjusted (coarse grains at high temperature or small grains at low temperatures). It is therefore behaving remarkably well given that it is tested significantly out of its adjustment window. Slight modifications to decrease nucleation kinetics for coarse grains at low temperature could help. But it could prove artificial as long as it can not be compared with actual experimental data combining the characterization of recrystallization and of a variety of γ'-precipitation configurations. Here again, full γ'-precipitation model would be needed, which was unrealistic in the scope of this study. Nevertheless, the predicted results are already rather close to experiments anyways.

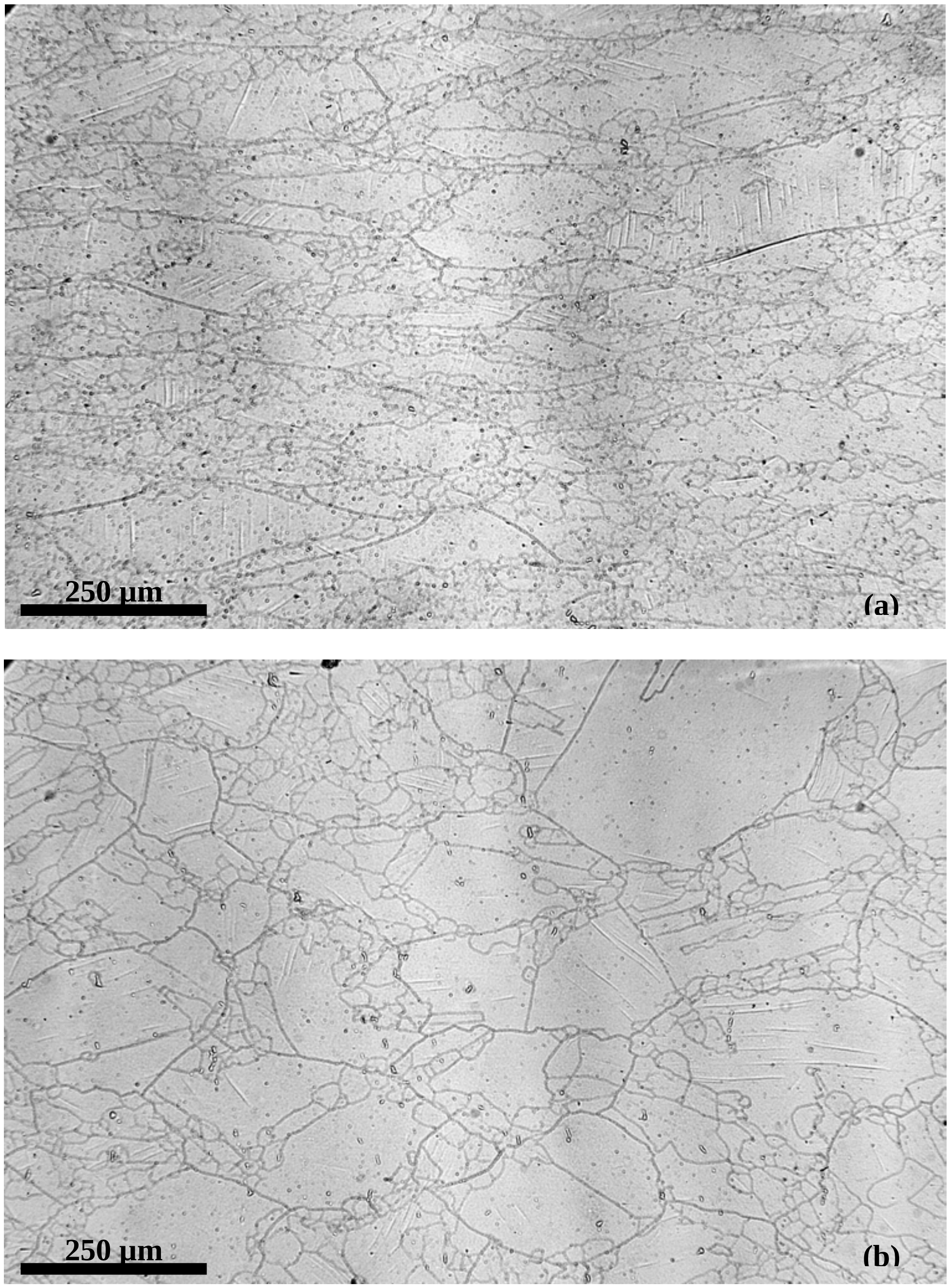

Figure 4: #9 Mid-radius (a) and outer-radius (b)

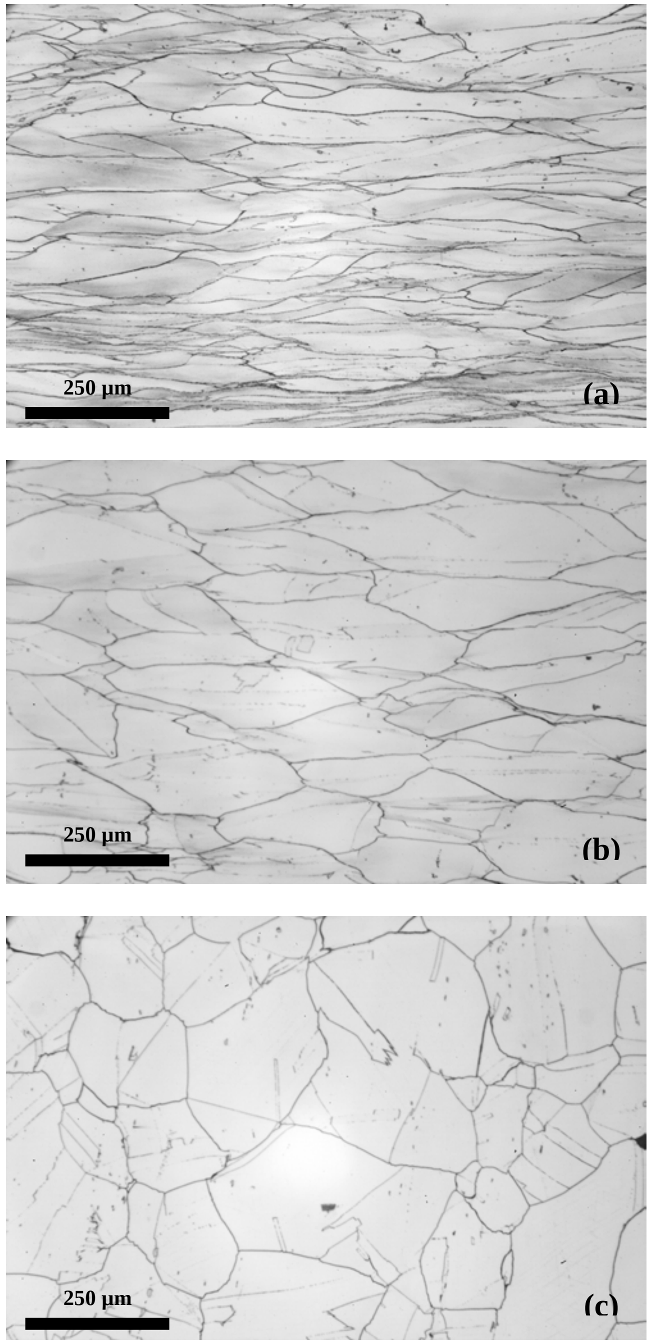

Figure 5: #4 center (a), mid-radius (b), and outer-radius (c)

In the end, these double-cone tests and re-heats validate the assumptions made for model development in regard to the effect of γ'-precipitation on recrystallization kinetics.

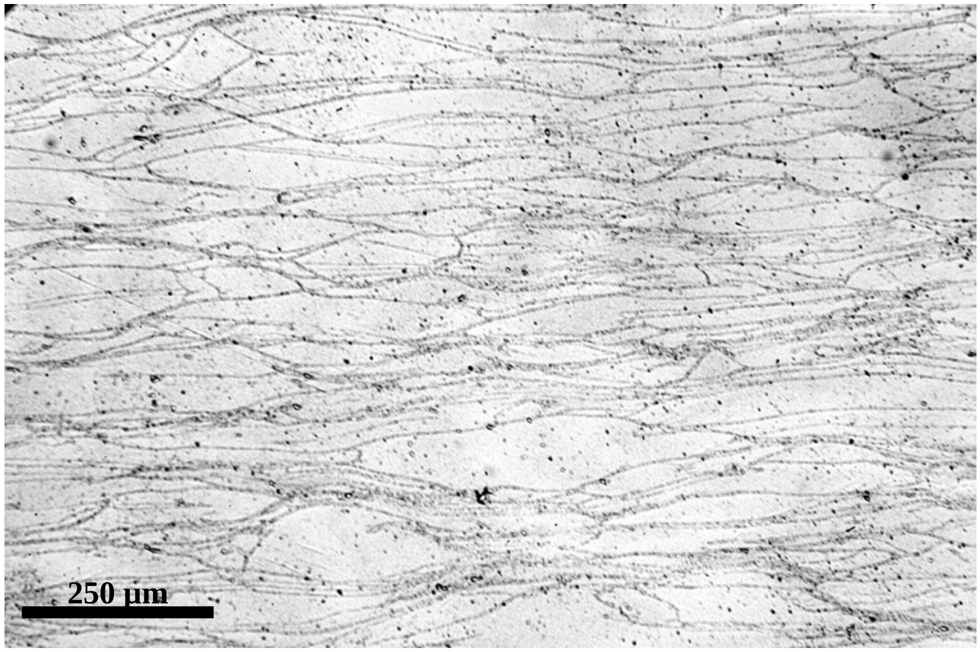

Figure 6: #10 center (incipient recrystallization necklace)

After this study oriented towards the effects of γ'-precipitation on recrystallization, few uniaxial compression tests were performed on cylinders to investigate the relationship between the evolution of the substructure and nucleation. These tests were focused on small deformations to capture the incipient stages of the nucleation of recrystallized grains. A list of these tests in summarized in Table 2. Wrought samples come from the same Waspaloy rolled bar as before. Without heat treatment, initial grain size had previously been characterized from 80 to 100 µm. Ingot samples were cut in a section of the Waspaloy ingot used before as well by Weaver et al.

Sample #	Type	Temperature (°F)	Strain rate (s^{-1})	Strain
1	Wrought	1950 5min, 1850	0.005	0.32
2	Wrought	1950	0.01	0.17
3	Wrought	2050	0.01	0.130
4	Wrought	1950	0.01	0.32
5	Ingot transverse	2050	0.01	0.27
6	Ingot axial	2050	0.01	0.30

Table 2: List of nucleation tests

Overall, wrought samples exhibit features very similar to those observed on 718 [6]. Samples 2 and 3 have been subjected to the lowest deformation (Figure 7). They show the very beginning of the development of a substructure with smooth color gradients across grains and a few low angle sub-boundaries. Recrystallization however has not been initiated yet.

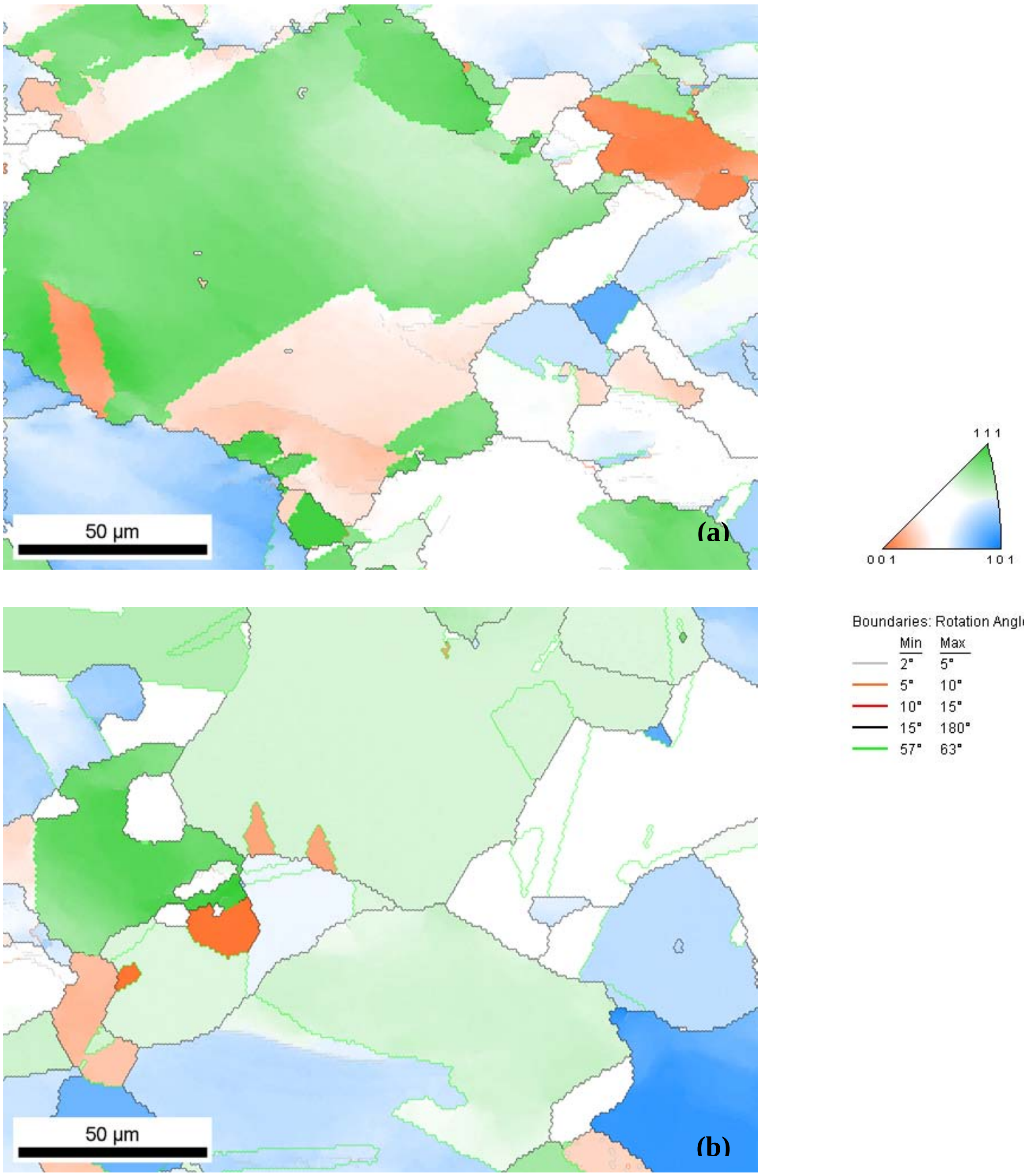

Figure 7: Nucleation samples #2 (a) and #3 (b)

With larger strains, samples 1 and 4 show progress with an increased and widespread disorientation of sub-boundaries and some nucleation. Sample 1 was deformed at a lower temperature (1850°F) than sample 4 (1950°F); the deformation temperature of sample 1 is below the γ'-solvus. Recrystallized grains are significantly smaller in that case. The model indicates for these samples recrystallized fractions of respectively 10% and 50%, and recrystallized grain sizes of 6 µm and 20 µm. In the case of sample 4, the temperature is so high that nuclei grow too quickly to provide clear indications about the nucleation sites and mechanisms. Sample 1 however is indicative of a strong correlation between nucleation sites and zones that exhibit numerous sub-boundaries. There are few instances of nuclei found inside grains on sub-boundaries that tend to fragment those initial grains.

The representation of twin boundaries was attempted by coloring in green all grain boundaries whose disorientation is between 57° and 63°. There seems to be a bug in the post-treatment of the TSL software as those green boundaries are drawn frequently where a sub-boundary would be expected. It disturbs the overall perception as to the influence of twin boundaries in the nucleation process. If these green boundaries are counted as regular boundaries, the 6-µm average recrystallized grain size appears fairly close to that on the OIM maps of sample 1. Nevertheless, there seems to be more grain boundary migration than considered in the model. Consequently, nucleation by bulging is probably more frequent than expected. The overall impact of this observation is unclear. In particular, with regard to model development, it is not sure that additional equations evaluating the contribution of bulging per se would improve the model. They would just add new adjustment parameters, complexity, and risks of instability.

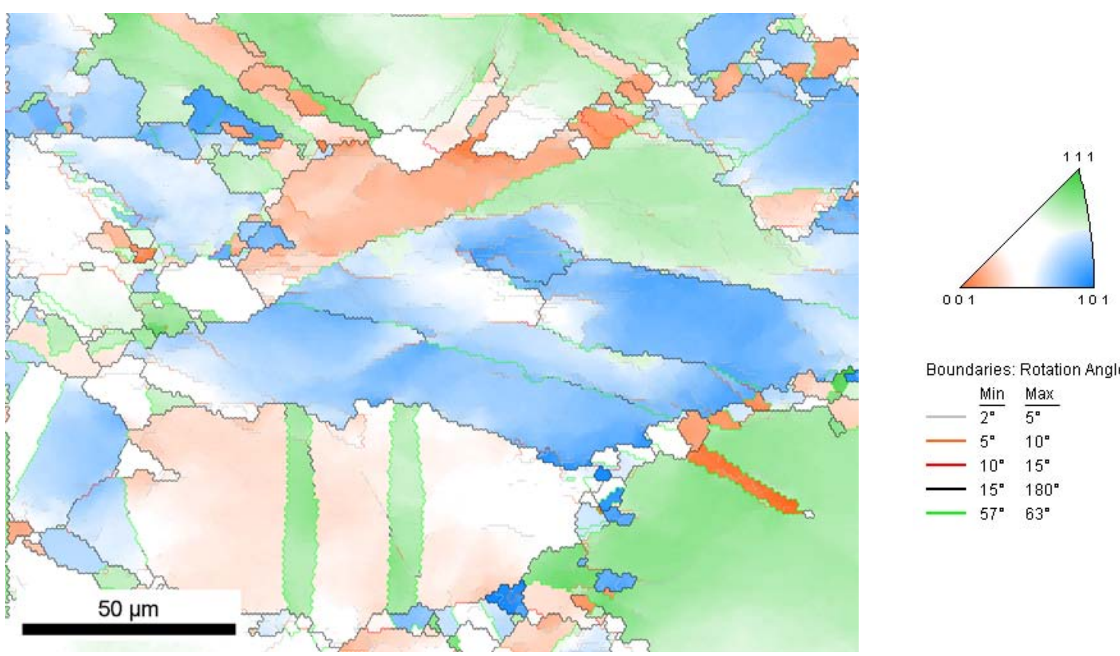

Figure 8: Nucleation sample #1

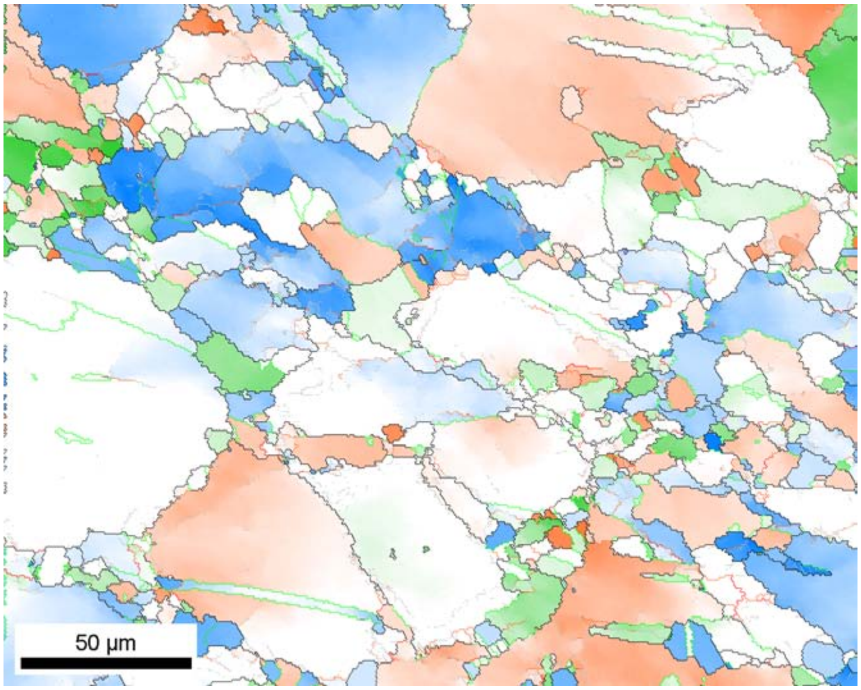

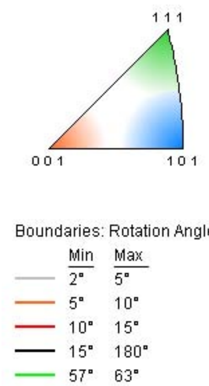

Figure 9: Nucleation sample #1

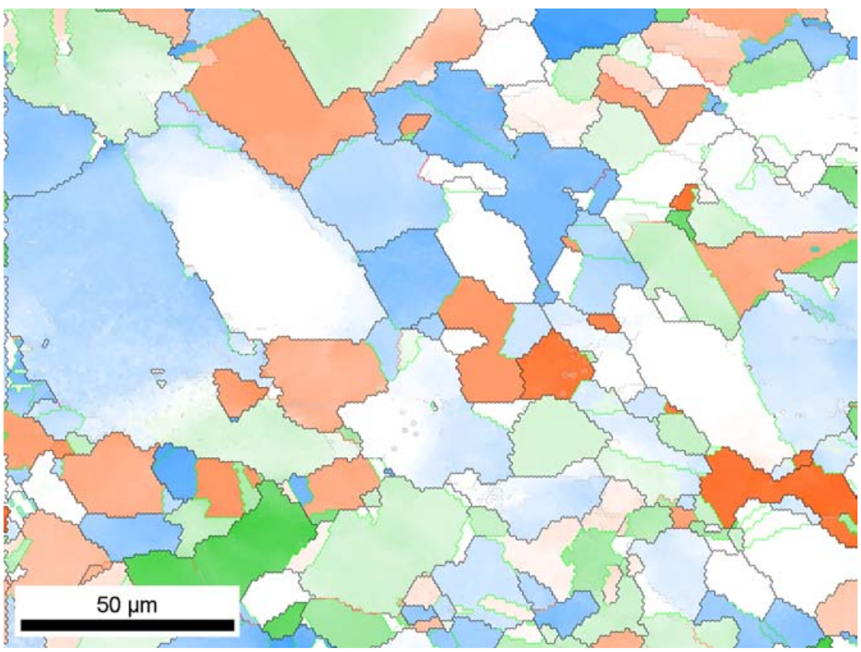

Figure 10: Nucleation sample #4

The last two samples (#5 and #6) were taken from an ingot. The compression axis was either orthogonal to the axis (Sample 5, Figures 11 and 12) of the coarse ingot grains or parallel to it (Sample 6, Figure 13). Both have sensibly the same strain of 0.3.

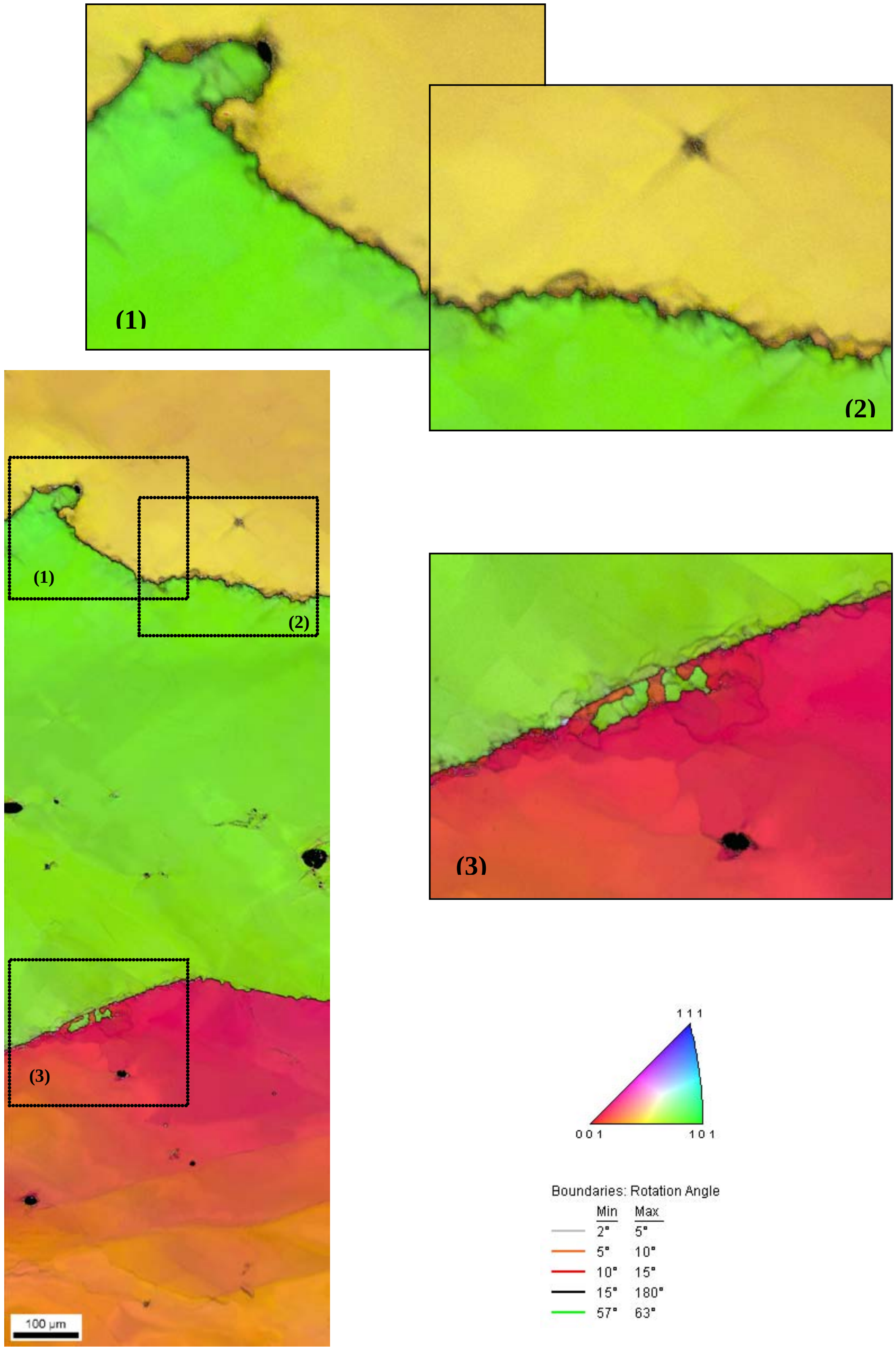

Figure 11: Nucleation sample #5 (Transverse)

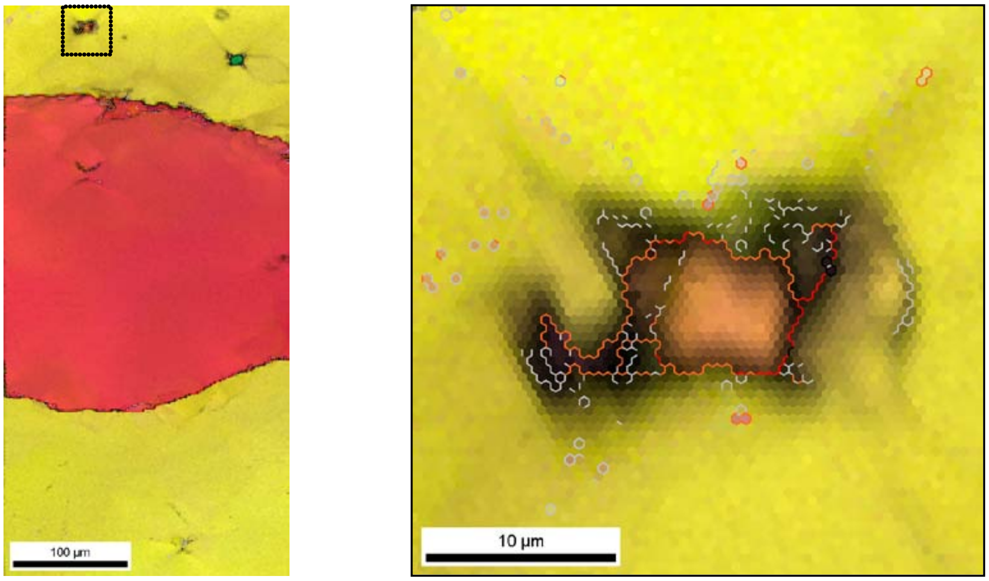

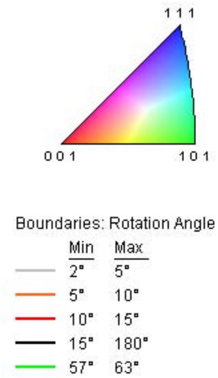

Figure 12: Nucleation sample #5 (Transverse)

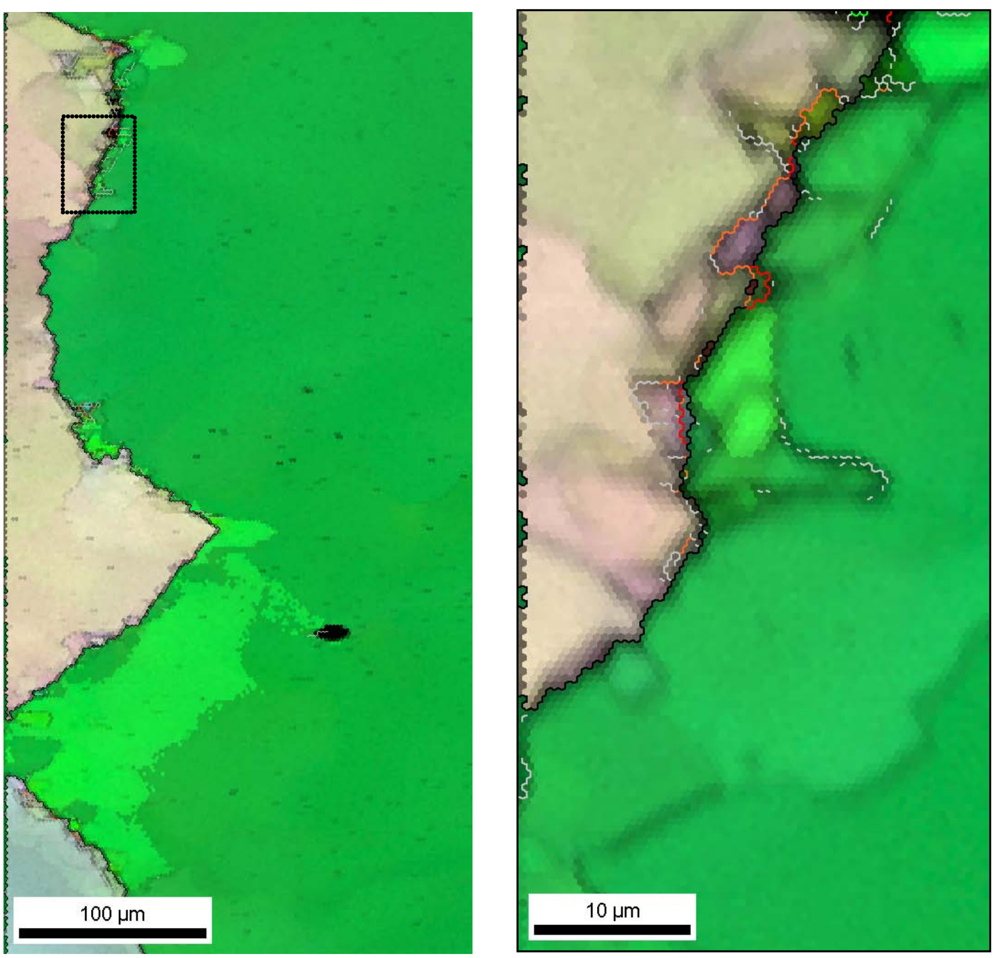

Figure 13: Nucleation sample #6 (Axial)

Overall, the observations made on these samples are in good agreement with hypothesis used to develop the model. First, there is a clear difference of behavior between the sub-boundaries located near initial grain boundaries and those located inside the grains near coarse particles. Therefore the assumption necessary for model development that a distinction be made between the evolutions of sub-boundaries located near initial grain boundaries and those in the volume near coarse particles was correct. Specifically, this distinction supposes a delayed evolution of the sub-structure around particles when compared to surface sub-structure, which is quite confirmed by the observation of EBSD maps.

This is particularly true in the case of axial grains. They were found to require disorientation kinetics of sub-boundaries in the volume up to 2.5 times slower than those of other orientations so as to fit experimental recrystallization kinetics. Experimental observations by OIM corroborate this hypothesis. An X strain pattern and sub-boundaries are clearly visible around coarse particles in the case of the transverse sample. In contrast, the (unfortunately only) coarse particle seen on the axial sample does not seem to disturb strain or crystal orientation.

Furthermore model optimization indicated that the disorientation kinetics of sub-boundaries located near initial grain boundaries is affected by ingot-grain orientation by only 10-20%. This is well confirmed by the comparison of transverse and axial samples: little difference is observed experimentally between the sub-structures close to initial grain-boundaries for those two samples. It means that the disorientation kinetics of the substructure on each side of a grain boundary is dictated for the most part by incompatibilities of deformation between the two crystals rather than by the orientations of those two crystals per se.

Here again, the bulging of initial grain boundaries appears to have a larger contribution than expected, as can be seen on Figure 11 insert 3. The extent to which such nucleation mechanism should be accounted for is unclear. Even if it is not taken in account per se in the model, the overall behavior of the latter is sufficiently accurate. Additional equations to represent bulging would probably not induce a better precision, while they would make the model more complex and thus potentially unstable.

In conclusion, this experimental work validates the more questionable assumptions made during model development. A few discrepancies were identified, but their importance is not demonstrated. Additionally, model modifications would probably have more detrimental consequences than positive ones since more equations implies more coefficients and more risks of numerical instability.

After these experimental studies, subscale model-validation is now presented.

Subscale validation of the microstructure-evolution model

The work now presented was carried out with an industrial partner chosen by the Air Force Research Laboratory. This industrial partner possesses a 1,000-Ton press which allows the forging of subscale pieces, typically a few inches in diameter. For the present study, a cylindrical sample geometry was chosen, with dimensions of ∅3” x 6”. Two samples were cut from as-rolled Waspaloy bar stock. A third sample, 1/2” thick only, was used to measure as-heated grain size.

Samples were heated in a furnace for one hour to reach a forging temperature of 2050°F. Grain size at the end of soak time was evaluated to 200µm. The first sample was upset down to 1.84” (69% reduction in height). The second one, after a 30-second waiting time on die, was side-pressed down to 1-5/8” (44% reduction from initial diameter). The first sample underwent a water quench after deformation as soon as transfer permitted. The side-pressed sample was held between the dies for two minutes prior to transfer to an air-cool table. Table 3 and 4 compile the times recorded for the successive forging events, which were used to determine the elapsed times used to set up Deform simulations of the two forging processes.

Events	Recorded times (s)	Elapsed times (s)
Furnace door opened	0	0
Piece placed on bottom die	10	10
Start forging	15	5
End forging	19	4.15
Piece in quench tank	29	10

Table 3: Recorded times for forging events of upset

Events	Recorded times (s)	Elapsed times (s)
Furnace door opened	0	0
Piece placed on bottom die	11	11
Start forging	42	31
End forging	43	1.3
End of hold between dies	2:49	125

Table 4: Recorded times for forging events of side-press

Because the side-press required a 3D simulation, the Deform simulation could not reach high enough resolution near the surface to capture its sharp temperature gradient, unless a very large mesh were used. However, the microstructure-evolution model can not handle more than 50,000 nodes or it needs too much memory. The side-press test was therefore not investigated in much detail.

In a contrasting way, the upset could be simulated in Deform-2D with a fine-enough mesh, which in 2D can be obtained with just 5,000 nodes. It allowed to capture the sharp temperature gradient that develops at the sample surface due to the contact with relatively cold dies (Figure 14). The need for such level of detail is made evident by comparing the outer regions of the die-contact zone on the temperature map of Figure 14 with the macro of Figure 15. The fine-mesh 2D-simulation of the upset thus offers the ability to test the sensitivity of the microstructure-evolution model in meaningful conditions.

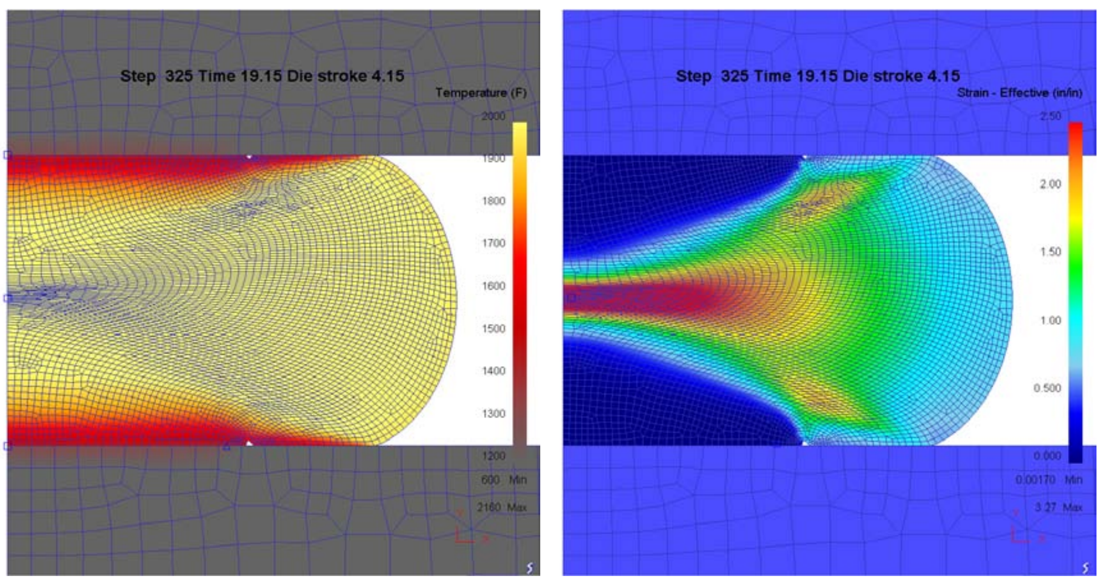

Figure 14: Temperature and strain maps at the end of the upset

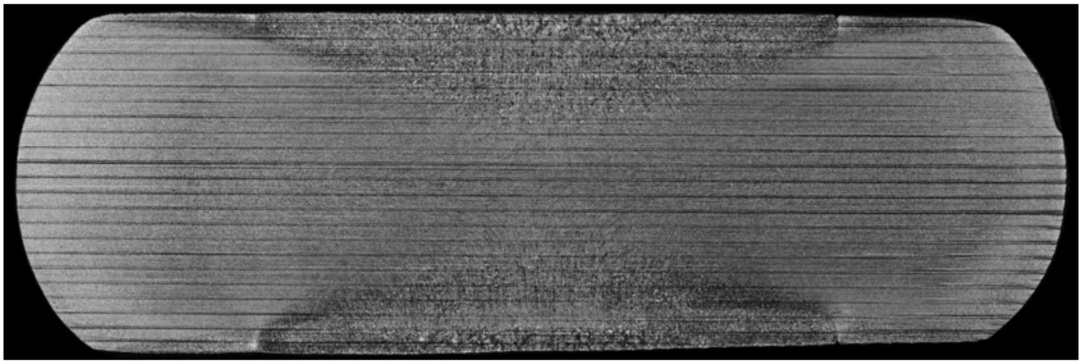

Figure 15: Macro slice of the upset sample

A number of slices were added to the cut plan of the upset sample (Figure 16) in provision for a study of microstructure coarsening during subsequent heat treatments. Regarding the as-forged slice, a detailed characterization of the variety of microstructures present on the section was planned (Figure 17). The goals were to locate precisely the transitions between the recrystallized zones and the unrecrystallized regions that were affected by die chill and low deformation; evaluate the effect of slightly lower temperatures where the surface lost heat to the ambient air and by radiation; the amount of grain growth due to the transfer time before water quench at the center, where adiabatic heating actually increased temperature by 150°F.

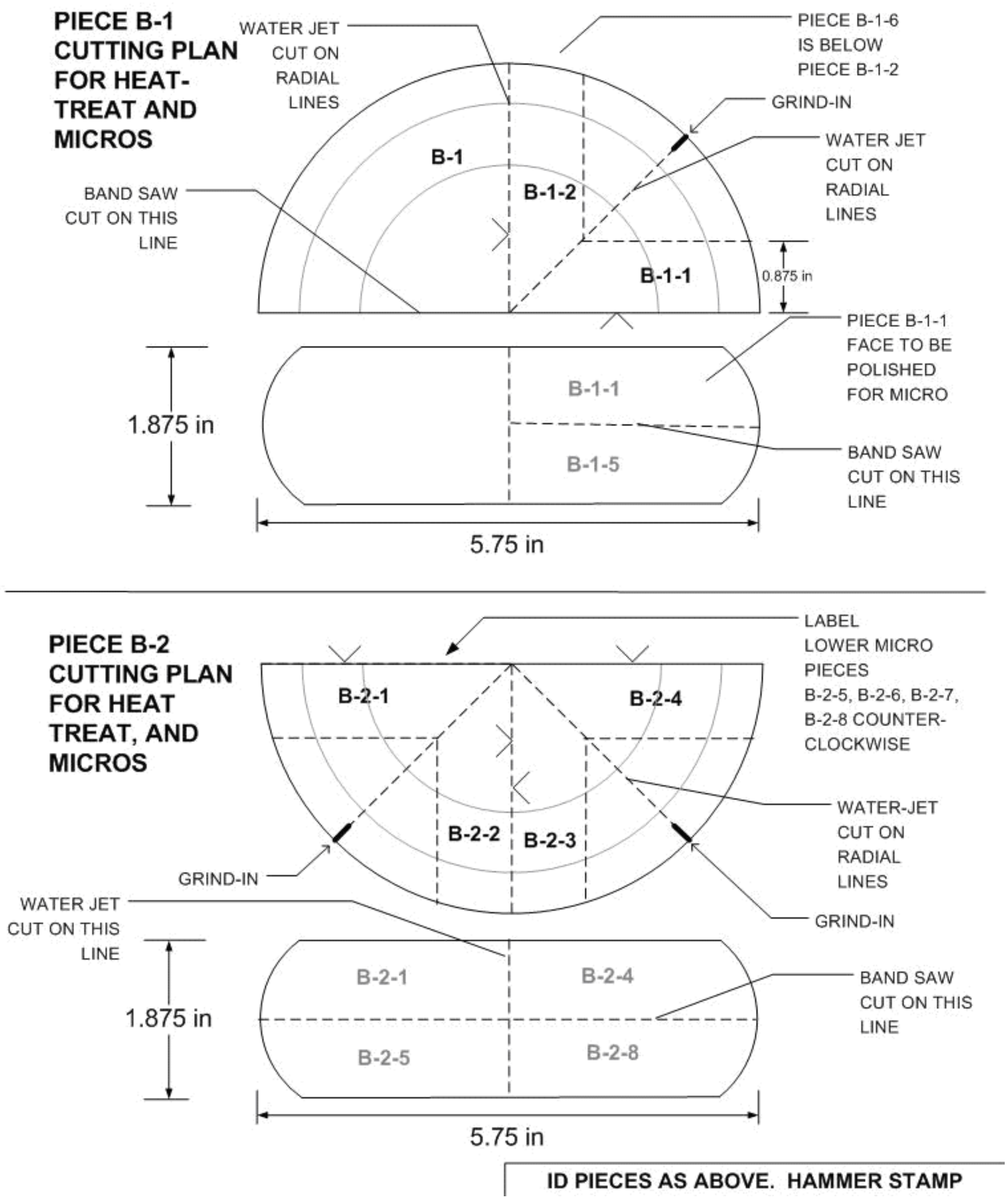

Figure 16: Cutting plan

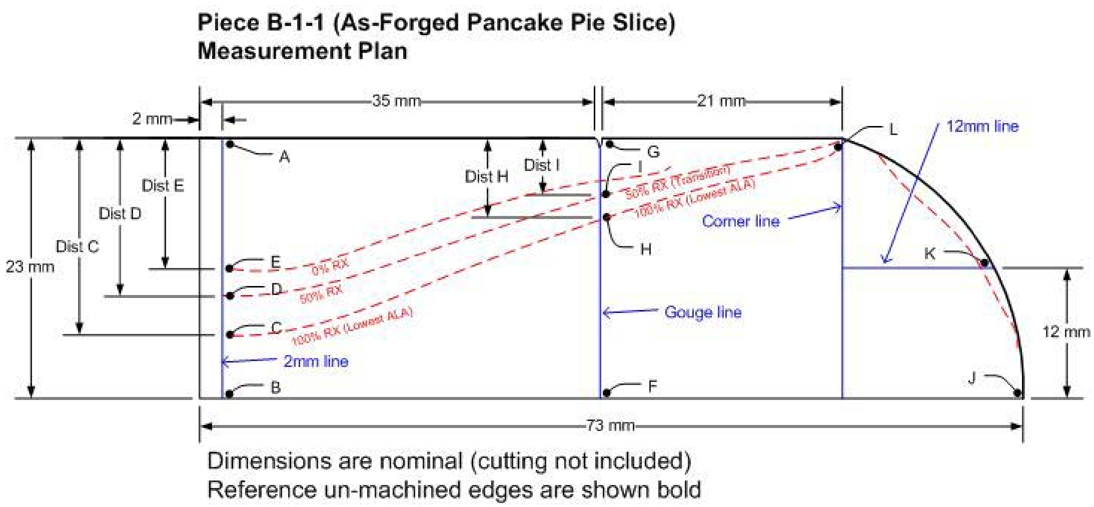

Figure 17: Measurement plan

While the characterization of these microstructures was performed by the metallographic laboratory of the industrial partner, Deform-simulation results were extracted in order to run the microstructure-evolution model and attempt a prediction. In most areas, it appeared to provide reasonable results. However, close to the surface, model instability was noticed (Figure 18). The macro-slice of Figure 15 does not exhibit such feature. The source of that instability had to be identified and the model corrected.

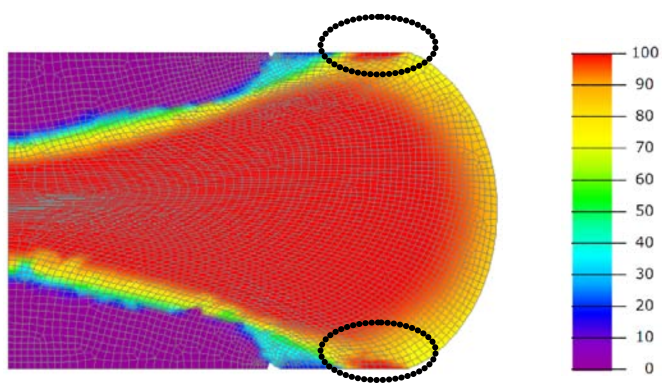

Figure 18: First attempt of the microstructure-evolution model – Recrystallized fraction (pct.)

Analysis of the thermomechanical data provided the explanation for the instability. The affected zone has a very specific thermomechanical history characterized by 1) a significant strain (~0.8), most of which happens during 2) a quick drop of temperature as the contact with dies is established, followed by 3) a fast reheat when inner heat diffuses back to the surface during the transfer of the sample in the air to the quench tank. It is during the latter that the instability happens. It results from the instantaneous (or so-considered by the model) dissolution of γ' precipitates which releases grain boundaries and allows the high stored energy to trigger an exaggerated progress of recrystallization.

In consequence, a security was added to the model. This security feature prescribes the instant dissolution of γ' precipitates when temperature rises above the γ'-solvus if the material underwent deformation while temperature was lower than 980°C/1800°F. In that case, dissolution is delayed until the material has been above the solvus for three consecutive minutes. The latter is a bit too sharp a statement. But a better representation would suppose a full γ'-precipitation model. Nevertheless, after three minutes above the solvus, recovery would have lowered energy enough to bring the model back to normal regime. Stability is then guaranteed and only a little recrystallization delay might be expected as a worst case scenario.

Provided this slight modification, the comparison of the model results with values measured by the industrial partner's metallographic lab according to the plans of Figure 17 is presented in Figure 19. It reveals the very good adequacy of the model with actual material behavior during hot working.

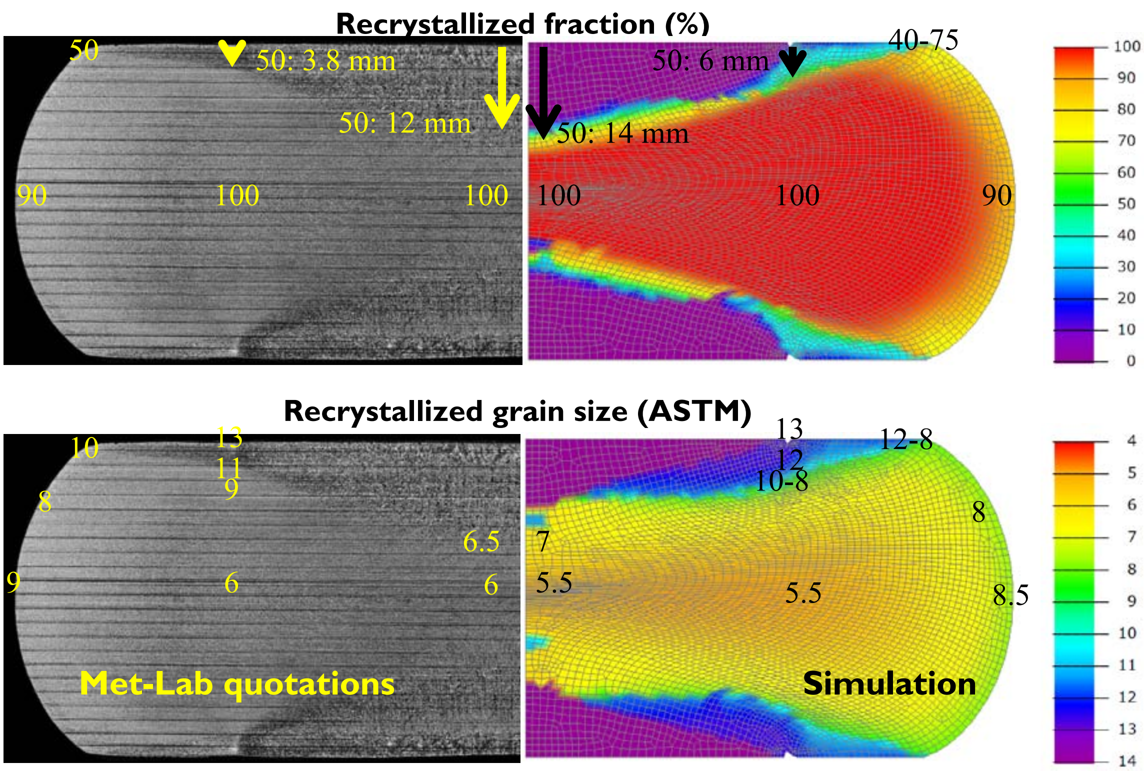

Figure 19: Comparison of model prediction with measurements

While this subscale-validation project was in progress, the implementation of new functions for the application of the model on 3D FEM-simulations was carried out. These aspects are presented in the following section.

Implementation of functions for model application on 3D FEM results

The application of the microstructure-evolution model on 3D FEM results does not differ much from its application on 2D FEM results. It still consists in passing to the module for numerical integration of the model the values [t, T, ε] for each node sequentially. Given the way meshes have been implemented, viz. in templates, the access to data embedded in 2D and 3D meshes is virtually identical. The implementation of the 3D application started almost just as a copy and paste of the 2D numerical integration functions. However, the few adaptations needed were extremely complex to implement, debug, and validate, because it is not possible to fully visualize results in 3D. Significant work was therefore done to alleviate that difficulty by implementing a number of peripheral functions that aim at creating 2D representations of a 3D meshes, and so leverage existing 2D mesh drawing capabilities.

Needless to say, 3D→2D transformations raise quite complex geometric issues. It started with the implementation of functions that identify the surface of a 3D mesh and then converts it into the 2D mesh that results from its observation from any side. Then the focus was put on the implementation of functions that create the 2D mesh which derives from the section of a 3D mesh by a plane for any normal direction X, Y or Z, and at any position in the piece. The 2D mesh resulting from that operation holds the temperature, strain and microstructural data interpolated from the 3D mesh in the section plane.

3D meshes are usually coarser than 2D meshes due to computer limitations. Therefore additional effort was paid to design functions that refine 3D meshes by inserting new nodes and reconnecting new elements accordingly. This does not aim at improving the thermomechanical precision as it is just an interpolation of existing results. But it allows the testing of the model sensitivity to gradients on a finer space scale. These functions are quite resource intensive however. And so would be the transport functions needed to continue microstructure calculations across the typical remeshing triggered during 3D FEM simulations, even though they are less frequent than in 2D. Such transport functions were therefore not implemented in 3D. A better alternative was pursued instead to address both refinement and remeshing issues at once.

From the user side, this new approach requires the generation of a secondary mesh in Deform, of the exact same dimensions as the one used in the actual simulation. That secondary mesh should be finer, given the purpose of refinement. Two functions were implemented to perform the following tasks. The first loads the secondary mesh and attaches it onto the coarse mesh that was used in the thermomechanical Deform-3D simulation. The attachment process consists in identifying the element of the coarse mesh to which each node of the fine secondary mesh belongs. In that process, the barycentric coordinates of each fine-mesh node in reference to the nodes of the coarse-mesh element to which it belongs are generated and stored. Then the second function manages the fine-mesh nodes as if they were tracking points. At each stored simulation step, it simply calculates the node data (coordinates, temperature, strain) as the weighted sum of the data of the nodes of the coarse-mesh element to which the node belongs; the weights used are precisely the barycentric coordinates previously identified. In the advent of a remeshing operation, the first function is called again to attach the (deformed) fine mesh onto the new coarse mesh. Only the attachment process is resource intensive as it searches, element by element, the one to which each node belongs. But once that is done, the tracking/interpolation at each simulation step is very fast. These operations result in a list of files of the same total number as the coarse mesh result-files exported from Deform-3D; but those new files contain the interpolated evolution of the fine mesh as if it had been used to perform the thermomechanical Deform-3D simulation in the first place, without any remesh interruption. That list of files can readily be used for the integration of the microstructure-evolution model on the thermomechanical history carried by the fine mesh.

After the implementation, testing, and debugging of these new functionalities had been completed (Figures 20 and 21), their first application in conjunction with the microstructure-evolution model consisted in the comparison of the same cogging process performed with either cold or warm dies, so as to evaluate the impact of die temperature on microstructures. The results of these comparative simulations are compiled in Figures 22 to 29. Warm dies appear to have very limited impact upon microstructures.

At this point, the integration of the microstructure-evolution model on 3D FEM results was technically possible in the software. And the model itself had been successfully validated using a subscale forging process performed at the R&D facility of the industrial partner. The application of the microstructure-evolution model of Waspaloy during thermomechanical processing to actual industrial primary conversion of ingots into billets was therefore the next logical step.

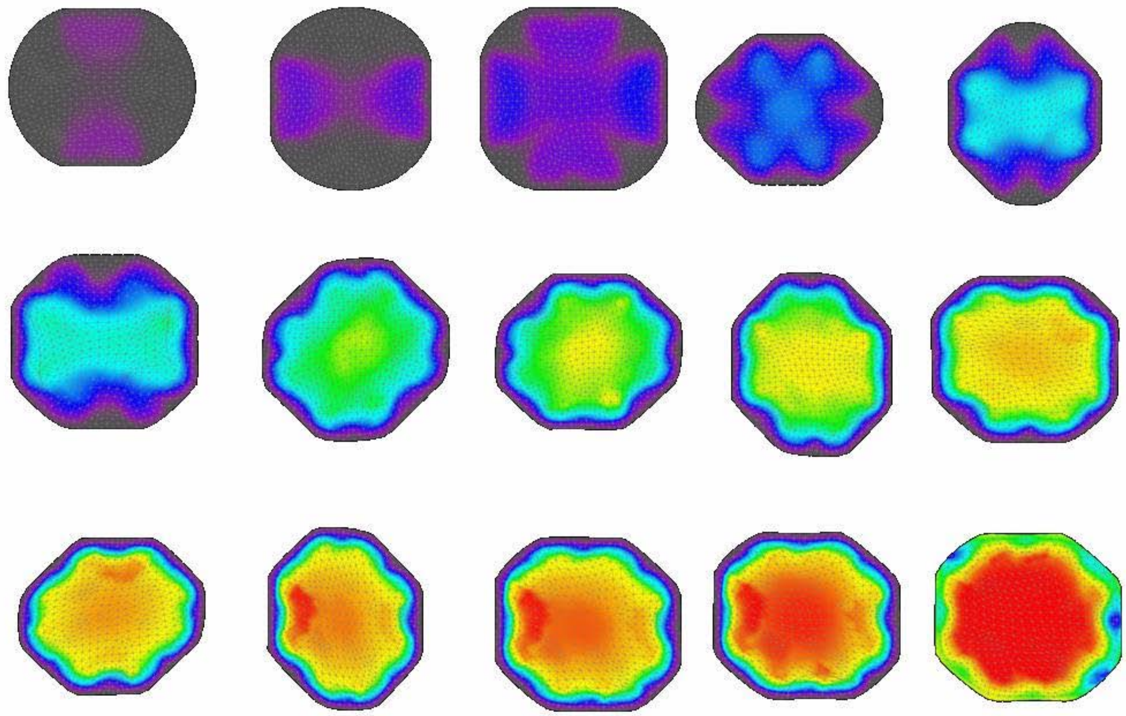

Figure 20: Sections of a Waspaloy ingot during cogging at various stages: Recrystallized fraction

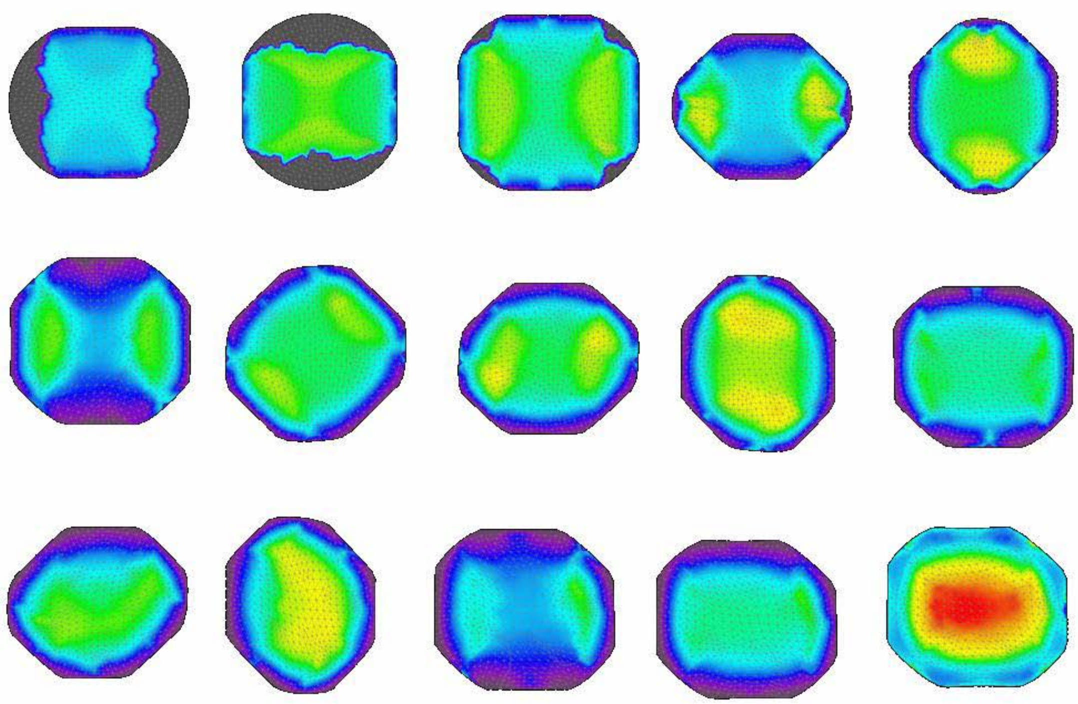

Figure 21: Sections of a Waspaloy ingot during cogging at various stages: Recrystallized grain size

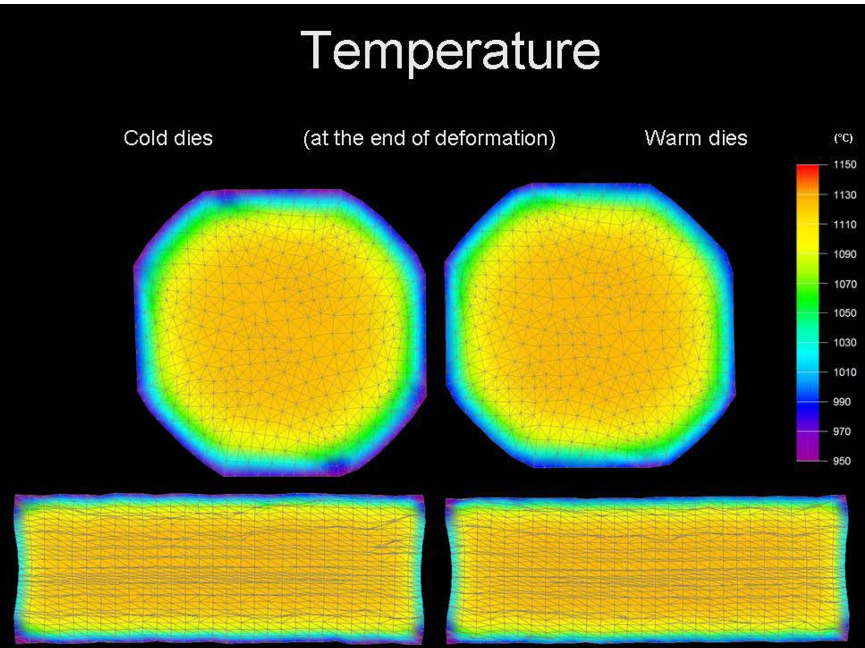

Figure 22: Temperature at the end of deformation

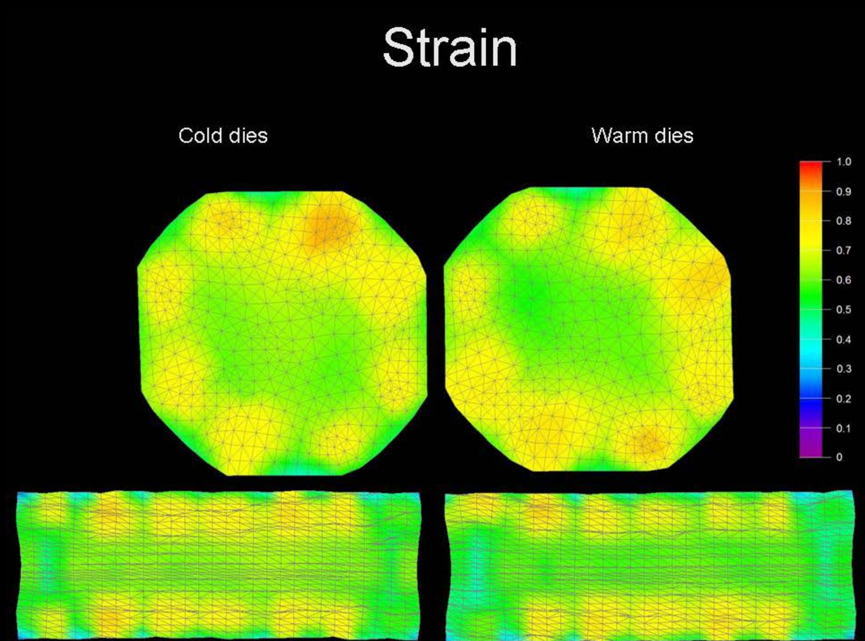

Figure 23: Strain at the end of deformation

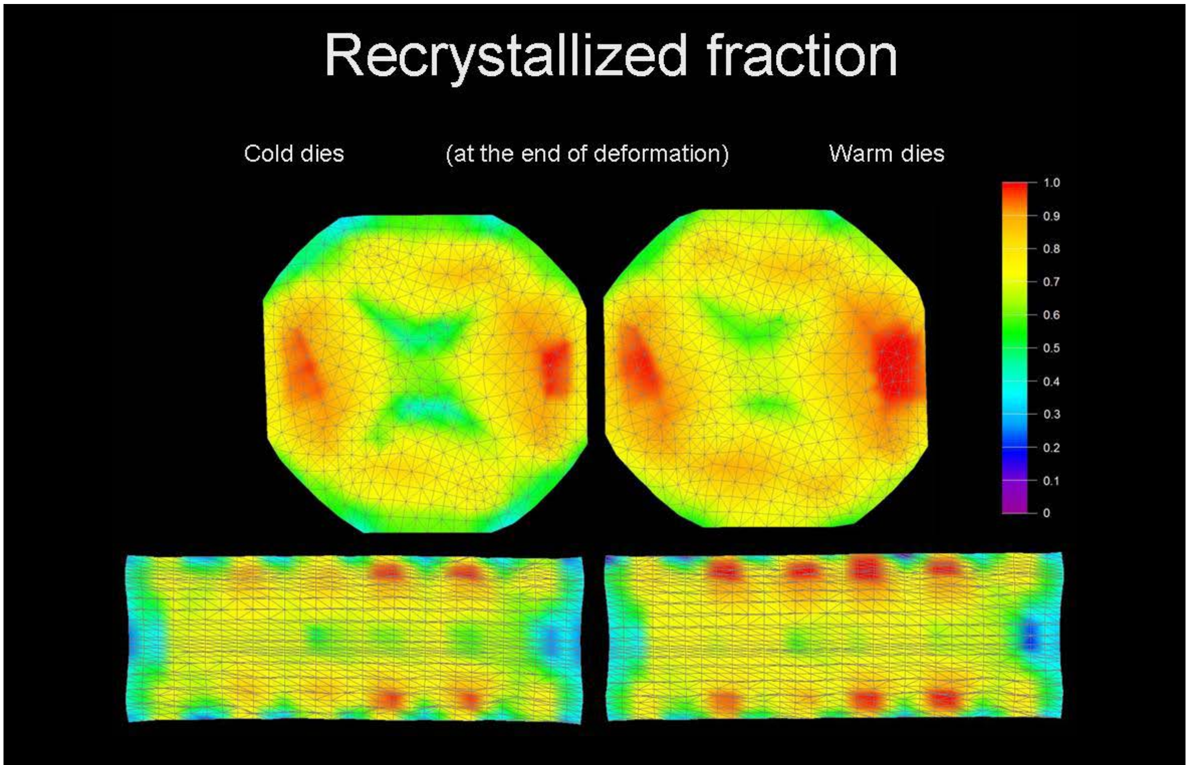

Figure 24: Recrystallized fraction at the end of deformation

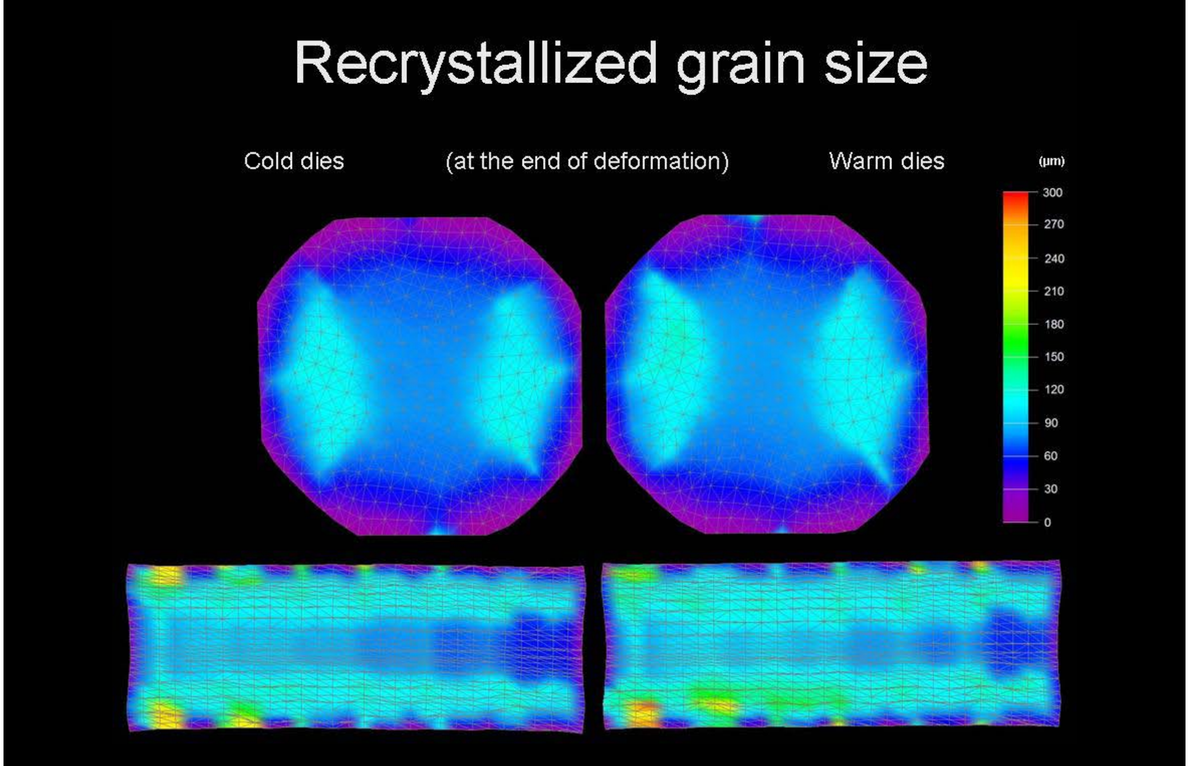

Figure 25: Recrystallized grain size at the end of deformation

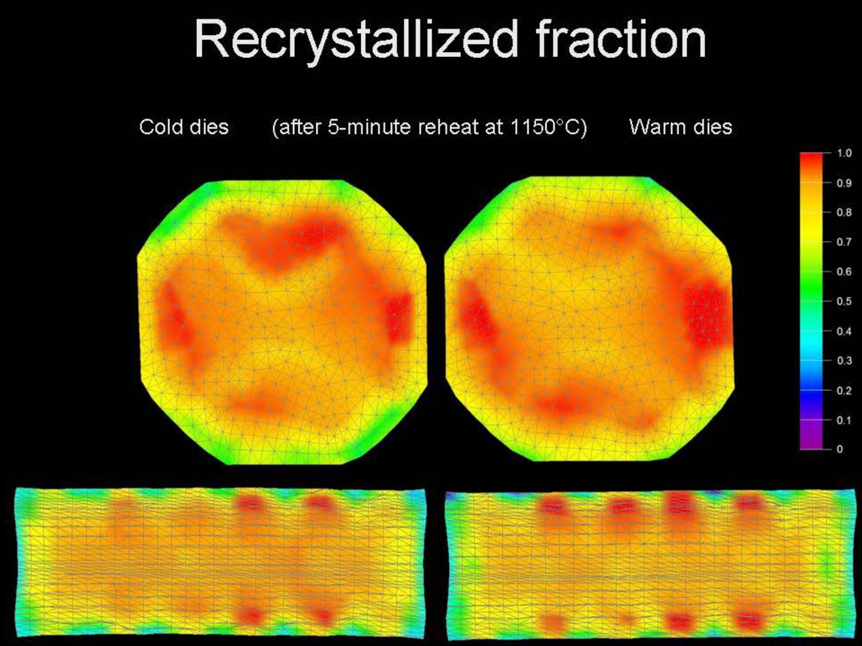

Figure 26: Recrystallized fraction after a 5-minute reheat

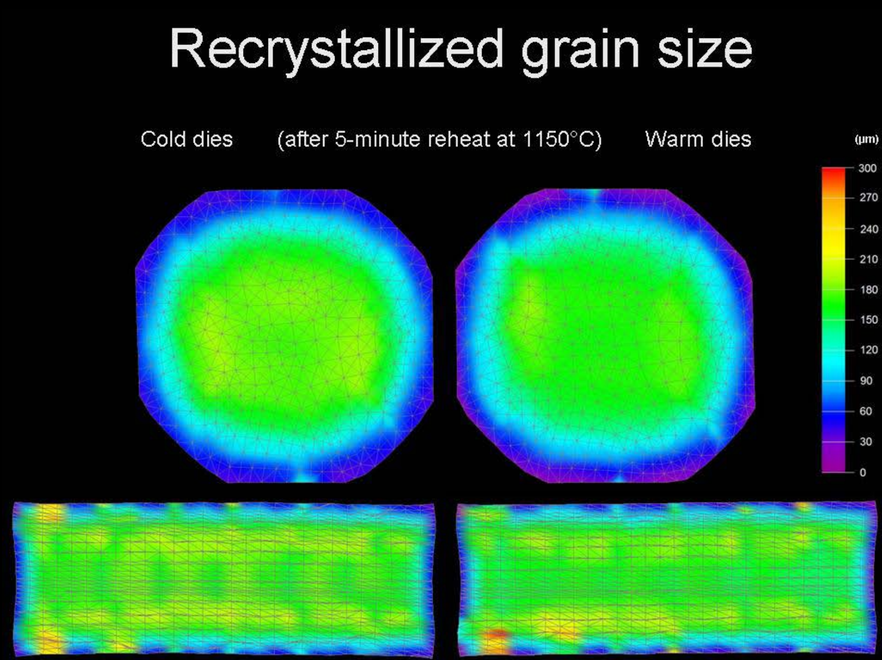

Figure 27: Recrystallized grain size after a 5-minute reheat

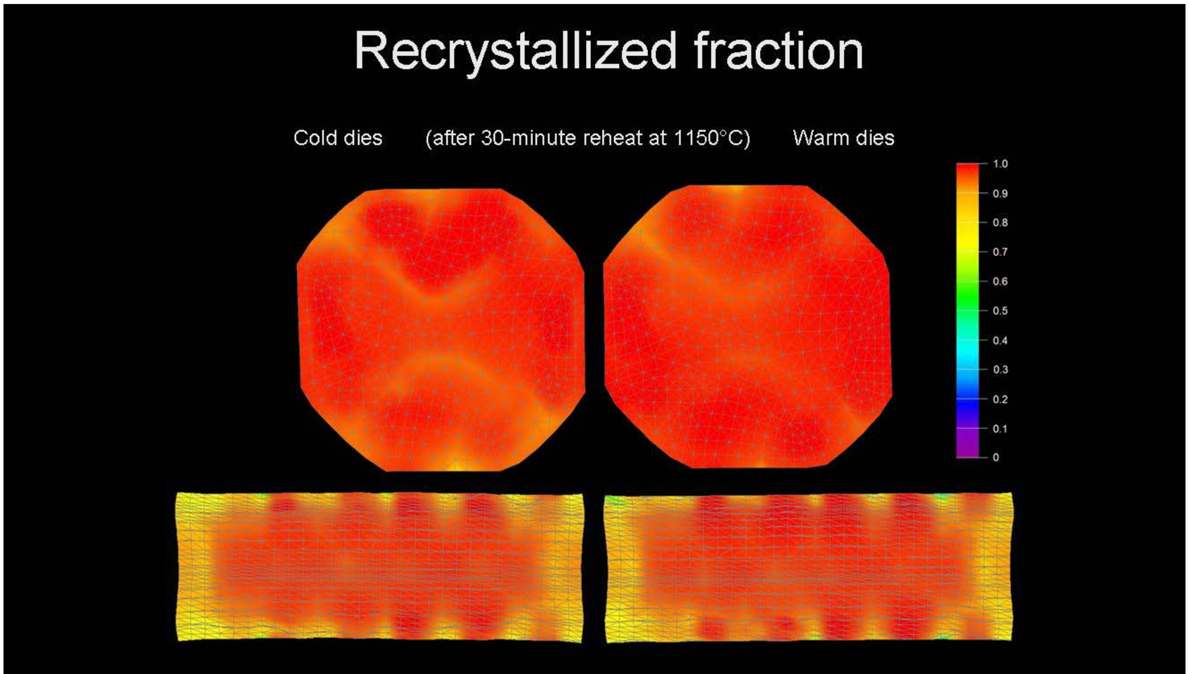

Figure 28: Recrystallized fraction after a 30-minute reheat

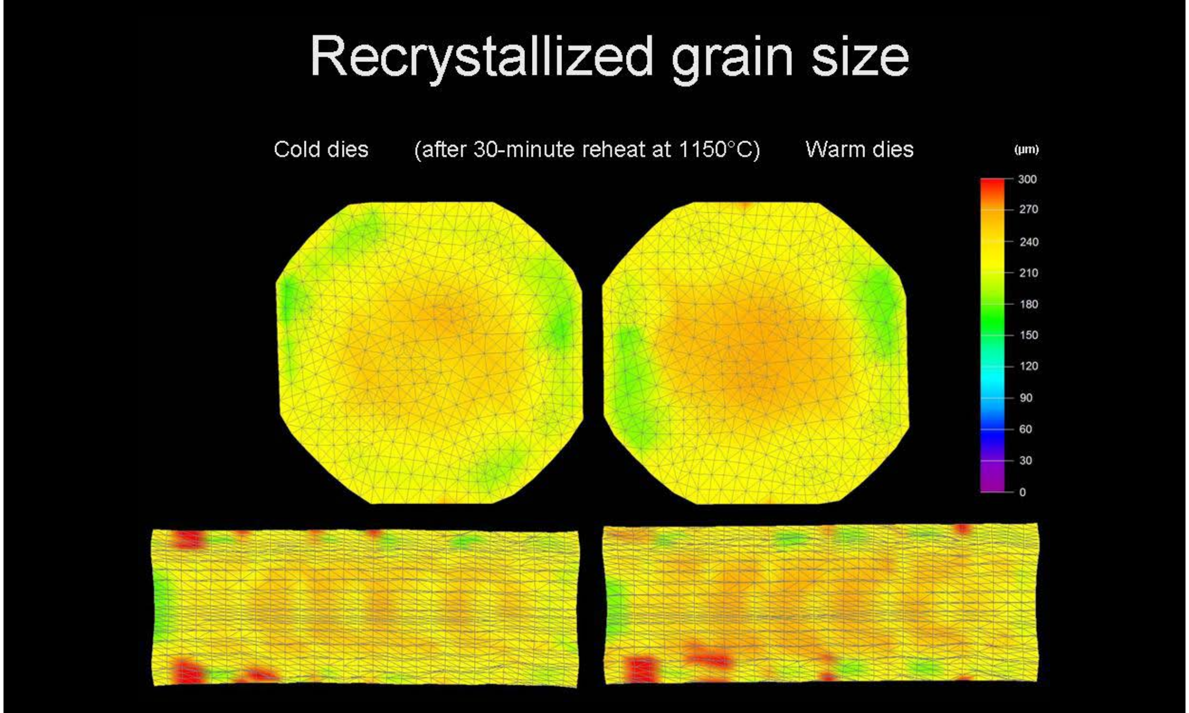

Figure 29: Recrystallized grain size after a 30-minute reheat

Application of the microstructural model to industrial processes

At the end of the 1990's, the Air Force Research Laboratory undertook a large investigation regarding a recurring production issue raised by industrial partners/providers: the occurrence of so-called ALA (as large as) grains in some forged products. This is one of the most common problems for Nickel-base superalloys. In the present case, emphasis was put on larger diameter Waspaloy products. Smaller diameter products are not as prone to ALAs because additional diameter reduction facilitates their elimination. When coarse ALA grains subsist, billets undergo so-called cut-backs to eliminate the zones affected by this defect. This can result in significant yield losses that imply higher production costs, which may ripple down to the final products bought by the Air Force at higher prices, be it for new engines or spare parts. One of the major missions of the AFRL is to provide support to American manufacturers in reducing their production costs, with the expectation that it will translate in cost reductions for the Air Force as well in the long run and help maintain United States aerospace supremacy.

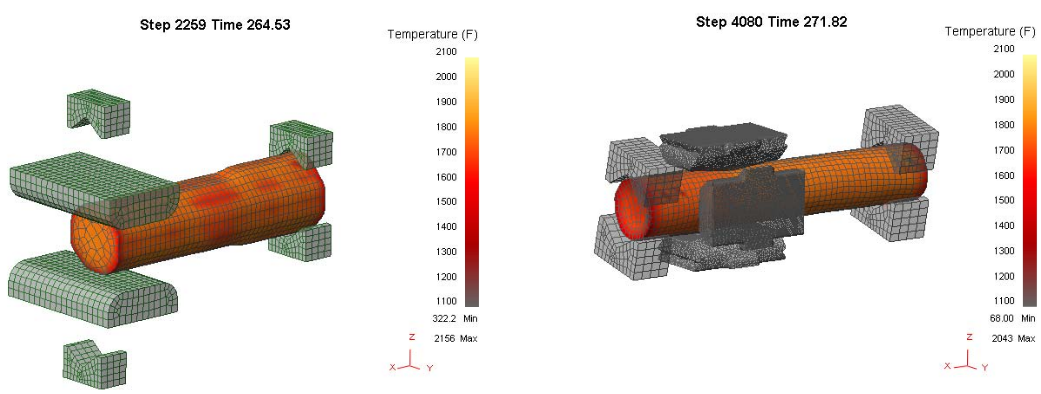

Figure 30: Cogging and GFM simulations

Regarding the Waspaloy products of interest for the AFRL and for its industrial partner in this study, production begins with the conversion of ingots on a press until an intermediate diameter. The billets are then transferred to a GFM to undergo a number of rotary forging passes until the final diameter is reached. Out of the variety of processing routes and products, emphasis was put on three of them. It thus required carrying out the Deform-3D simulations of the three Press-and-GFM sequences (Figure 30). These simulations were defined in the cogging template of Deform-3D using parameters of temperatures, holding times, cogging sequences, GFM reductions, etc. derived from the combination of 1) the definition of practices as documented by the industrial partner and 2) data recorded during actual production at the press and at the GFM by a myriad of sensors such as surface temperature, press tonnage, manipulator movements, GFM power, etc... Deform-3D results were extracted and treated for mesh refinement (Figure 31). And the microstructure-evolution model was used for each of the simulations.

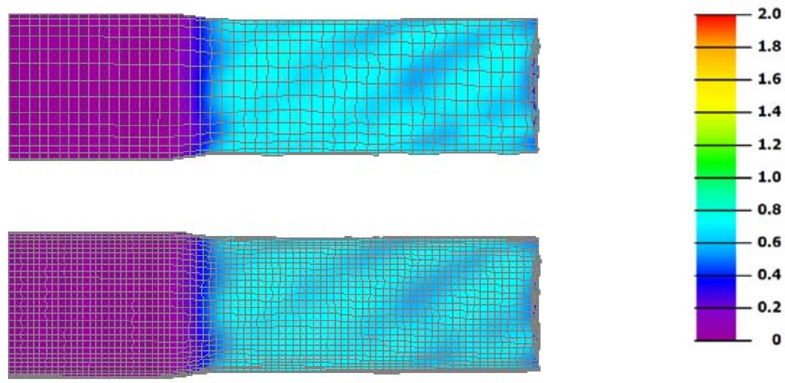

Figure 31: Comparison of the surface strain patterns for a coarse mesh (as extracted from Deform-3D) with its corresponding fine mesh at the same step of a GFM simulation

Because press and GFM simulations were carried out separately, meshes do not translate from the end of the press simulation to the beginning of the subsequent GFM simulation, in particular because cuts and grinding operations may have been performed to eliminate incipient cracking before transfer to GFM. This implied the necessity to implement an additional microstructure-initialization function. This function is able to read the results of a simulation and to map them onto a new mesh. It is then possible to use the recrystallized grain size from a previous simulation as the initial grain size of a new one. In the present case, it allows the initialization of the microstructure for the GFM simulation with the local recrystallized grain sizes of the press simulation that preceded it (Figure 32).

The results presented on Figure 32 match actual measurements on products. Furthermore, their detailed analysis, along with those of simulations slightly modified to represent possible process variations, suggests that the ALAs found in finished billets may be remnants of the recrystallized grains that appeared during the cogging operations. In particular, the application of a temperature offset of -25°F is sufficient to impede their complete recrystallization (Figure 33). It shows that the process for large diameter billets is rather sensitive to inevitable industrial process variations. ALAs coming from earlier stages in the process can not be ruled out at this point. But a solution has to be tested first for the ALAs coming from the latest possible step, and see if it is sufficient. If not, then the search for a solution to eliminate upstream ALAs would have to be undertaken.

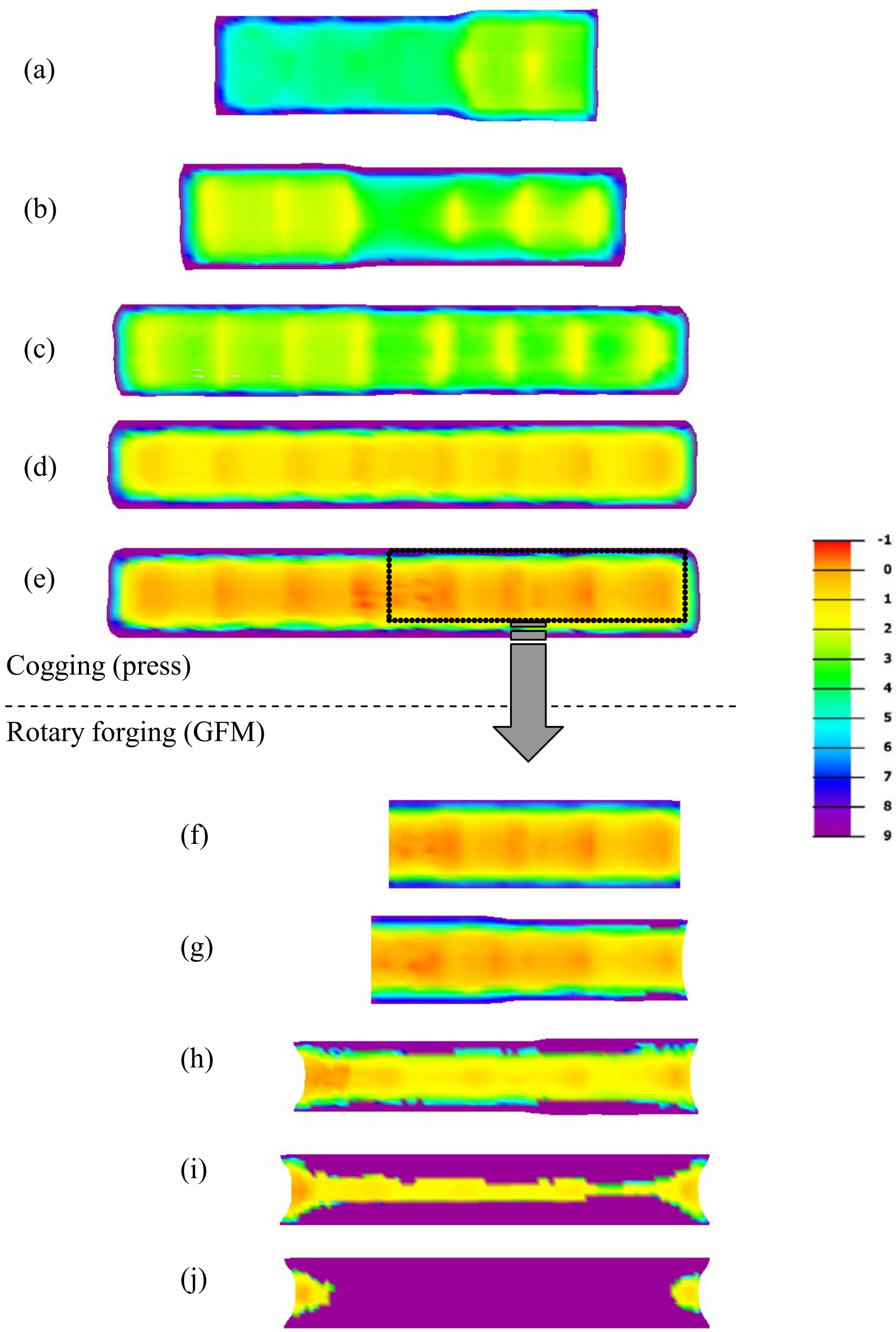

Figure 32: Sections showing the size of the recrystallized grains that appeared during cogging: at various stages of the cogging process (a, b, c, d); at the end of the cogging process (e); after their transfer for microstructure initialization for the GFM simulation (f), and their progressive disappearance during the GFM process (g, h, i, j) (Results presented in ASTM)

(a)

(b)

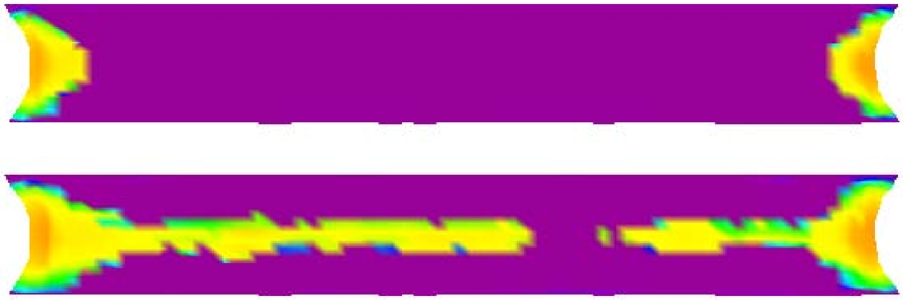

Figure 33: Comparison of predicted ALA grains for the nominal practice (a) with a temperature offset of -25°F (b)

As the model could reproduce correctly the behavior of the current practice, it was applied again to predict the behavior of an alternate practice proposed by industrial partner engineers. It aims at reducing the sensitivity to above-mentioned process variations. The Deform simulation of that purely virtual, never implemented practice was carried out and the model was applied to extracted, refined meshes. Analysis of the prediction results indicates that the goal of reducing process sensitivity would be met, without deterioration of other properties. The alternate practice will therefore be tested on one or two billets first. And if successful, it will be implemented for all future large diameter Waspaloy products with grain-size requirements. Statistics cumulated over months will demonstrate if the occurrence of cut-backs due to ALAs has decreased significantly.

Conclusion of the development of the mesoscale microstructure-evolution model of Waspaloy and its application

Since the time when industrial partners submitted the ALA-grains problem to the AFRL at the end of the 1990's, numerous studies have been performed by the AFRL in order to identify a solution. The AFRL investigated homogenization heat-treatments first [7]; then it characterized the recrystallization of ingot structures of Waspaloy [1-3] to complement data obtained before on wrought material [4]; using those experimental data, the development of a novel mesoscale model of microstructure evolution could be investigated through a previous contract with Universal Technology Corporation [5]; and finally, during the presently-reported UTC contract, the industrial application of all this work was carried out; a diagnosis could be reached and a reasonable solution proposed.

Exploratory work for the development of next-generation microstructure-evolution modeling software

All the microstructure-evolution modeling presented so far was performed using a computer software called RX-MOD designed by the contractor, namely Jean-Philippe Thomas, during his PhD. The first lines of code of RX-MOD had been written in the summer of 2000; by the end of his PhD in the summer of 2004, it had become a fully operational software for the mesoscale modeling of recrystallization and associated precipitation of secondary phases. During the subsequent years of cooperation with the AFRL, a number of modifications and improvements were implemented. But the original software architecture had not been designed from start to accommodate such evolution.

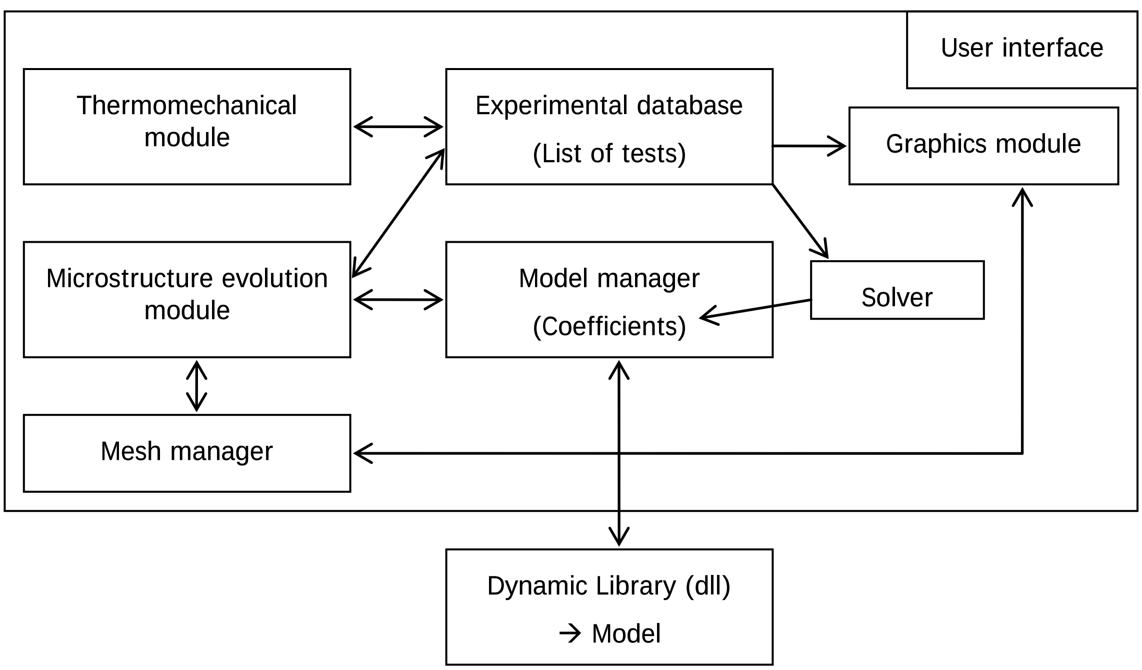

Figure 34: RX-MOD architecture

Furthermore technical choices that used to make sense back in 2000 when Windows 98 was prevalent, when processor frequencies were only reaching the gigahertz and when memory was just in double digits of megabytes, are not relevant anymore. In particular, while the variety of modules that compose the code rely on similar functions, e.g. for data management, they often operate on different, adapted formats due to required optimization. It results in difficult-to-manage code redundancy. It also leads to the virtual impossibility of implementing extended communication between these modules beyond original plans. Regarding software interface, RX-MOD is built against the Microsoft Foundation Classes (MFC) library. Originally designed for Windows 98 and adapted for Windows XP, this library is becoming obsolete. It is being replaced by the Microsoft .NET Framework in the software industry. Basically, what these observations point out is that RX-MOD has reached the end of its first life cycle.

As this diagnosis is reached, the fixes to adequately design “RX-MOD 2.0” seem evident at first glance: create a common foundation for all data management and other frequent functionalities; remodel the interface, in English, and build it against the .NET Framework. A number of so-called “Core” libraries were therefore designed. Among those new libraries are Core System, Core IO, Core Data, Core Geom, Core Mesh, Core Graph, etc… As of 2008, they are actually still built against the MFC library. However, all are built using the same principles, which result in a common foundation that can act as a buffer that isolates high level functionalities from the operating system / MFC / .NET Framework, and guarantee that they are written in standard, portable, maintainable C++.

Nevertheless, as this project progressed, it appeared more and more clearly that this approach was not addressing the deeper issues such as the possible evolution of recrystallization modeling, the context in which models are used, or the potential lying in actually leveraging the synergy of the various modules of the software. By ignoring these issues and continuing on this path, the project would result in the same RX-MOD as before, just easier to use and maintain, maybe a little bit more efficient, but unable to provide the environment for the development of new kinds of models for the coming years as it has been since 2000. The very paradigm of RX-MOD had to evolve beyond the resolution of short term technical issues.

First, as the name chosen for RX-MOD suggests, its purpose is to handle recrystallization modeling. To some extent, that was inappropriate from start. Because the architecture of models for the precipitation of secondary phases was not clearly defined yet during early development stages of the first version of RX-MOD, a precipitation module was implemented in a flexible manner, more flexible in fact than the recrystallization one, the basics of which were already well known. As a result, RX-MOD turned, from start, into a recrystallization modeling software that was offering more flexibility for precipitation than for recrystallization… Even if the primary goal here is the design of software that will handle recrystallization models, it just makes no sense to limit it to that since other peripheral aspects, like precipitation, will necessarily come in the picture. Therefore it is an unavoidable fact that RX-MOD should assume the purpose of handling microstructure-evolution modeling in general. And by doing so, it solves the inadequate, artificial separation of recrystallization and precipitation in two distinct modules by managing them under one single concept.

Second, a long standing issue of RX-MOD regards its thermomechanical module. Its role is to create the thermomechanical history of the sample which will be used as integration path by the recrystallization model. Receiving the nominal definition of a test as input, it calculates the whole history, from the heat-up ramps, to adiabatic heating, to heat exchange with furnace environment and anvils, to final air cool or water quench. To do so, simple geometries for samples and anvils are assumed in order to be easily discretized in rectangles, which are used in a finite difference integration scheme; their deformation during tests is described in ideal conditions such that the initial rectangles remain rectangles on which finite differences can still be applied. The application of a strain-concentration factor is supposed to replicate the overall effect of a possible friction. When the first version was being designed, an FEM-based thermomechanical module was thought of, and quickly rejected. Such an undertaking was deemed unrealistic. There was a large disproportion between the end-use of such project and the overwhelming effort it would require. And therefore, the project settled for a finite-difference-based thermomechanical module. The evolution of RX-MOD throughout the years now leads to a different evaluation. Significant mesh-related capabilities have been implemented; and it is almost like if all needed mesh-related functions are present but the core FEM ones.

Regarding the simulation of thermomechanical processes, FEM has been a major topic of research and development for three decades. The main predictions of FEM models are strain and temperature distributions, and load/tonnage. Apart the latter, these predictions are of interest only in relation to microstructures, which are the ultimate goal for industrial purposes. It may be useful to remind that actually FEM is only a step, not the end *per se*. FEM simulation is becoming more and more a mature technology; most development is oriented towards modules and interfaces tuned for specific simulation needs such as cogging/GFM. Actually, nowadays, such new modules address processes that are increasingly away from thermomechanical processing *stricto sensu*. On the other hand, the potential of physics-based microstructure-evolution modeling only starts revealing its potential. It is therefore questionable that the complex issues at hand with the latter have to be dealt within the constrained space allowed by FEM software packages. In a proper software configuration, microstructure-evolution modeling should be prevalent over FEM issues, not the inverse as it is currently the case in any commercial FEM package. Software for microstructure-evolution modeling should allow the user to tap into embedded FEM functionalities when needed, not be limited within them. Some could argue that in the end, when the model is used, whether FEM makes some place to a microstructure-evolution model or a microstructure-evolution model uses FEM functionalities does not change anything. This is true; but how is the physics-based microstructure-evolution model supposed to be designed, tuned and optimized in the first place? Consequently, the articulation of FEM simulation and microstructure-evolution modeling needs to be re-evaluated.

It appears clearly that the balance between the end-use of FEM capabilities in RX-MOD and the effort required for the integration of such capabilities has significantly evolved since 2000. An attempt for the addition of FEM-related functions to the RX-MOD software was decided. To do so, the use of free FEM libraries such as those available on the internet was considered. However, they would still constitute a somewhat separated module, whereas the goal here is to insure accessibility from anywhere in the code. Therefore FEM functionalities had to be implemented in the Core Mesh library, upon the same mesh objects as those used anywhere else in the code. The implementation of brand new FEM functions was therefore undertaken. These new functions are still rather prototypical. They have not reached satisfactory reliability yet as they may not always converge. Nevertheless, they could capture correctly the influence of strain-rate sensitivity in tension (Figure 35) as well as the deformation of a ∅10mm by 15mm uniaxial compression sample with friction (Figure 36). These results are very encouraging. Additional work would probably allow significant further improvements.

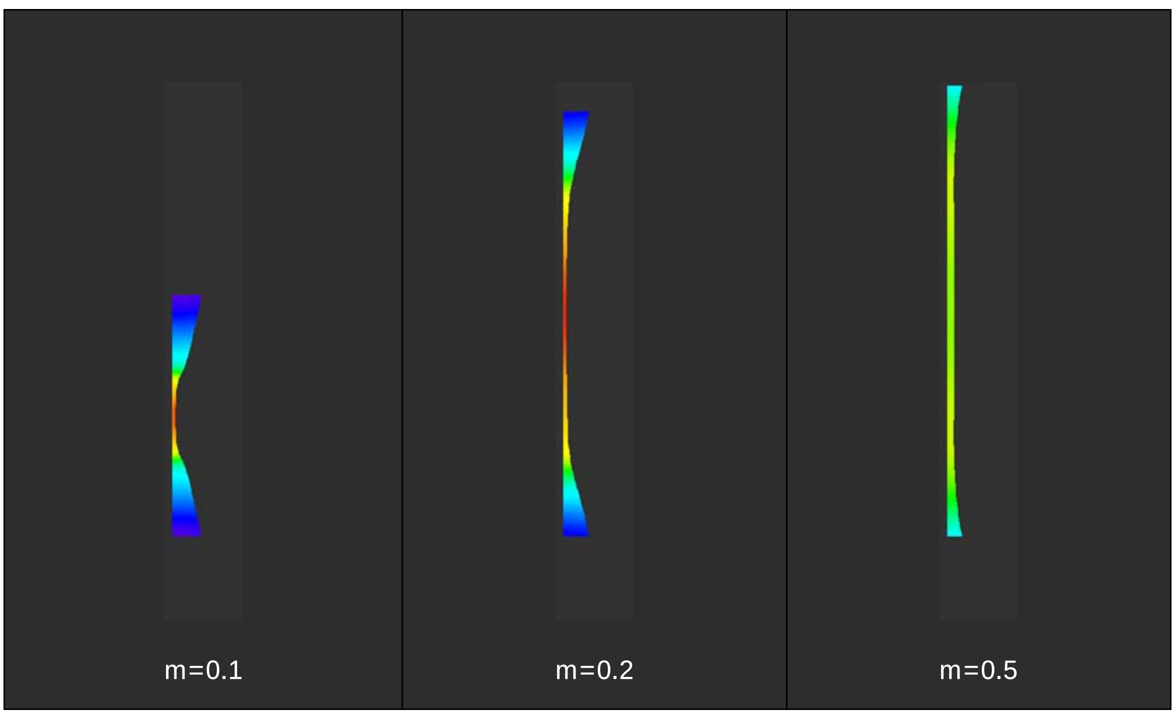

Figure 35: Tension test in plane strain for three strain rate sensitivity values

Calculated by the prototypical FEM functionalities to be implemented in RX-MOD 2.0

Data management, graphics, etc. performed by the new core libraries - Colors represent strain

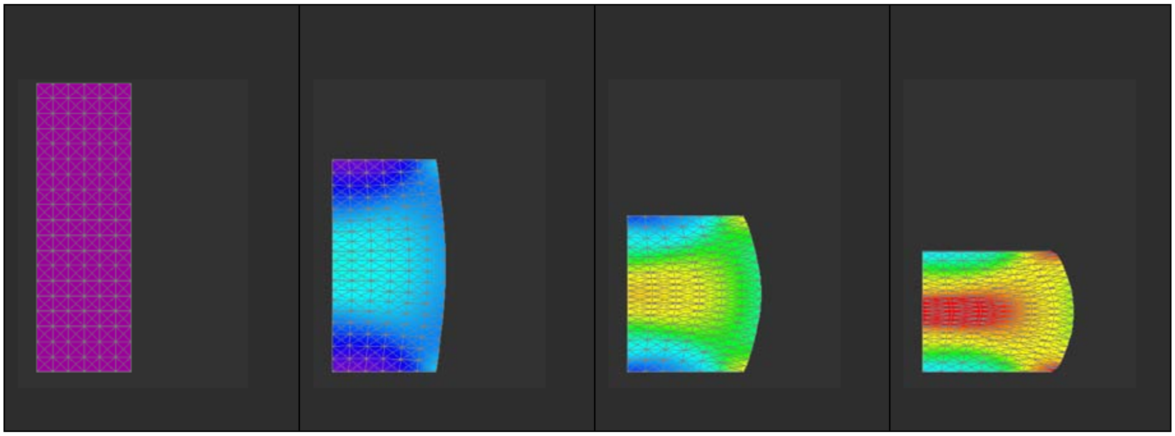

Figure 36: Uniaxial compression of a ∅10mm x 15mm sample with friction
Calculated by the prototypical FEM functionalities to be implemented in RX-MOD 2.0
Data management, graphics, etc. performed by the new core libraries - Colors represent strain

FEM functions need specific input with regards to thermal properties and mechanical behavior. It forced to re-examine the structure in which such data were generated or stored in RX-MOD 1, viz. the “Material” class. It contained the thermal properties; the coefficients for the Norton-Hoff flow-stress law used by the finite-difference-based thermomechanical module to evaluate adiabatic heating; the coefficients of the models of recrystallization and precipitation; the data and functions needed to load and interact with the dynamic linked library (dll) that hosts the models; the list of pointers to modeling functions loaded from the dll. For RX-MOD 2.0, the new “Material” class is a key component for intended modeling flexibility. The Material class contains holders of all the information that is provided by the dynamic linked library with regards to the models it contains, the data it needs to function, the data it outputs, etc. All this is allowed by the Core Data library which provides the tools needed to describe these formats in a concise way. For example, recrystallization models rely on a number of functions such as dislocation generation, recovery, etc. In RX-MOD 1.0, it was fixed to 20 functions, for one single model. In RX-MOD 2.0, several models with a variable number of functions are allowed. When the dll is loaded, it first sends a format object that contains the number of models and their names. These are allocated by the Material class. Then the dll sends, for each model, a format object containing the number of functions and their names. They are then allocated for each model. Provided a clear hierarchy and its appropriate description, it is possible to manage flexible modeling.

The incorporation of FEM functionalities requires a clear articulation with the Material class, which naturally should provide FEM input, viz. thermal and flow-stress functions. Thermal functions such as heat diffusivity or heat capacity do not require flexibility beyond being implemented freely in the dll to depend on temperature in any way deemed suitable by the user. For mechanical data, at first, a flow-stress function was be implemented aside the thermal ones.

However, this introduces a dissymmetry with the flow-stress predicted by microstructure-evolution models and thus complicates their use. The concept of microstructure-evolution model as-handled by the software was therefore extended to include models that only give Von Mises flow-stress in response to a temperature, strain, strain-rate input. To some extent, they can be seen as microstructure-evolution models, just in an even more rudimentary and macroscopic way than Avrami models for instance. Consequently, all microstructure-evolution models are required to provide a flow-stress to be able to respond to FEM functionalities. If ranged from most simple to most complex, the very first model of the dll should be just a Norton-Hoff type of law capable of providing reasonable flow-stress values. Such a macro flow-stress law would insure the possibility of at least the calculation of the thermomechanical history of samples through the thermomechanical module.

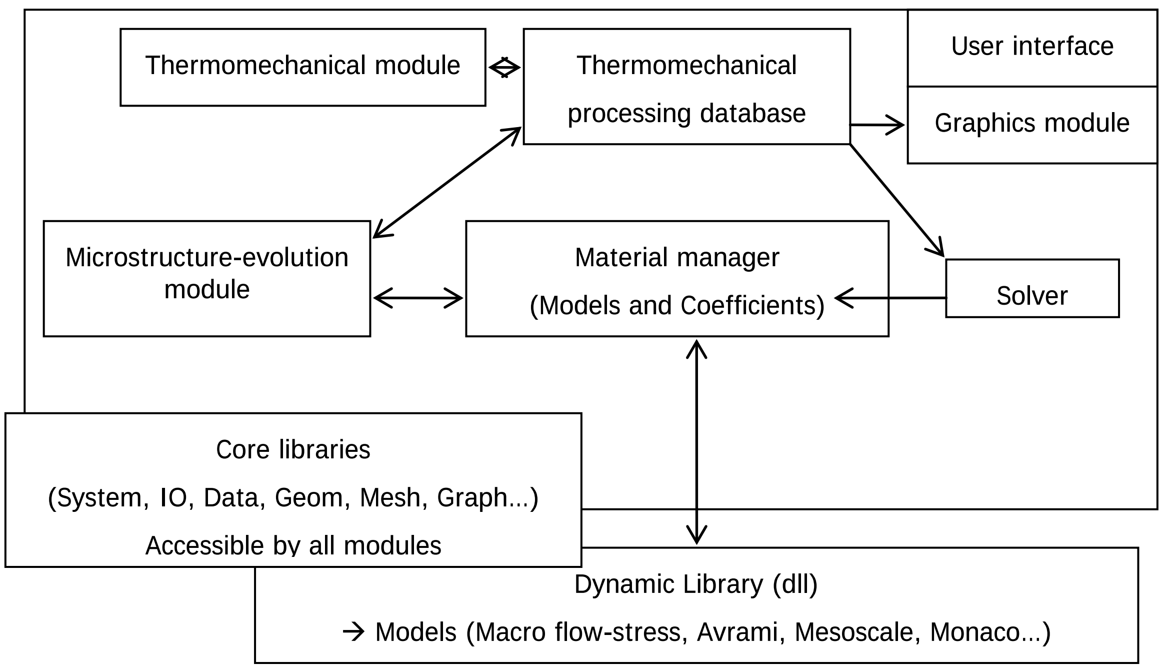

Figure 37: Projected RX-MOD 2.0 architecture

These thermomechanical histories would be saved as FEM simulations. And the history of the center of samples would be extracted from these FEM simulations by means of tracking point functions. It will not be possible to differentiate an internally generated FEM simulation from one imported from an external FEM package such as Deform, if not by their level of complexity. The experimental database, which used to contain only the list of tests, the thermomechanical history of the center point of samples, and microstructure results, will have to become a more general thermomechanical processing database. These modifications have not been implemented yet. It partly comes from the remaining difficulty to fully grasp the use of the different microstructure-evolution models at different levels or layers.

The concept of levels/layers is very important in RX-MOD 2.0; although its definitive contours are not quite clear yet. Even its name is not. What has been identified is that interrogations rise recurrently with regards to the combinations/sequences of use of software capabilities. For instance, the order of development of a Mesoscale model would be:

1) Enter the definition of all tests along with measured data (Stress-strain curves, recrystallized fractions, recrystallized grain sizes, etc…)

2) Run a rough initialization of thermomechanical paths as a direct translation of the nominal definition of tests.

3) Run the “microstructure-evolution model” of the macro flow-stress law on those rough thermomechanical paths and use results to tune its coefficients to fit the measured flow-stress curves.

4) Use the newly adjusted macro flow-stress law for a better evaluation of thermomechanical histories through FEM simulations. Potentially, due to adiabatic heating and friction not accounted for in item 2, loop item 3 and 4 until the parameters of the macro flow-stress law are de-correlated from the softening effect of adiabatic heating embedded in the measured data.

5) Develop/adjust the Mesoscale model to fit all available data using the thermomechanical paths provided by the FEM simulations based on the best iteration of the macro flow-stress law of items 3-4.

6) If the flow stress provided by the Mesoscale model ends up being more precise than the macro flow-stress law, re-run the FEM simulations, but using the flow-stress provided by the Mesoscale model this time. If significant changes arise, loop back to item 5.

One can see that such a sequence would involve multiple changes in the levels at which the models are used. Said differently, in terms of set-up of the calculations, at item 3, the macro flow-stress law being adjusted is used in the “microstructural layer” on a tracking point. At item 4, that macro flow-stress law switches to the “mechanical layer” on meshes. At item 5, the macro flow-stress law is still used in the “mechanical layer” on meshes, and the Mesoscale model is in the “microstructural layer” on tracking points. At item 6, the Mesoscale model would occupy both the “mechanical layer” and the “microstructural layer” on the full mesh. In the case of a simulation performed by Deform and imported, only in the “microstructural layer” would be activated with the Mesoscale model. In the case when the mesh imported from Deform is used to track a finer mesh, a different sort of layer relationship appears between the native "thermo-mechanical layer" of the coarse Deform mesh and the finer mesh on which the Mesoscale model is used in the "microstructural layer". A very interesting use of the finer mesh would consist in re-calculating the thermal evolution to better capture surface gradients; each element of the fine mesh would derive its strain, strain rate, and therefore adiabatic heating, from the strain available in the native coarse mesh. In such scenario, the native coarse mesh would be the "mechanical layer", the fine mesh would provide the "thermal layer", and the Mesoscale model would be the "microstructural layer".

This concept of layer becomes even more interesting if one considers the use of meshes to support hybrid Cellular Automata (CA) - Monte-Carlo (MC) types of models. Such meshes will be called "micro-meshes" in order to reflect that they belong to the "microstructural layer" and that they assume large numbers of very fine element-cells. Needless to say, they require large amounts of memory. However, one of the key assumptions of usual MC and CA models is that of a regular, isotropic, thus non-deformable, grid of cells. Such "rigid" assumption is generally considered as having a negligible impact. We have not found any study investigating the behavior of distorted grids, if only because it would impose a clear understanding of the way regular-grid models function in regard to probabilities of picking neighbors and switching cells. Such investigation is the core of the development of an extension of Cellular Automata and Monte-Carlo models into what will be called Monaco modeling in RX-MOD 2.

A prototypical Monaco model was implemented using triangle meshes only so far. It requires more information than the typical connectivity table; although most of that additional information derives from the latter. This information comprises the list of elements to which a node belongs (dual of the connectivity table); the list of first order neighbors of an element (sharing a side); the list of secondary neighbors of an element (sharing only a node). In 3D, there are three orders of neighbors ranging from common face, to common side, to common node; but 3D appears to be beyond current computer capabilities. Some geometric values are also needed such as, for each element-cell, the probability that a given first order neighbor is picked (based on the ratio of the length of the common side divided by the total circumference of the element); the distance between the centers of gravity of adjacent element-cells; and the depth of the element relative to each side orthogonally (Figure 38).

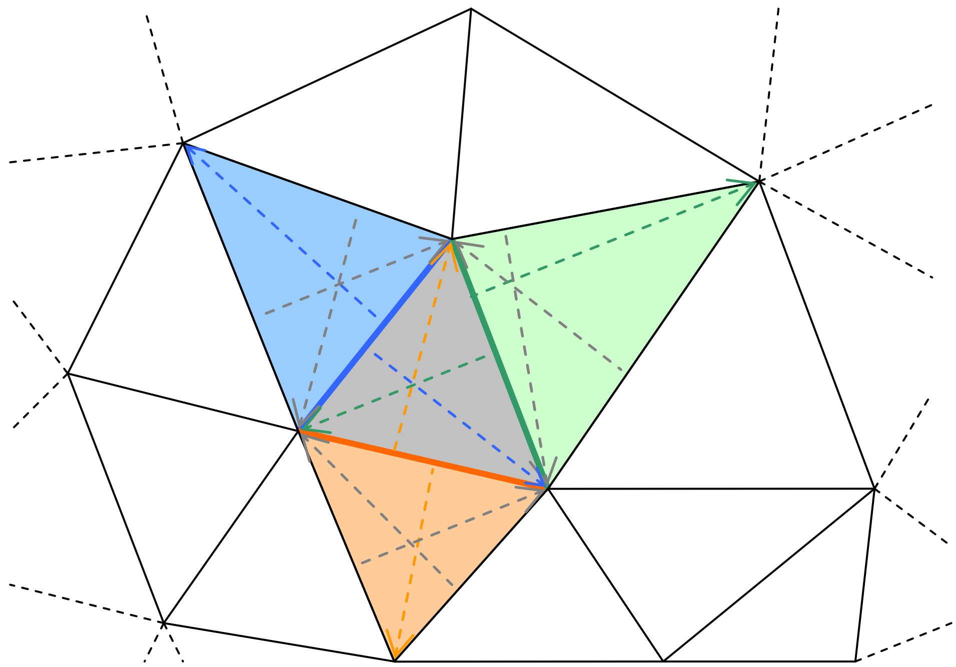

Figure 38: representation of an element-cell; its first order neighbors are highlighted; the depth of the element-cell relative to the side of each neighbor is materialized by an arrow

The model then functions as follows: first, an element-cell is picked randomly in the micro-mesh, and one of its first order neighbors is picked in accordance with the above-mentioned probabilities. A type of interaction is chosen between CA-type (dislocations, for recrystallization) or MC-type (grain-boundary energy for grain growth; it involves the second-order neighbors). Then the driving force for the switch is calculated either based on a dislocation-density difference between the two cells (CA-type of interaction) or as the energy difference between the two configurations (switched vs. un-switched for MC-type of interaction). If the driving force is positive, it is multiplied by the grain boundary mobility and by a (small) time step. It results in a boundary-migration distance. For a small-enough time step, this distance is shorter than the depth of the element relative to the side of the considered first-order neighbor, distance by which the boundary would have to move to operate the switch. The division of the two is therefore the probability of switching the cell within the considered time step. In the case of a negative driving force for an MC-type of interaction, a probability of switch is evaluated nevertheless using an exponential expression representing thermal fluctuations. This would however need more understanding. To calculate the probability of switch, one could normalize the boundary-migration distance by the distance between the centers of gravity, or the sum of the two distances between the orthocenters and their common element-cell side. However, the first option, viz. using the element depth relative to the moving side seems more meaningful. Nevertheless, overall, the definition of those probabilities aims at replicating the switch behavior of a regular grid of cells, as well as accounting for its distortion when the micro-mesh is attached to a mesh being deformed.

To test those new functionalities, a micro-mesh was attached upon the simulation of Figure 36 and used for a Monaco simulation. The local temperature and strain of the "macro-mesh" of Figure 36 (thermo-mechanical layer) are interpolated and provided at each step to the element-cells of the micro-mesh (microstructural layer) as input for their evolution and switch probabilities. The results are presented in Figure 39. Pushing the concept of layers forward, one can use a Monaco simulation to provide mechanical information to the macro-mesh. Using the same macro-mesh as that of Figure 36, the flow-stress was provided to each macro-element as the average of the flow-stresses of the micro-element-cells it contains. In this case, the "mechanical layer" (the macro-mesh) receives flow-stress input from the "microstructural layer" (the micro-mesh). And in return, the micro-mesh receives information regarding its deformation, strain and temperature from the macro-mesh. The results of a simulation assuming no friction are presented in Figure 40. In that simulation, each grain was provided with a random Taylor factor to account for the effect of the latter on strain homogeneity. It exhibits the typical alternate 45° bands of higher and lower strains that derive from the Taylor factor variation between initial grains. The new embedded FEM functionalities seem to behave properly, even in this advanced coupling scheme. However, a new set of boundary conditions allowing a form of mechanical periodicity would be needed to avoid the free-surface undulations that develop on the right-hand side. A real microstructure would be more constrained than represented here.

One can see that the proper management of interactions between layers is the key to leverage the full potential of RX-MOD 2. Additional thinking will have to be put into it before the integration of all the modules of the software is carried out. This will insure that no interesting combination is made impossible and simultaneously that these combinations can be managed easily and intuitively by the user. Such questioning is at the frontier or rather in the overlap region of software development and microstructure-evolution modeling research. Their appropriate management is nevertheless very important, as demonstrated by the results presented in the first part of this report that were allowed by RX-MOD 1, or by the already advanced capabilities of RX-MOD 2.

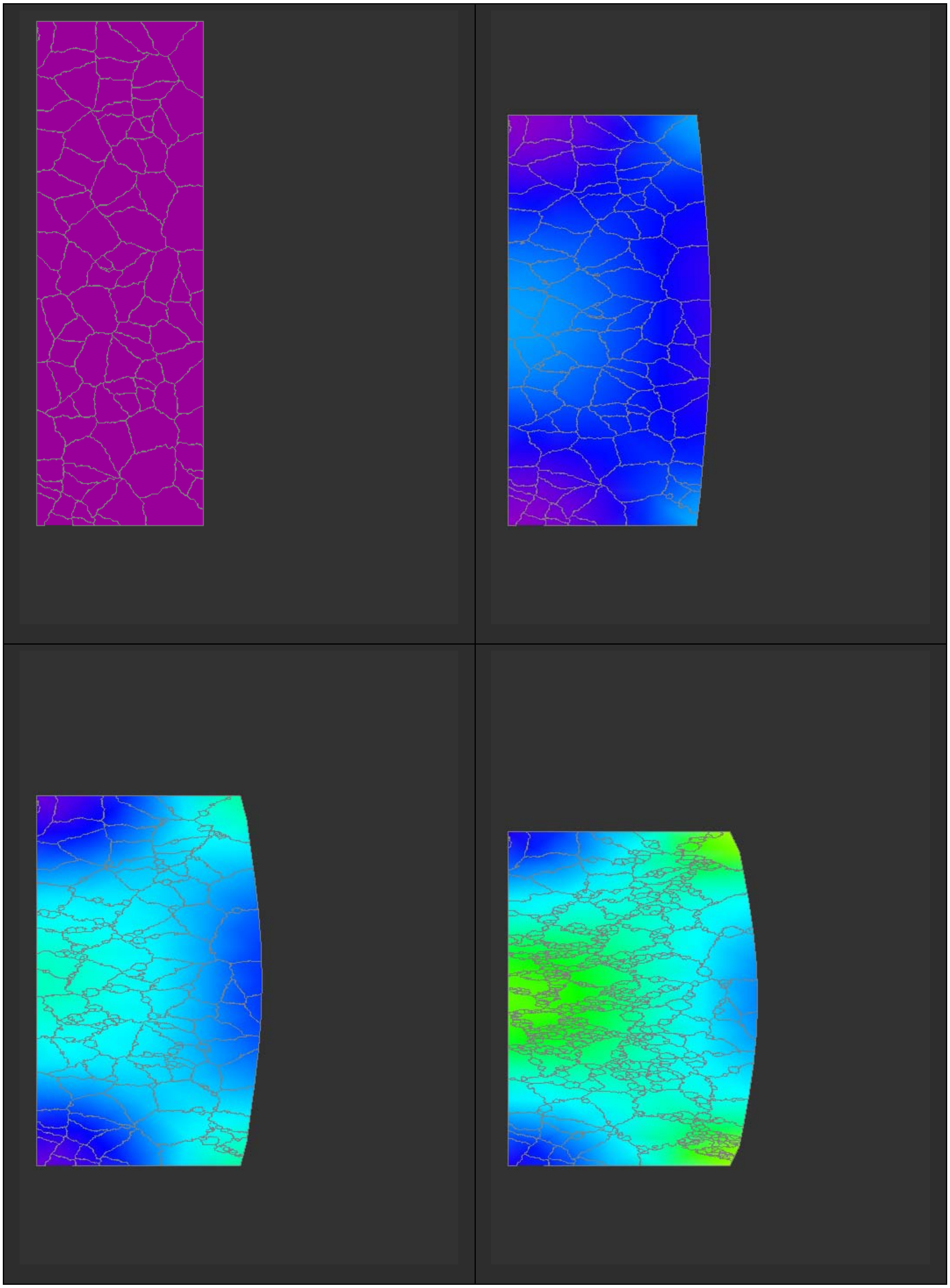

Figure 39: Monaco simulation attached on the thermomechanical simulation of Figure 36

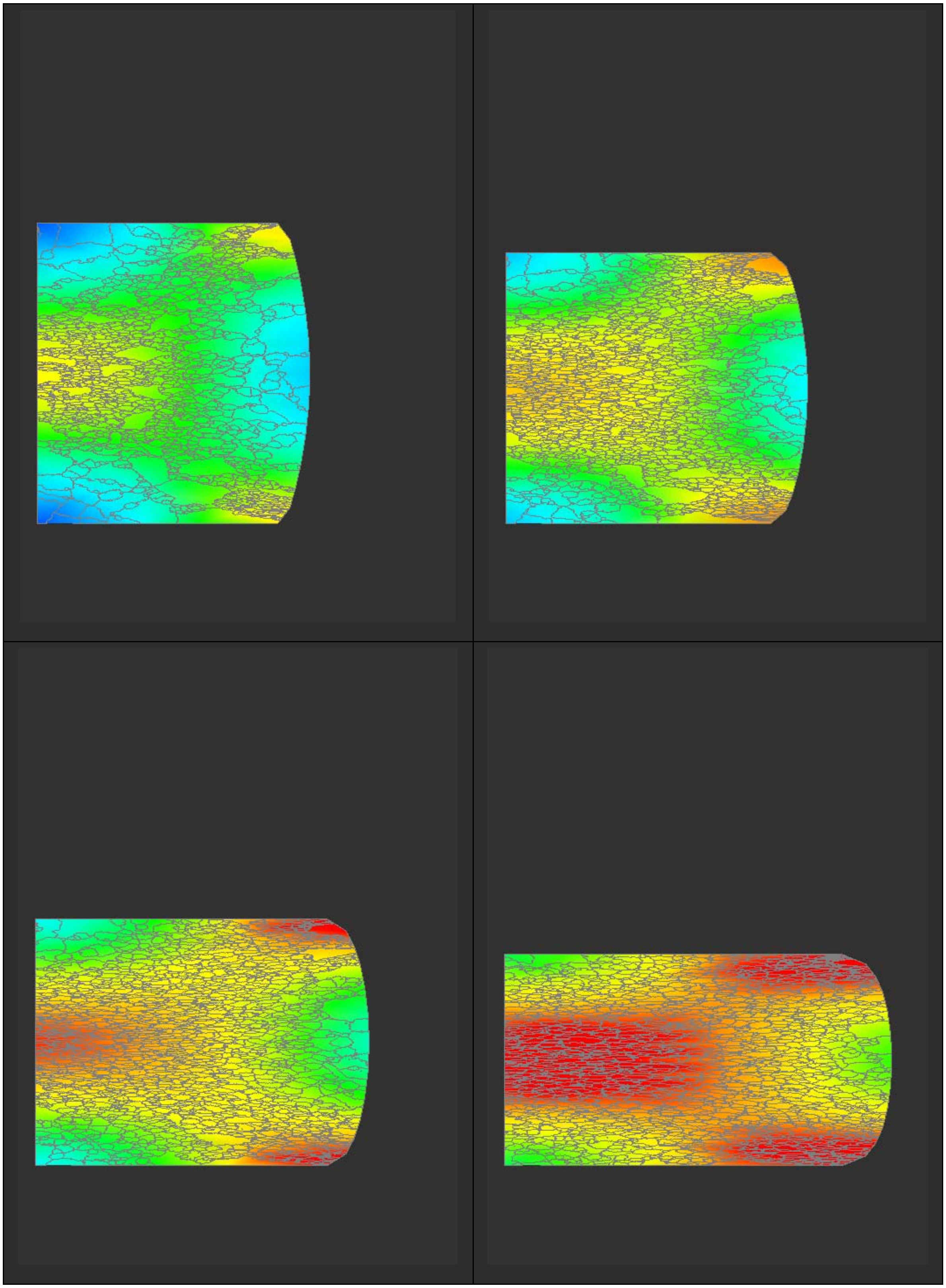

Figure 39: Monaco simulation attached on the thermomechanical simulation of Figure 36

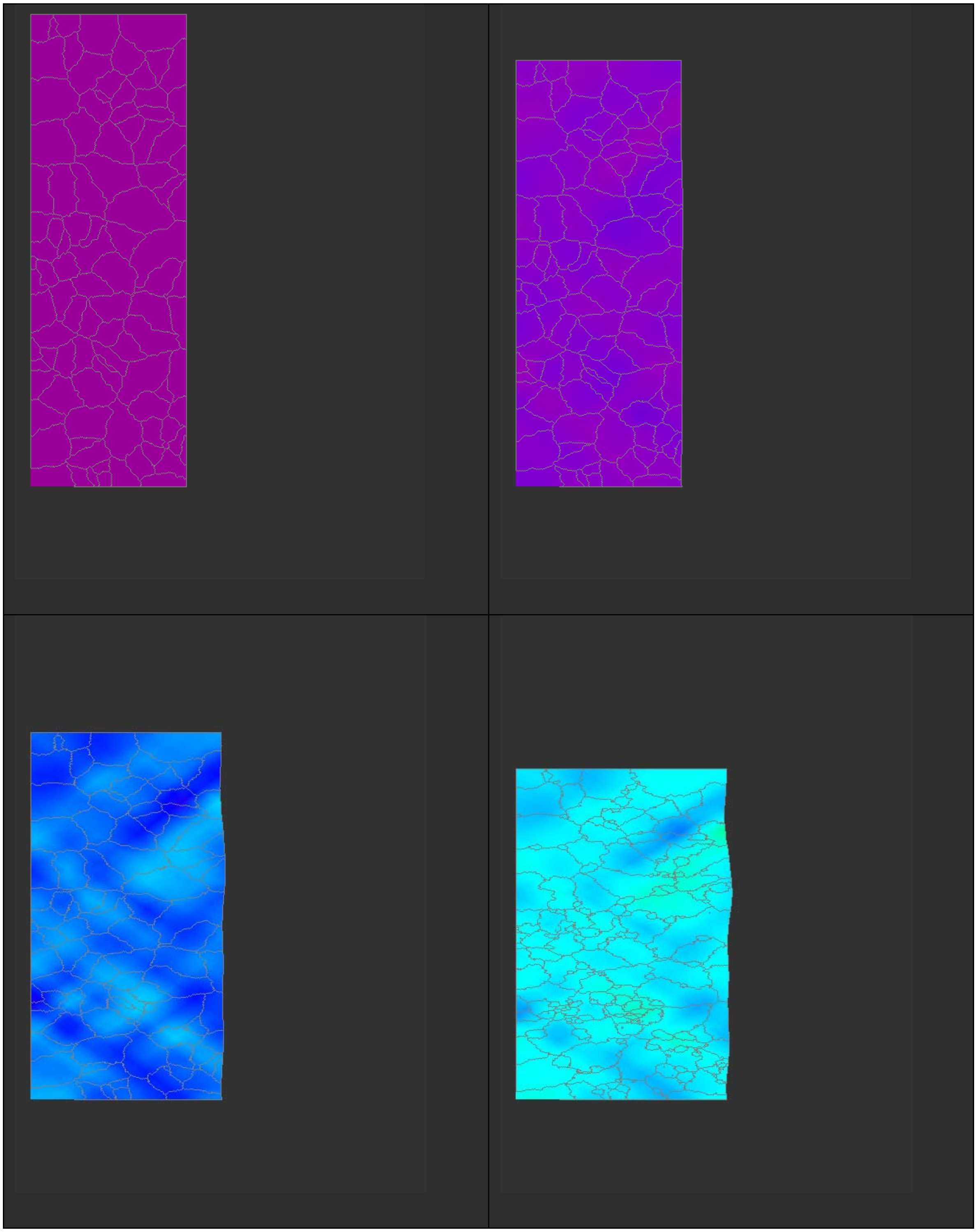

Figure 40: Monaco simulations providing the flow-stress to the mesh of Figure 36, no friction

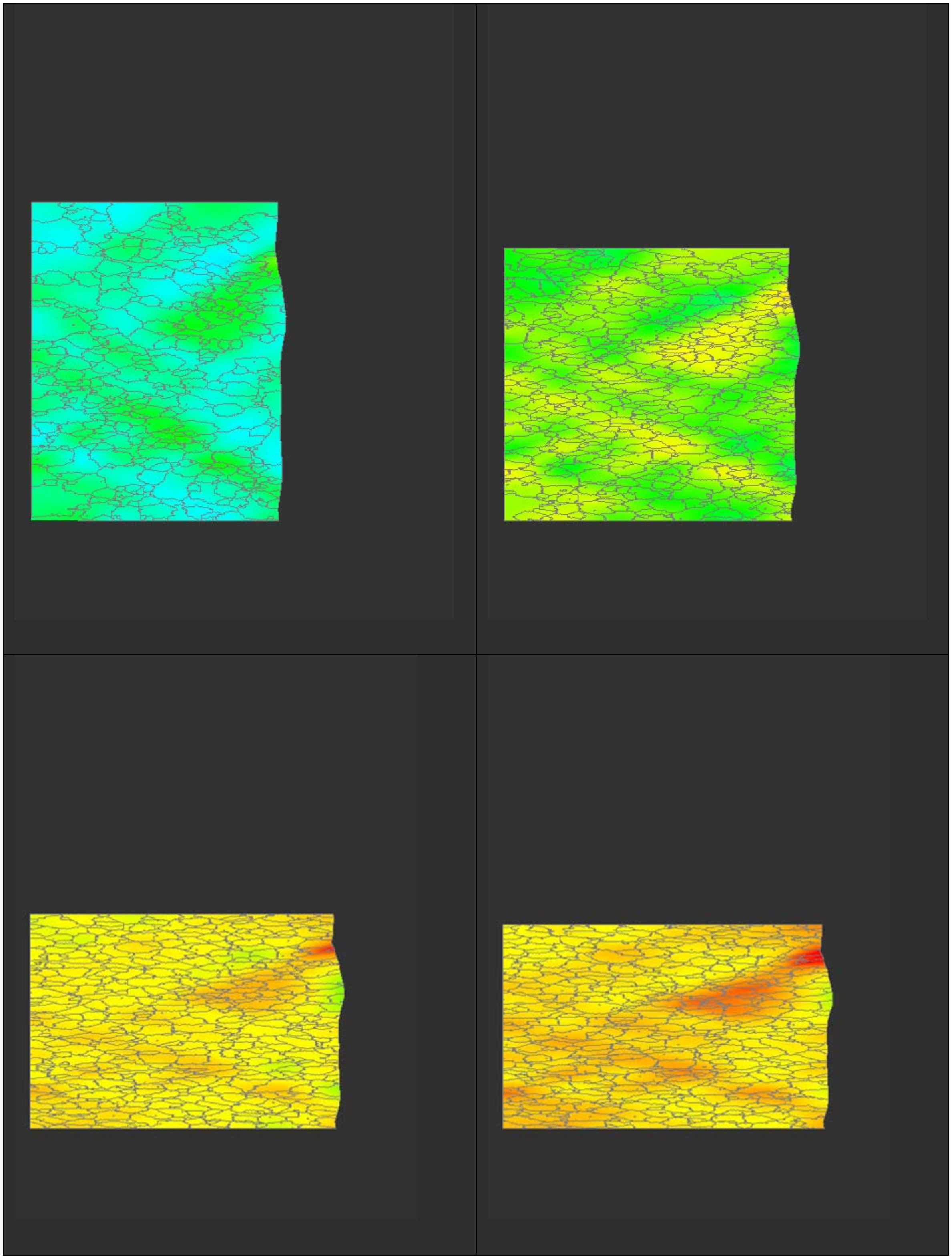

Figure 40: Monaco simulations providing flow-stress data to the mesh of Figure 36, no friction

Conclusion of the investigation for a next-generation microstructure-evolution modeling software

The examples of simulations performed in the prototypical modules developed for RX-MOD 2 reveal the potential lying in the coupling of functionalities that are usually considered separately. Depending on the level at which such functionalities are leveraged, they belong to thermal, mechanical or microstructural so-called layers. RX-MOD 2 aims at allowing the user to dispose freely of a variety of combinations to perform “multi-model” or “multi-layer” analysis and design models in an efficient fashion. This is made possible by 1) core libraries that provide a common foundation for all modules and 2) a modeling architecture that considers microstructure-evolution models as a continuum ranging from macro flow-stress, to Avrami models, to Mesoscale, to Monaco models (extensions of MC and CA on flexible grids) and maybe one day even to phase-field models (again, on flexible grids). In the same way that the first version of RX-MOD was a requirement for the successful development and application of meso-scale models of recrystallization for Nickel-base superalloy, RX-MOD 2 will be a necessity to handle future novel modeling techniques, applicable even beyond superalloys. One can easily see for instance the potential of combined FEM-Monaco simulations for the investigation of the globularization of α phase during hot working of α-β titanium alloys. There is still considerable work to be done though to fully reach these objectives. But current results should be seen as already very encouraging; for instance, to our knowledge, it is the first time that a figure such as Figure 41 can be drawn using a microstructure-evolution model. Ever increasing computer capabilities will soon allow such calculations over the section of whole billets. Hopefully RX-MOD 2 will be completed and ready in time to exploit such new hardware capabilities.

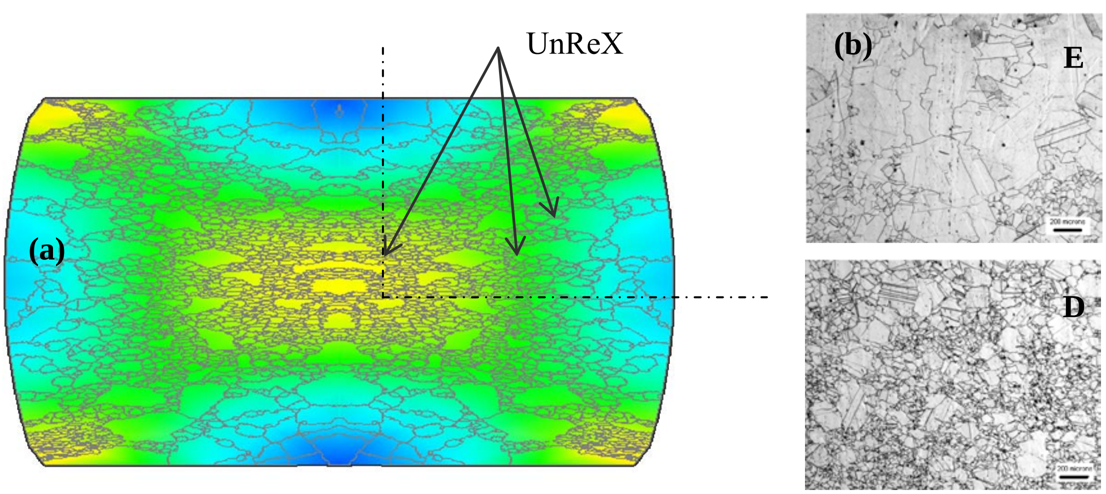

Figure 41: Monaco simulation on a pancake (a); for qualitative comparison, micrographs taken at locations D and E of Figure 17 on the actual subscale-validation pancake of Waspaloy (b)

Conclusion

A physics-based mesoscale model of recrystallization of Waspaloy was successfully applied to the industrial primary conversion of ingots into billets, in a combination of cogging and rotary forging processes. A most probable source of subsisting unrecrystallized ALA grains was identified for the larger diameter products in which they tend to occur. A modified practice was envisaged by the engineers of the partner industrial company as a solution. The simulation of this alternate practice showed noticeable improvements in terms of resilience to inevitable industrial process variations, without detrimental effects on other properties. The use of these modeling techniques adds security and increases confidence prior to actually implementing the practice in production. After about a decade since the AFRL was first consulted about that difficult-to-control production issue, these results can be seen as a great example of successful partnership between the Air Force and its suppliers.

The experience gained during this project allowed a more exploratory type of work with the development of so-called Core libraries and a few new modules in preparation of envisioned next-generation microstructure-evolution modeling software, deemed RX-MOD 2. The combination of these prototypical modules already exhibits remarkable novel modeling capabilities. In particular, it reconciles various modeling methods by managing them as a continuum of complementary approaches rather than in opposition. And it proposes a software architecture such that microstructure aspects can take advantage of embedded FEM functionalities. Still, a significant amount of work would be needed to fully reach the goals of a user-friendly, powerful, stable, versatile computer tool for microstructure-evolution modeling.

References

[1] S.L. Semiatin, P.N. Fagin, M.G. Glavicic, D. Raabe, Scripta Mat. 2004, vol. 50, pp 625-29

[2] S.L. Semiatin, D.S. Weaver, P.N. Fagin, M.G. Glavicic, R.L. Goetz, N.D. Rey, R.C. Kramb, M.M. Anthony, Metall. Mater. Trans. A, 2004, vol. 35A, pp 679-93

[3] D.S. Weaver and S.L. Semiatin, Scripta Mat., 2007 vol. 57, pp 1044-1047

[4] G. Shen, S.L. Semiatin, and R. Shivpuri, Metall. Mater. Trans. A, 1995, vol. 26A, pp 1795-1803

[5] J.P. Thomas, F. Montheillet, and S.L. Semiatin, Metall. Mater. Trans. A, 2007, vol.38A, pp 2095-109

[6] J.P. Thomas, E. Bauchet, C. Dumont, and F. Montheillet, Superalloys 2004, K.A. Green, T.M. Pollock, H. Harada, T.E. Howson, R.C. Reed, J.J. Schirra, and S. Walston, eds., TMS Warrendale, PA, 2004, pp 959-68

[7] S.L. Semiatin, R.C. Kramb, R.E. Turner, F. Zhang, and M.M. Anthony, Scripta Mat., 2004, vol. 51, pp 491-95

Appendix: Article

A geometric framework for mesoscale models of recrystallization

A Geometric Framework for Mesoscale Models of Recrystallization

J.P. THOMAS, F. MONTHEILLET, and S.L. SEMIATIN

Geometric aspects are a major issue in models of recrystallization that rely on statistical grain-population descriptions, because the growth of recrystallized grains has to be compensated by the loss of volume of deformed grains, thus leading to concomitant variations in all geometric variables. A geometric framework for such models was thus designed. It is based on mesostructure units (MSUs), each of which represents an aggregate of similar grains. The evolution of MSUs is controlled by two kinds of inputs, nucleation rates and grain-boundary velocities, from which the evolution of microstructure is described in an internally consistent fashion. The geometric framework was applied initially to the necklace recrystallization of fine-grain microstructures, *viz*., the usual form of recrystallization comprising nucleation on initial grain boundaries. It was extended to describe particle-stimulated nucleation (PSN) in order to treat geometric effects related to intragranular recrystallization, as is found in coarse ingot microstructures. For both the necklace-only and necklace-and-PSN cases, test cases using simple inputs were performed to validate the behavior of the geometric framework.

DOI: 10.1007/s11661-007-9247-x

I. INTRODUCTION

MODELING tools for the prediction of microstructure evolution are needed to optimize thermomechanical processes, *i.e*., to obtain desirable mechanical properties and to reduce both process design time and manufacturing cost. The usual method, based on the so-called Avrami or Johnson-Mehl-Avrami-Kolmogorov (JMAK) formulation, has been applied with some success for a number of years. In particular, its implementation in finite-element-method (FEM) subroutines, requiring minimal additional computational power, has provided a very useful tool for manufacturers.[1] However, such models become increasingly phenomenological as their domain of application is extended over wider ranges of temperature, strain, and strain rate, and for complex sequences of dynamic, metadynamic, and static recrystallization, as illustrated in Reference 2.

As long as dynamic recrystallization can be neglected or represented using reasonable approximations, it is possible to integrate a number of mechanisms and couple them inside the framework of an Avrami formulation.[3] However, the Avrami approach poses a number of limitations related to its lack of a true physical basis outside the context of classical static evolution. For example, it is incapable of properly incorporating the influence of precipitates on dynamic recrystallization,[4] and its extension to deal with partial waves of dynamic or metadynamic recrystallization is questionable.[5] Geometric and texture effects are also rarely included in such instances. A more fundamental weakness of this phenomenological approach, even when focusing on a specific alloy, relates to the extensive and, hence, expensive experimentation required to characterize microstructure evolution over the full range of temperature, strain rate, and history variables and, thus, to fit such models. Furthermore, it is usually not possible to extend Avrami relations derived for one material to another, even in the same alloy class, because the model parameters have limited physical meaning.

Models of microstructure evolution based on the Monte-Carlo[6] and cellular-automata[7,8] techniques also have their own advantages and limitations. They provide an enhanced representation of the physics of evolution. Nevertheless, they require substantial computational power, thus preventing their application at every node of an FEM mesh. In such cases, analysis is limited to a rather small number of tracking points.

To meet the needs of industry, a new type of recrystallization model is required. Such a model should combine the key advantages of the Avrami approach (*i.e*., reasonable computational requirements) and physics-based models (*i.e*., the formulation and input parameters should be as meaningful as possible). Computational requirements concern not only the coupling of the microstructure model with the FEM process model, but also various aspects of the optimization routine used to adjust model parameters in order to replicate the laboratory data that provide the basis of the material description. Because of the complexity of the thermomechanical processes at both the macroscales and microscales, computational restrictions preclude the

J.P. THOMAS, Visiting Scientist, Air Force Research Laboratory, AFRL/MLLMP, is with the Universal Technology Corporation, Dayton, OH 45432. F. MONTHEILLET, CNRS Senior Scientist, is with the Ecole Nationale Supérieure des Mines, Centre SMS, CNRS UMR 5146, 42023 Saint-Etienne Cedex 2, France. S.L. SEMIATIN, Senior Scientist, Materials Processing/Processing Science is with the Air Force Research Laboratory, Materials and Manufacturing Directorate, AFRL/MLLMP, Wright-Patterson Air Force Base, OH 45433. Contact e-mail: lee.semiatin@wpafb.af.mil
Manuscript submitted October 19, 2006.
Article published online July 25, 2007.

local description of microstructure evolution for every grain. Instead, a simplified grain-population description which is based on a statistical approach at the mesoscale appears to offer promise.

Geometric evolution is a central issue in mesoscale models of recrystallization because, first, the loss in volume of some grains through nucleation has to be compensated for by an increase in the volume of some other entity and, second, the growth of the recrystallized grains has to be compensated for by the loss in the volume of other (deformed) grains. The latter consideration includes the so-called impingement of recrystallized grains: in the context of dynamic recrystallization, the deformed grains may be not only the ones present at the very beginning of deformation; those of the previous generations of recrystallized grains may also be present. Hence, the impingement of the recrystallized grains during dynamic recrystallization rarely leads to the end of grain-boundary migration. As a result, the ability of mesoscale models to represent adequately the progress of recrystallized zones, the subsequent waves of the recrystallization that occur inside these zones, and, therefore, the dynamic steady state when recrystallization is complete depends primarily on the way in which geometric aspects are managed.

Given the complexity of the geometric issues, early mesoscale models neglected most of the evolution inside recrystallized zones during deformation.[9] Some improvements have been made, although the concept of impingement of grain boundaries stopping migration is typically assumed.[10,11] By contrast, the mesoscale model presented in Reference 12 focused on the steady state of dynamic recrystallization. In terms of geometry, the core of this model lay in the implicit evaluation of the probabilities of contact between grains of different types based on the surface of their boundaries. The same probability expressions were also used explicitly for the mesoscale modeling of static grain growth.[13] Inasmuch as this latter approach seems promising and applicable for a number of cases, it was thus chosen as the basis for the present work.

Mesoscale models should also reflect the distinction between the driving forces and mechanisms of microstructure evolution activated by deformation, on the one hand, and geometric evolution *per se* on the other. To deal with the strictly geometric effects of nucleation and grain growth discussed earlier, geometric variables should be constrained into a somewhat independent, yet internally consistent, framework that ensures that their coupled evolution satisfies volume conservation and that the geometric description of microstructures remains meaningful. In the present work, such a geometric framework for a statistical, mesoscale model for microstructure evolution is introduced. For purposes of statistical representation, grains of similar condition/state are aggregated into so-called mesostructure units (MSUs). Each MSU is defined by variables that can be seen as averages over the specific grain population which the MSU represents. Geometric variables include the volume density of the specific type of grains and the average dimensions or volume of the grains. A few other variables, such as the Taylor factor or the dislocation density, can be added to represent deformation-related properties and driving forces; the incorporation of these latter variables is briefly treated in Reference 5 and will be discussed more extensively in a companion publication.

The geometric framework was designed to respond to two types of inputs: nucleation rates and grain-boundary velocities. These inputs are provided by the other part of the model; *i.e.*, the one that is related to the microstructure-evolution mechanisms and driving forces, an example of which is summarized elsewhere.[5]

Inspired by previous models,[5,12] the present geometric framework was developed in the context of a larger program the objective of which is to develop and validate models of microstructural evolution during the primary processing of ingots of nickel-base superalloys such as Waspaloy.[14] In the sections that follow, the fundamental rules used to design the geometric framework are introduced first. The application of the framework for a strictly-necklace-recrystallization topology and its response for various simple input expressions are then described. Subsequently, the framework is extended to treat particle-stimulated nucleation (PSN) and the development of intragranular recrystallized areas. The challenges involved in quantifying the recrystallization behavior during ingot processing are discussed last.

II. FUNDAMENTAL ASPECTS OF THE GEOMETRIC FRAMEWORK

The definition and number of MSUs in the geometric framework depend on the specific use of the model. To represent a microstructure in which recrystallization occurs, at least two MSUs are required: one for the initial grains and one for the recrystallized grains (which consume the initial grains). However, additional MSUs may be beneficial in obtaining a more refined insight into microstructure evolution. For example, for multi-hit processes such as cogging, at least one other MSU is needed to distinguish between the recrystallized grains that appear during the current deformation step and those that appeared during previous bites, inasmuch as the latter grains are expected to be coarser and have higher dislocation densities than the ones developed during the current hit. In the present work, which aims at providing a general description of this geometric framework, the total number of MSUs is denoted as N_{MSU}. The N_{MSU} can be as low as 2 or 3, as discussed earlier, but it could be 50 or more as well, if the goal were to represent the distribution of strain hardening or grain sizes in the recrystallized structure with great accuracy. Large numbers of MSUs lead to computationally intensive models, however.

A. *Key Definitions*

Each MSU is designated by an index which varies from 1 to N_{MSU}; the numbering convention is that higher indices are assigned to the MSUs that contain more recent grains. Thus, MSU 1 comprises initial grains, while MSUs with higher indices are originally "empty" (*i.e.*, contain no grains). The progressive filling and growth of MSUs of higher indices makes their volume, and thus the recrystallized fraction, increase.

In the isotropic case, the grains (for any MSU i) are assumed to be spheres of diameter D_i. Their volume density is denoted as n_i. The volume enclosed in the individual grain, v_{ei}, and the total volume of MSU i, V_i, are given by the relations

$$v_{ei} = \frac{\pi}{6} D_i^3 \quad [1]$$

$$V_i = n_i v_{ei} = n_i \frac{\pi}{6} D_i^3 \quad [2]$$

(In Eq. [1] and subsequent equations, the subscript e is used specifically for variables the definition of which relies on the surface enveloping each grain in the microstructure.)

The case of anisotropic grains is illustrated in Figures 1 and 2. It involves the definition of three dimensions, D_{xi}, D_{yi}, and D_{zi}, as the principal axes of the ellipsoid that provides the best-fit of the average grain of MSU i; v_{ei} and V_i are then given by

$$v_{ei} = \frac{\pi}{6} D_{xi} D_{yi} D_{zi} \quad [3]$$

$$V_i = n_i v_{ei} = n_i \frac{\pi}{6} D_{xi} D_{yi} D_{zi} \quad [4]$$

The total volume of the microstructure is the sum over i of all MSU volumes given by Eqs. [2] or [4]. The volume conservation issue appears clearly, as all geometric values are connected to this sum. Thus, the variation of any of them has to be compensated by the simultaneous change of some other(s). Practically, MSUs are initialized so that the total volume of the microstructure is equal to the unit volume. As a consequence, once volume conservation is assured during the entire course of microstructure evolution, the values V_i thus represent the volume fractions occupied by each MSU from which the recrystallized fraction(s) can be deduced in a straightforward manner.

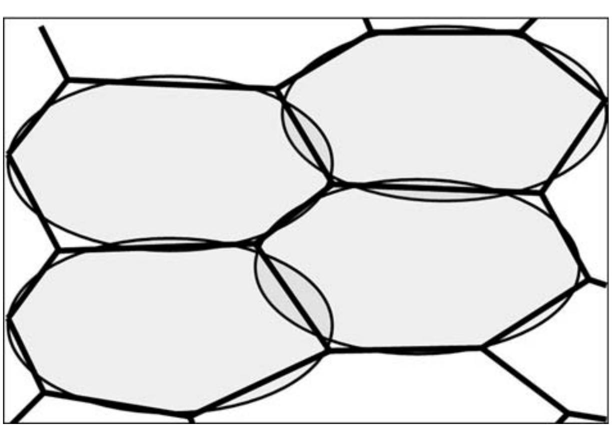

Fig. 1—Section of a schematic grain structure with the corresponding ellipsoidal-grain approximation.

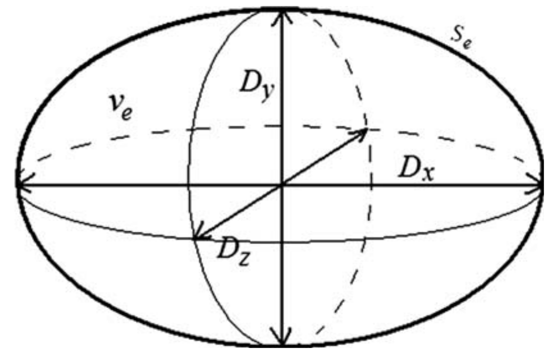

Fig. 2—Geometry of the ellipsoidal-grain approximation.

As a general and fundamental rule, the time rate of change of the volume of a grain, $\dot{v}$, is equal to the volume swept by its migrating grain boundary. Denoting the migration rate (which is normal to the grain boundary) as $\dot{u}$ and the boundary surface area as s, $\dot{v}$ is given by

$$\dot{v} = s\,\dot{u} \quad [5]$$

Because the rate of variation of the grain dimensions is twice the average boundary velocity $\dot{u}_i$ of a grain of MSU i, Eq. [5] is readily verified for isotropic (spherical) grains. In this case, the surface area s_{ei} is given by

$$s_{ei} = \pi D_i^2 \quad [6]$$

and the rate of variation of the volume enclosed by the grain boundary is

$$\dot{v}_{ei} = \pi D_i^2 \frac{\dot{D}_i}{2} = s_{ei} \dot{u}_i \quad [7]$$

For anisotropic grains, the corresponding equation (which reduces to the proper expression in the limit of a spherical grain) is

$$\dot{v}_{ei} = \frac{\pi}{3}\left(D_{xi}D_{yi} + D_{yi}D_{zi} + D_{zi}D_{xi}\right)\,\dot{u}_i \quad [8]$$

which leads to the following for the surface area in order to satisfy Eq. [5]:

$$s_{ei} = \frac{\pi}{3}\left(D_{xi}D_{yi} + D_{yi}D_{zi} + D_{zi}D_{xi}\right) \quad [9]$$

Equation [9] is different from typical expressions for the surface area of an ellipsoid, which can be expressed analytically only for the specific cases of prolate and oblate spheroids. The reason for this discrepancy lies in the fact that when the surface of an ellipsoid migrates under the effect of a pressure, it does not remain ellipsoidal, contrary to the assumption underlying the derivation of Eq. [8] Compared to the exact solutions for oblate and prolate spheroids, however, Eq. [9] provides a result that differs by a maximum of ~30 pct for highly anisotropic shapes. In addition, it has the advantage of straightforward numerical evaluation applicable in all instances, even when all three principal axes are of different lengths in which case the surface area should be evaluated using an elliptic integral. As a consequence, Eq. [9] provides a useful estimate for anisotropic grains the shapes of which approximate, but are not equivalent to, ellipsoids. Furthermore, this approximation is useful in addressing issues related to space filling, contact, and MSU interactions discussed later.

The density of the grain envelopes of MSU i in the whole structure, denoted S_{ei}, is defined as

$$S_{ei} = n_i s_{ei} \qquad [10]$$

In Figure 3, this value for recrystallized grains, S_{e2}, is the sum of all grain envelopes represented in that section by thin lines. In zones such as the dashed square, the grain-boundary density inside MSU i only, S_{vei}, is defined by

$$S_{vei} = \frac{s_{ei}}{2\, v_{ei}} = \frac{1}{D_{xi}} + \frac{1}{D_{yi}} + \frac{1}{D_{zi}} \qquad [11]$$

The factor of 1/2 in Eq. [11] is added to account for the fact that each grain boundary is the combination of two grain envelopes and thus avoids double-counting of the grain boundary between adjacent grains. As it is defined to describe zones for which the grains of only one MSU are represented, it is useful to evaluate interactions between grains of the same MSU.

B. *Principal and Secondary Variables*

Among the interrelated variables mentioned here, several are chosen to be the principal ones to describe the microstructure and to be those from which all others can be deduced. In this regard, volume conservation is a major concern, and model results are obtained *via* numerical integration using Runge–Kutta-type algorithms which involve linear combinations of derivatives evaluated at different steps. Hence, it is preferable that all derivatives be written in terms of volumes and not involve other variables such as grain size *per se*. By this means, the linear combination of a set of volume-conserving volumetric time rates of change results in a new set that is naturally volume conserving as well.

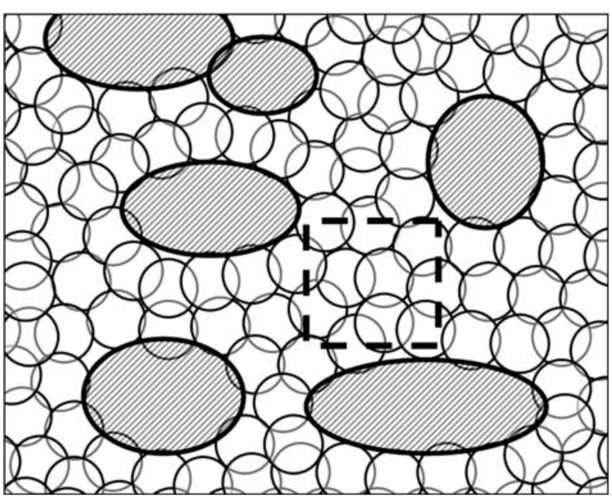

Fig. 3—Schematic cross section of a two-MSU microstructure. Initial grains (MSU 1) are cross-hatched, and their envelopes are thick lines. Recrystallized grains (MSU 2) are white and their envelopes are thin lines; surface areas s_{e1} and S_{e1} are represented by thick lines; s_{e2} and S_{e2} are represented by thin lines. The total envelope surface area S_{etotal} ($= S_{e1} + S_{e2}$) counts each grain boundary twice. In the dashed square, only interactions between grains of MSU 2 occur; they are treated using the grain-boundary density $S_{ve2} = 0.5\ s_{e2}/v_{e2}$.

For the case of the necklace-only topology, MSUs are primarily defined by their volume V_i, the volume of their grains v_{ei}, and two anisotropy parameters α_{xyi} and α_{xzi}, only the derivatives of which have to be determined for subsequent integration. The parameters α_{xyi} and α_{xzi} are defined as the ratios of D_{yi} to D_{xi} and D_{zi} to D_{xi}, respectively. For each MSU i, these four principal variables are enough to deduce the secondary variables which include the density of grains n_i (Eq. [2]) and an additional intermediate, equivalent grain size D_{eqi}:

$$D_{eqi} = \left(\frac{6\, v_{ei}}{\pi}\right)^{1/3} \qquad [12]$$

All three grain dimensions are derived from the equations

$$D_{xi} = \frac{D_{eqi}}{\left(\alpha_{xyi}\alpha_{xzi}\right)^{1/3}} \qquad [13]$$

$$D_{yi} = D_{xi}\, \alpha_{xy\,i} \qquad [14]$$

$$D_{zi} = D_{xi}\, \alpha_{xz\,i} \qquad [15]$$

The surface quantities s_{ei}, S_{ei}, and S_{vei} are obtained from Eqs. [6], [9], [10], and [11].

For isotropic (spherical) grains, the anisotropy parameters α_{xy} and α_{xz} are equal to unity. Thus, D_i is equal to D_{eqi} and does not require further treatment during integration. For anisotropic grains, once the rate of variation of the volume enclosed within the grain is known, the variation rate of the grain dimensions can be obtained by rearranging Eq. [5] and applying the assumption that the variation rates for all three grain dimensions are the same, *i.e.*, twice the average grain-boundary velocity:

$$\dot{D}_i = \dot{D}_{xi} = \dot{D}_{yi} = \dot{D}_{zi} = 2\frac{\dot{v}_{ei}}{s_{ei}} \qquad [16]$$

Then, the variation rates of the two anisotropy parameters can be derived as well; *i.e.*,

$$\dot{\alpha}_{xy\,i} = \frac{\dot{D}_{yi}}{D_{xi}} - \frac{D_{yi}}{D_{xi}}\frac{\dot{D}_{xi}}{D_{xi}} = \frac{\dot{D}_i}{D_{xi}}\left(1 - \alpha_{xy\,i}\right) \qquad [17]$$

$$\dot{\alpha}_{xz\,i} = \frac{\dot{D}_{zi}}{D_{xi}} - \frac{D_{zi}}{D_{xi}}\frac{\dot{D}_{xi}}{D_{xi}} = \frac{\dot{D}_i}{D_{xi}}\left(1 - \alpha_{xz\,i}\right) \qquad [18]$$

For the necklace-only topology, only the rates of variation of the volume of the MSUs and their grains, $\dot{V}_i$ and $\dot{v}_{ei}$, respectively, are thus necessary to calculate the geometric evolution of the whole microstructure.

III. GEOMETRIC FRAMEWORK FOR NECKLACE TECHNOLOGY

In this section, the dependence of $\dot{v}_{ei}$ and $\dot{V}_i$ on the grain-boundary velocities $\dot{u}_{ij}$ between grains of each pair i-j of MSUs and the nucleation rates $\dot{n}_i^{\text{nucl}}$ generated by each grain of MSU i are summarized. The nucleus volume, v^{nucl}, is assumed to be known and to be the same for all MSUs.

The geometric description for the volume variations due to the generation of nuclei is very simple, but becomes increasingly complex when quantifying volume variations related to the interactions between different MSUs, the interactions between grains of the same MSU, and the incorporation of nuclei into the MSU of highest index. The volume variations due to nuclei generation are given by

$$\dot{v}_{ei}^{\text{nucl}-} = \dot{n}_i^{\text{nucl}} v^{\text{nucl}} \quad [19]$$

$$\dot{V}_i^{\text{nucl}-} = n_i \dot{v}_{ei}^{\text{nucl}-} \quad [20]$$

The volume variations associated with the other phenomena are summarized in the following sections.

A. *Interactions between Grains of Different MSUs*

In order to calculate the interaction of the grains of MSU i with those in another MSU j, it is necessary to decompose the volume variation of their grains into the sum of the volume variations due to interactions with all MSUs:

$$\dot{v}_{ei}^{\text{migr}} = \sum_{j=1}^{N_{\text{MSU}}} \dot{v}_{ij}^{\text{migr}} = \sum_{j=1}^{N_{\text{MSU}}} s_{ij}\,\dot{u}_{ij} \quad [21]$$

Here, $\dot{v}_{ij}^{\text{migr}}$ is the volume variation of a grain i due to its interaction with grains of MSU j, s_{ij} represents the statistical probability of the surface of contact of a grain of MSU i with the grains of MSU j, and $\dot{u}_{ij}$ is the migration rate of a grain i–grain j boundary. Assuming a uniform probability of contact with grains of any MSU j among all the grains of the microstructure, s_{ij} is given by

$$s_{ij} = q_j s_{ei} \quad [22]$$

$$q_j = \frac{n_j s_{ej}}{\sum_{k=1}^{N_{\text{MSU}}} n_k s_{ek}} = \frac{S_{ej}}{S_{\text{total}}} \quad [23]$$

in which q_j is the probability that a grain-envelope surface element is in contact with the envelope of a grain of MSU j (and thus defines a grain boundary with that grain), when chosen randomly among all grain envelopes of the microstructure. The S_{total} is the total grain-envelope surface density present in the microstructure, *viz*., twice the total grain-boundary surface density (Figure 3). The probability q_j is thus a specific fraction of the envelope/boundary of a grain of MSU i. This choice is consistent with previous approaches.[5,12,13]

Figure 3 illustrates the simple case of a two-MSU microstructure. Because recrystallized grains (MSU 2) are fine and numerous, the probability/fraction $q_2 = S_{e2}/S_{\text{total}}$ has reached a value close to 1.0 as recrystallization progressed. In other words, the probability that a grain-envelope element is in contact with the grain envelope of a recrystallized grain is very high, and conversely, the probability of interaction with an initial grain is very low. Initial grains thus interact mostly with recrystallized grains but rarely with other initial grains, a behavior typical of a necklace topology.

The volume variation of a grain of MSU i due to its interaction with grains of MSU j is then given by

$$\dot{v}_{ij}^{\text{migr}} = s_{ij}\,\dot{u}_{ij} = s_{ei}\,q_j\,\dot{u}_{ij} = s_{ei}\frac{S_{ej}}{S_{\text{total}}}\,\dot{u}_{ij} \quad [24]$$

and the volume variation of the whole MSU i due to its interaction with MSU j is

$$\dot{V}_{ij}^{\text{migr}} = n_i s_{ij}\,\dot{u}_{ij} = n_i s_{ei}\,q_j\,\dot{u}_{ij} = S_{ei}\,q_j\,\dot{u}_{ij} \quad [25]$$

It can be readily shown that volume conservation is ensured; *i.e*.,

$$\dot{V}_{ij}^{\text{migr}} = n_i s_{ei}\frac{n_j s_{ej}}{S_{\text{total}}}\,\dot{u}_{ij} = -n_j s_{ji}\dot{u}_{ji} = -\dot{V}_{ji}^{\text{migr}} \quad [26]$$

B. *Interactions between Grains of the Same MSU*

Equations [24] and [25] are useful for interactions between grains of different MSUs. However, they are not applicable to the interaction among grains of their own MSU, because in-MSU interactions must leave the volume of the MSU unchanged while the migration of the boundaries that separate the grains of the MSU occurs. To deal with this case, analysis is focused on zones in which the grains of only one MSU are present, such as inside the necklace, for the case of a two-MSU microstructure (*e.g*., the dashed square of Figure 3). This case thus involves the use of the grain-boundary density S_{vei} defined by Eq. [11]). This relation is differentiated. Assuming an equal variation rate for each of the principal dimensions of the grains (as is assumed in Eq. [16]), the following is obtained:

$$\dot{S}_{vei} = -\dot{D}_i\left(\frac{1}{D_{xi}^2} + \frac{1}{D_{yi}^2} + \frac{1}{D_{zi}^2}\right) \quad [27]$$

Grain growth is related to the boundary density that disappears as a result of boundary migration. In other words, some moving boundaries meet each other, and only one boundary remains where there were two. However, at the scale of the whole microstructure, not all grain envelopes of MSU i are affected by this phenomenon, inasmuch as some are involved in interactions with grains of other MSUs. The contribution of in-MSU interactions is the balance after subtracting interactions with other MSUs, *i.e*., q_i. As a result, the volume swept by grain boundaries of MSU i, specifically inside zones where only grains of MSU i are present, is given by

$$\dot{V}_i^{\text{swept}} = S_{vei}\, q_i\, \dot{u}_{ii} \qquad [28]$$

Equation [28] is the equivalent for the in-MSU interactions of Eq. [25]. It gives the volume variation of MSU i related to the interactions between its own grains, which results actually in a null-volume variation, because it is taken over itself. Its only effect is to make the grain boundaries contained by this swept volume disappear:

$$\dot{S}_{vei}^{\text{migr}-} = S_{vei}\, \dot{V}_i^{\text{swept}} = \left(\frac{1}{D_{xi}} + \frac{1}{D_{yi}} + \frac{1}{D_{zi}}\right)^2 q_i\, \dot{u}_{ii} \qquad [29]$$

Combining Eqs. [27] and [29], the contribution ($\dot{D}_{ii}^{\text{migr}}$) of boundary migration within an MSU to the grain-size variation of this MSU is obtained; *i.e.*,

$$\dot{D}_{ii}^{\text{migr}} = \frac{\left(1 + \frac{1}{\alpha_{xy\,i}} + \frac{1}{\alpha_{xz\,i}}\right)^2}{1 + \frac{1}{\alpha_{xy\,i}^2} + \frac{1}{\alpha_{xz\,i}^2}}\, q_i\, \dot{u}_{ii} \qquad [30]$$

For isotropic grains, Eq. [30] becomes

$$\dot{D}_{ii}^{\text{migr}} = 3\, q_i\, \dot{u}_{ii} \qquad [31]$$

In Eq. [31], the factor of 3 (instead of 2) may seem surprising. It is explained by the connection between grain-boundary velocity and the apparent grain-size variation of an MSU in which some grains grow and, most important, others disappear; *i.e.*, there is not a constant population. In such a case, MSU i is an aggregate of grains that would exhibit in reality a variety of sizes or stored energies. Depending on the purpose of the modeling, this could be an overly simplified representation. However, the geometric framework should not be modified depending on the context in which it is used. Hence, in practice, this approximation is either activated or prevented through the definition of the input of the framework. Specifically, the values for the velocity of the boundaries between the grains of a given MSU will be either zero or will assume some positive value (based on the dislocation density or grain-boundary curvature of MSU i and described by the driving force equations), if this feature is to be used. Lacking physical meaning, negative values are not possible.

From the rate of change of the grain size, the rate of change of the grain volume is readily derived as

$$\frac{\dot{v}_{ii}^{\text{migr}+}}{v_{ei}} = \frac{\dot{D}_{ii}^{\text{migr}}\left(D_{xi}D_{yi} + D_{yi}D_{zi} + D_{zi}D_{xi}\right)}{D_{xi}D_{yi}D_{zi}} = S_{vei}\, \dot{D}_{ii}^{\text{migr}} \qquad [32]$$

C. *Incorporation of Nuclei by the MSU of Highest Index*

The incorporation of nuclei generated by the structure into the MSU of highest index (N_{MSU}) implies a volume increase of this MSU, and one can expect a refinement of its grain size. The rate of change of the volume of the MSU is the product of the total number of nuclei generated per unit time, $\dot{n}_{\text{total}}^{\text{nucl}}$, and the volume of the individual nucleus; *i.e.*,

$$\dot{V}_{N_{\text{MSU}}}^{\text{nucl}+} = \sum_{k=1}^{N_{\text{MSU}}} \dot{V}_i^{\text{nucl}-} = \dot{n}_{\text{total}}^{\text{nucl}}\, v^{\text{nucl}} \qquad [33]$$

The differentiation of Eq. [2] for the case of the nuclei-receiver MSU (index N_{MSU}) yields

$$\dot{V}_{N_{\text{MSU}}}^{\text{nucl}+} = \dot{n}_{\text{total}}^{\text{nucl}}\, v_{e\,N_{\text{MSU}}} + n_{N_{\text{MSU}}}\, \dot{v}_{e\,N_{\text{MSU}}}^{\text{nucl}} \qquad [34]$$

The combination of Eqs. [33] and [34] gives the rate of change of the volume of grains of the nuclei-receiver MSU as

$$\frac{\dot{v}_{e\,N_{\text{MSU}}}^{\text{nucl}}}{v_{e\,N_{\text{MSU}}}} = -\,\frac{\dot{n}_{\text{total}}^{\text{nucl}}}{n_{N_{\text{MSU}}}}\left(1 - \frac{v^{\text{nucl}}}{v_{e\,N_{\text{MSU}}}}\right) \qquad [35]$$

As expected, the incorporation of nuclei induces a refinement of the grains of the MSU, inasmuch as the size of the nuclei is smaller than that of the grains of the MSU.

If the structure is completely recrystallized and, hence, all grains are in the MSU of highest index, interactions still occur and all nuclei are produced only within this MSU. The migration of the boundaries within the MSU produces a grain-size increase (Eq. [32]). Further nucleation tends to reduce its grain size (Eq. [35]). As a consequence, the geometric framework enables the model to function and reach a dynamic steady state even when only one MSU remains.

The simple addition or subtraction of the various rates of volume change enables the framework to incorporate inputs composed of nucleation rates and grain-boundary velocities into the volume variation rates of each MSU and of its grains, which can be readily integrated over time.

D. *Tests of the Framework Using Simple Input*

The geometric framework was encoded using C + +. The core program comprised a generic MSU class the data sets of which consist of the primary geometric variables of MSUs. Various member functions were used to evaluate the secondary variables needed by the framework (grain dimensions, grain-boundary surfaces, *etc.*) The mesostructure was not implemented as a class but rather as a template that depends on a parameter class. It manages a flexible array of objects of its parameter class, which are expected to be MSUs when the template is instantiated. To calculate the geometric evolution in response to the inputs (the rates of nucleation and grain-boundary velocity), the mesostructure template relies on the values returned by the member functions of the objects of its array. These member functions have names and formats that are basically those of the generic geometric MSU class. This means that when it is instantiated, the mesostructure template must be built against a parameter class that features at least the member functions of the generic geometric MSU class.

In practice, two steps are required to connect the geometric framework with mechanisms and driving forces to execute a complete mesoscale model. First, the generic geometric MSU is derived into a class that contains additional data sets (such as Taylor factor, dislocation density, *etc.*) and new member functions as needed. Second, the mesostructure template is instantiated against this new MSU class. This instantiation results in a mesostructure class in which all geometry evolution is managed transparently. Only the mechanisms of evolution, driving forces, and energy storage remain as the main focus for the model development and adjustment. For the simple tests presented in this article, the MSU derivation was concise, because only constant rates were used without explicit relation to any actual driving forces. However, for a mesoscale model applicable to an actual material, additional variables and a set of driving force equations, such as those briefly discussed in Reference 5, are needed.

The capabilities of the geometric framework for the necklace-only topology were evaluated using several hypothetical cases. These were based on constant rates of nucleation and grain-boundary migration varying by orders of magnitude. Although hypothetical in nature, the values used here were suggested by observations for Waspaloy within the temperature range of 1000 to 1120 °C and for strain rates between 0.01 and 1 s^{-1}.[4]

The first test of the framework was performed on a single MSU (which would apply if the microstructure were fully recrystallized) in order to evaluate the dynamic equilibrium provided by Eqs. [32] and [35]. A constant boundary velocity of 20 μm per unit strain and a nucleation rate of 1 nucleus per 10 μm^2 of grain boundary per unit strain were assumed for various initial grain sizes (Figure 4). The same steady-state grain size, indicative of a balance between nucleation and grain growth, was reached for all initial grain sizes tested.

A case comprising two MSUs was also analyzed to establish the influence of the competition between nucleation and grain-boundary migration on recrystallization. The first MSU was initialized with a 100-μm grain size. The second MSU, which incorporated the nuclei, was initially empty; its volume defined the recrystallized fraction of the structure. Various nucleation and migration rates were chosen to reach a recrystallized fraction of 50 pct at a deformation of approximately 0.5 for each of the chosen parameter combinations (Figure 5). The balance between nucleation and migration indirectly mirrors the influence of the strain rate on the recrystallization kinetics. At high strain rates, there is relatively little time for boundary migration and, thus, nucleation is responsible for most of the recrystallization. Conversely, most recrystallization at low strain rates occurs due to grain-boundary migration. An Avrami analysis of the obtained recrystallization kinetics revealed that an increase in the strain rate was accompanied by a decrease in the Avrami exponent (Figure 6).

The metadynamic evolution of recrystallization was tested by considering a zero nucleation rate after deformation and either a constant or a decreasing grain-boundary migration rate (Figure 7). The following expression quantified the influence of metadynamic recovery such as would give rise to a decreasing grain-boundary velocity:

$$\dot{u}_{\text{metadynamic}} = \dot{u}_{\text{dynamic}} \left(1 - \exp\left(\frac{t}{t_{\text{characteristic}}}\right)\right) \qquad [36]$$

Very strong metadynamic recovery was found to inhibit the completion of recrystallization, as shown in Figure 7.

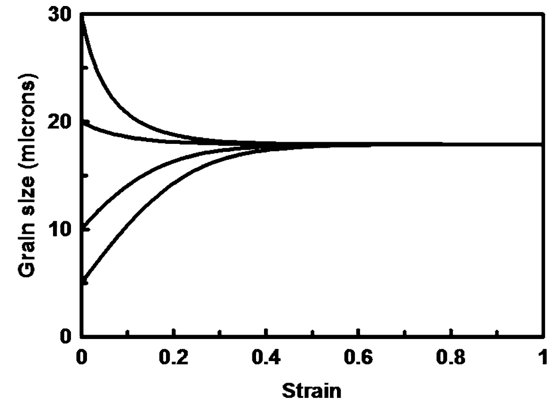

Fig. 4—Model results for the evolution of grain size during a single-MSU dynamic simulation. The nucleation rate was 1 nucleus per 10 μm^2 of grain boundary and per unit strain, the grain-boundary velocity was 20 μm per unit strain, and $v^{\text{nucl}} = 100\ \mu m^3$.

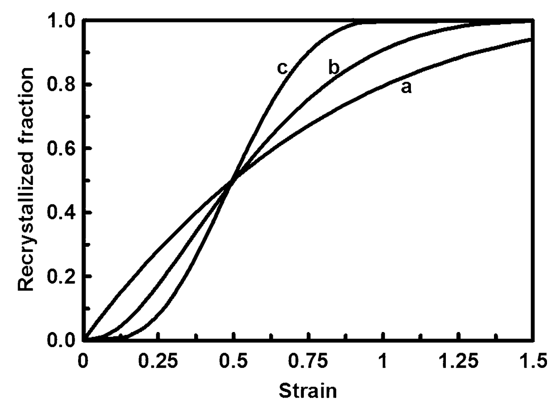

Fig. 5—Model results for recrystallized fraction during a two-MSU simulation of dynamic recrystallization. Nucleation rates were 1 nucleus per (*a*) 5 μm^2, (*b*) 100 μm^2, and (*c*) 5000 μm^2 of boundary and per unit strain; grain-boundary velocities were (*a*) 0 μm, (*b*) 42 μm, and (*c*) 105 μm per unit strain. $v^{\text{nucl}} = 100\ \mu m^3$.

IV. GEOMETRIC FRAMEWORK FOR NECKLACE-AND-INTRAGRANULAR TOPOLOGY

The approach presented in Section III is valid as long as the various grains only interact at their envelope surfaces. However, PSN of recrystallization within

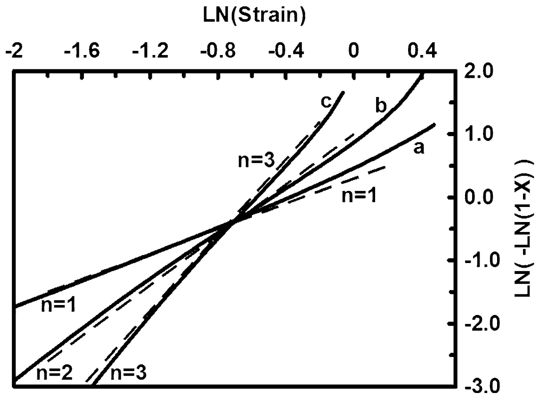

Fig. 6—Avrami analysis of the recrystallized-fraction curves in Fig. 5. X denotes the recrystallized fraction; the slope of the curves is the Avrami exponent n.

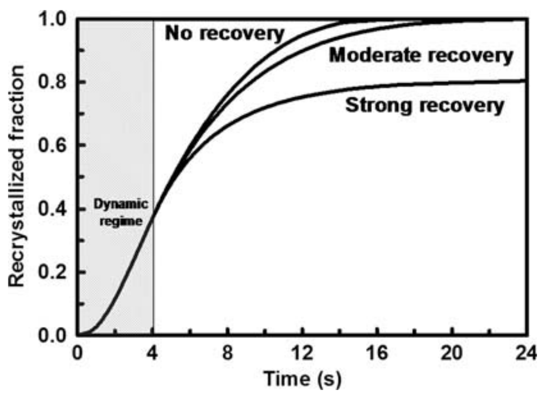

Fig. 7—Model predictions for the recrystallized fraction in two-MSU simulations of dynamic and metadynamic recrystallization. The nucleation rate was 1 nucleus per 100 μm^2 of grain boundary and per unit strain; the grain-boundary velocity was 42 μm per unit strain (equivalent to 4.2 μm/s to simulate a 0.1 s^{-1} strain rate during the dynamic regime). In Eq. [36], tested $t_{\text{characteristic}}$ values were 5 s (strong recovery), 20 s (moderate recovery), or an infinite time (no recovery). $v^{\text{nucl}} = 100\ \mu m^3$.

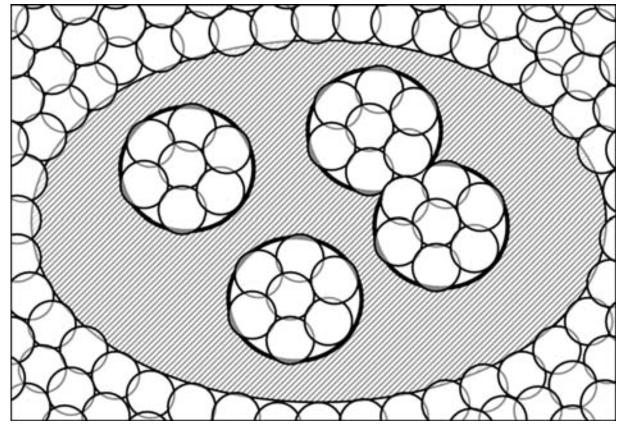

Fig. 8—Cross section of a two-MSU microstructure representing intragranular recrystallization within an ingot grain. The initial ingot grain (MSU 1) is cross-hatched, and recrystallized grains (MSU 2) are white. The thick lines delimit intragranular recrystallized zones, which would resemble bubbles in three dimensions; these thick lines are the location of a new kind of grain interaction not described by the equations for the necklace-only topology. s_{b1} and S_{b1} are thus represented by these thick lines; s_{e1}, S_{e1}, s_{e2}, and S_{e2} are represented by the thin lines.

grains has been observed during the breakdown of coarse-grain superalloy ingot materials such as Waspaloy.[14] In such cases, the previous assumptions are not valid, inasmuch as the contact between grains of different MSUs does not lie solely along their envelopes. Rather, interfaces develop within the initial matrix due to the generation of recrystallized grains that nucleate (and subsequently) grow inside the initial grain(s), as illustrated in Figure 8. Therefore, the preceding equations have to be modified to account for a topology comprising both necklace and intragranular features.

Not all grains are subjected to intragranular nucleation. In practice, only relatively large initial grains exhibit such a topology. For fine initial grains, nucleation can also be enhanced by second-phase particles, but the intragranular recrystallized zones in these instances merge rapidly with the developing necklaces; as such, their intrinsic geometric influence can be neglected. Consequently, the intragranular topology is only activated for the first N_{bt} MSUs of the structure when they are initialized for the case of coarse ingot grains. N_{bt} is strictly less than N_{MSU}. It means that the current recrystallized grains, stored in the MSU of highest index, do not represent sites for subsequent intragranular nucleation. In addition, in order to limit complexity, it is assumed that the only MSUs with grains that can fill the intragranular areas of others are those with indices that are greater than N_{bt}. In other words, intragranular recrystallized zones cannot be generated inside the intragranular zones of other MSUs through secondary PSN generation. This is not really a restriction, because the MSUs with an index strictly between N_{bt} and N_{MSU} will contain grains that recrystallized during the previous steps or hits of the simulated process. One can thus expect that they will not be coarse enough to develop the intragranular topology.

At the onset of PSN, intragranular zones contain only grains that nucleated on PSN particles. However, once recrystallized grains surround a particle, second and further generations of nuclei are generated in a manner formally similar to that of the necklace topology; *i.e.*, new nucleation sites for nuclei are provided at the new grain boundaries. Intragranular zones then spread out over the matrix, and, if the recrystallized grains they contain could be taken out, these zones would resemble growing bubbles. Therefore, the index "b" is used, in lieu of "e" for envelope, for variables that describe intragranular-related properties such as volume fraction, size, and surface area.

A. *Principal and Secondary Variables*

In order to take into account the intragranular zones, a new volume-related degree of freedom must first be defined. This volume has to allow space for the development of intragranular zones. Thus, henceforth, v_{ei} in Eq. [3] represents the total volume enclosed within the grain envelope of MSU i, but not necessarily the volume of material that belongs to the grain itself. The latter quantity is denoted as v_i, and obviously it is less than or equal to v_{ei}. For instance, in Figure 8, the volume enclosed in the ingot grain envelope, v_{e1}, contains recrystallized zones. Thus, the volume of material that actually belongs to the ingot grain (denoted by the cross-hatching) is $v_1 < v_{e1}$. The difference between the two quantities is simply the recrystallized volume occupied by zones that develop around PSN particles. Therefore, v_i is the fifth principal variable needed for the geometric description of MSU i. It enables the description of intragranular recrystallized zones in a realistic and physically admissible way by defining an additional set of secondary variables, as summarized here.

First, the fraction X_{bi} of intragranular recrystallized zones contained by a grain of MSU i, and by extension in the whole MSU i, is defined as

$$X_{bi} = 1 - \frac{v_i}{v_{ei}} = 1 - \frac{V_i}{n_i\, v_{ei}} \qquad [37]$$

A new material parameter is needed for an accurate definition of the microstructure: the density of sites of volume nucleation, denoted n_{PSN}. Typically, n_{PSN} will be equal to the density of second-phase particles that induce a large enough local spread of crystallographic orientations to activate nucleation.[15] The average volume $v_{\text{PSN}\ i}$ of a recrystallized zone that develops around a PSN site in the grains of MSU i can then be calculated. The volume of intragranular zones in a grain of MSU i is

$$\left(n_{\text{PSN}} v_{ei}\right)\ v_{\text{PSN}\,i} = v_{ei} - v_i \qquad [38]$$

Combining this relation with Eq. [37] leads to the desired relation

$$v_{\text{PSN}\,i} = \frac{X_{bi}}{n_{\text{PSN}}} \qquad [39]$$

Because the spatial distribution of particles may not be random, some clusters of PSN sites may behave as a single intragranular zone as $v_{\text{PSN}\ i}$ increases. A new function $N_{\text{cluster}}(v_{\text{PSN}\ i})$, which quantifies the number of clustered particles depending on $v_{\text{PSN}\ i}$, is then needed to evaluate the actual density of intragranular zones n_{bi} as $v_{PSN\ i}$ increases

$$n_{bi} = \frac{n_{\text{PSN}}}{N_{\text{cluster}}\left(v_{\text{PSN}\,i}\right)} \qquad [40]$$

When $v_{\text{PSN}\ i}$ is equal to zero, N_{cluster} assumes its minimum value of 1. In the case when no clustering occurs because the particles are randomly distributed, this function is also equal to unity.

The diameter D_{bi} of intragranular recrystallized zones that develop in the grains of MSU i is then given by

$$D_{bi} = \left(\frac{6X_{bi}}{\pi\, n_{bi}}\right)^{1/3} \qquad [41]$$

1. *Surface of interaction between the matrix of a grain and the intragranular recrystallized zones it contains*

In order to evaluate grain-interaction probabilities, the surface area between intragranular zones and the matrix of an initial grain must be calculated. If the assumption is made that intragranular zones are randomly distributed, the volume consumed by the growth of an intragranular zone is distributed between its surrounding matrix and its neighboring intragranular zones, with proportions equal to (on average) their respective volume fractions. In other words, due to the impingement between neighboring intragranular zones only a fraction 1-X_{bi} of the surface of intragranular zones is actually involved in interactions with the matrix of their initial grain. The surface area s_{bi} of interaction between the intragranular zones of a grain of MSU i and its matrix is then

$$s_{bi} = (1 - X_{bi})\ \left(v_{ei}\, n_{bi}\right)\ \pi\, D_{bi}^2 = v_i\, n_{bi}\, \pi\, D_{bi}^2 \qquad [42]$$

and the density of the surface of contact between the matrix and intragranular zones provided by the entire MSU i for the whole microstructure is

$$S_{bi} = n_i\, s_{bi} = V_i\, n_{bi}\ \pi\, D_{bi}^2 \qquad [43]$$

The interaction surface between intragranular zones and their surrounding grain makes it possible to investigate the various types of grain interactions and their respective contributions to recrystallization.

2. *Total grain-boundary densities*

As discussed with respect to Eq. [23], the calculation of the probability of contact of grains in one MSU (*i*) with those of another MSU (*j*) requires the evaluation of the fraction of the grain-interface density of MSU j relative to the total grain-interface density involved in these interactions. In the previous case of necklace-only topology, these grain interfaces were always the grain envelopes. However, when it comes to account for intragranular recrystallization, the situation is more complex, because two different types of grain interactions may occur.

The first and more common interaction is that investigated previously, *i.e.*, "envelope-envelope" interactions; the grain boundaries where such interaction takes place are defined by the contact of two grain envelopes.

The other interaction involves the contact of the envelope of a recrystallized grain with the initial grain along an intragranular interface (represented by thick lines in Figure 8 forming the so-called bubble referred to previously). By analogy with the previous envelope-envelope interactions, this other interaction is thus called a "bubble-envelope" interaction; the grain boundaries where such interactions take place are defined by the contact of a grain envelope with an intragranular bubble.

As a consequence, it is necessary to distinguish two total interaction surfaces denoted as $S_{e\,\text{total}}$ and $S_{b\,\text{total}}$, respectively. The latter is readily calculated as

$$S_{b\,\text{total}} = \sum_{k=1}^{N_{bt}} n_k s_{bk} = \sum_{k=1}^{N_{bt}} S_{bk} \qquad [44]$$

The total surface density of grain boundaries involved in envelope-envelope interactions,$S_{e\text{total}}$, is the total density of grain envelopes minus the part involved in bubble-envelope contact, which is $S_{b\,\text{total}}$, because all bubbles are in contact with the envelopes of some recrystallized grains (the impingement of intragranular zones is already accounted for in Eq. [42]):

$$S_{e\,\text{total}} = \sum_{k=1}^{N_{\text{MSU}}} S_{ek} - S_{b\,\text{total}} = S_{\text{total}} - S_{b\,\text{total}} \qquad [45]$$

Knowing these two total-boundary densities, it is possible to normalize grain-interaction probabilities.

3. *Partitioning of grain-interface areas between the two types of interaction*

A distinction is needed for individual grain-interface areas just as it was for total-boundary densities. For the grains of each MSU i, parameters q_{eei} and q_{bei} are defined as the fraction of their envelope in contact with the envelope of other grains or with the surrounding matrix, respectively, when they belong to an MSU some grains of which fill intragranular zones of low-index initial MSUs. For i less than or equal to N_{bt}, q_{bei} is zero inasmuch as these grains (initial grains) are not allowed to be in the intragranular recrystallized zones of other grains; in this case, q_{eei} is equal to 1. For other MSUs (i $> N_{bt}$), the assumption is made that each of them contributes to $S_{b\,\text{total}}$ proportionally to its own surface:

$$S_{ebc\,\text{total}} = \sum_{k=N_{bt}+1}^{N_{\text{MSU}}} S_{ek} \qquad [46]$$

$$q_{bei}\, n_i s_{ei} = \frac{S_{ei}}{S_{ebc\,\text{total}}} S_{b\,\text{total}} \qquad [47]$$

Equation [47] involves an intermediate parameter, $S_{ebc\,\text{total}}$, defined as the total density of the envelopes of the grains that can have nucleated in intragranular areas, and thus potentially contribute to $S_{b\,\text{total}}$, *viz.*, those with an MSU index strictly greater than N_{bt}. It can be simplified:

$$q_{bei} = \frac{S_{b\,\text{total}}}{S_{ebc\,\text{total}}} \qquad [48]$$

Furthermore,

$$q_{eei} = 1 - q_{bei} \qquad [49]$$

Equation [48] shows that all MSUs with envelopes that contribute to the surface of intragranular interfaces have the same partitioning between the two kinds of interactions.

4. *Interaction probabilities*

It is now possible to evaluate the probability of interaction for each pair of MSUs. The probability for a surface element of a grain boundary of MSU i to be an interface with a grain of MSU j (*i.e.*, the relations corresponding to Eqs. [23] and [24] but for the case of a necklace-and-intragranular topology) is now described. Two new parameters, q_{eeij} and q_{beij}, are defined as the probabilities of contact involving envelope-envelope and bubble-envelope interactions, respectively.

The first probability, q_{eeij}, is the fraction of the envelope of a grain i that is in contact with the envelope of another grain (q_{eei}), multiplied by the fraction (q_{eej}) of the density of the grain envelopes of MSU j (S_{ej}) which is also in contact with a grain envelope, among all boundaries defined by an envelope–envelope contact ($S_{e\,\text{total}}$):

$$q_{eeij} = q_{eei} \frac{q_{eej} S_{ej}}{S_{e\,\text{total}}} \qquad [50]$$

Basically, the role of the product $q_{eei}\, q_{eej}$ in Eq. [50] is to restrict both the grain i and the MSU j to envelope-only aspects, resulting in the same fraction as the one given by Eq. [23], the expression for the probability of interaction for the envelope-only/necklace-only topology. Equation [50] is thus the generalization of Eq. [23] to the necklace-and-intragranular topology, and consistency is ensured because both q_{eei} and q_{eej} are equal to unity when there are no intragranular recrystallized zones. Conversely, when intragranular recrystallized zones develop, the behavior of the complementary parts $1-q_{eei}$ and $1-q_{eej}$, *viz.*, q_{bei} and q_{bej}, must be taken into account.

The expression for q_{beij} depends on the value of i. If i is less than or equal to N_{bt}, then MSU i consists of ingot grains in which PSN can occur. Conversely, MSU j is composed of recrystallized grains, some of which are located in the intragranular zones of MSU i. Then q_{beij} is the fraction (q_{bej}) of the grain boundaries of MSU j (S_{ej}) in contact with intragranular interfaces (such as those of the grains of MSU i) relative to all interfaces between the intragranular recrystallized grains and the surrounding matrix ($S_{b\,\text{total}}$):

$$q_{beij} = \frac{q_{bej} S_{ej}}{S_{b\,\text{total}}} \qquad [51]$$

Conversely, if i is strictly greater than N_{bt}, MSU i is composed of recrystallized grains that can be inside the intragranular areas of MSU j. Then q_{beij} is the fraction (q_{bei}) of the grain envelopes of MSU i in contact with intragranular interfaces (such as those of the grains of MSU j), multiplied by the surface of intragranular interfaces present inside the grains of MSU j (S_{bj}), among all intragranular interfaces ($S_{b\,\text{total}}$):

$$q_{beij} = q_{bei} \frac{S_{bj}}{S_{b\,\text{total}}} \qquad [52]$$

Using these probabilities, it is possible to evaluate the time rates of change of MSUs and their grains in the various possible situations.

B. *Volume Variations of MSUs and Their Grains*

The rate of change of the volume of MSUs and of their grains depends on the interaction type, *i.e.*, both whether it is an envelope–envelope interaction or a bubble–envelope one and whether it is an interaction between grains of different MSUs or of the same MSU.

1. *Interactions between grains of different MSUs*

The interactions between different MSUs are the most numerous to deal with. The first, concerning interactions that involve only grain envelopes, affect v_{ei} and v_i with the same magnitude:

$$\dot{v}_{e\,ij}^{\mathrm{migr}} = \dot{v}_{ij}^{\mathrm{migr}} = q_{eeij}\, s_{ei}\, \dot{u}_{ij} \qquad [53]$$

$$\dot{V}_{ij}^{\mathrm{migr}} = n_i \dot{v}_{ij}^{\mathrm{migr}} \qquad [54]$$

The second, which are interactions between intragranular recrystallized grains and the ingot-grain matrix that surrounds them, consists of two symmetrical behaviors, depending on the location of grains. If we assume that i is less than or equal to N_{bt} and, conversely, that j is greater than N_{bt}, then the grains of MSU i contain some recrystallized j grains in their intragranular zones. For the former grains, there will only be a volume variation of the MSU and of its grains, but not of the volume delimited by their envelope because the latter is not involved:

$$\dot{v}_{e\,ij}^{\mathrm{migr}} = 0 \qquad [55]$$

$$\dot{v}_{ij}^{\mathrm{migr}} = q_{beij}\, s_{bi}\, \dot{u}_{ij} \qquad [56]$$

$$\dot{V}_{ij}^{\mathrm{migr}} = n_i \dot{v}_{ij}^{\mathrm{migr}} \qquad [57]$$

Conversely, for the j grains, all parameters will change, because their envelopes migrate through interaction with the intragranular interfaces of the first kind:

$$\dot{v}_{e\,ji}^{\mathrm{migr}} = \dot{v}_{ji}^{\mathrm{migr}} = q_{beji}\, s_{ej}\, \dot{u}_{ji} \qquad [58]$$

$$\dot{V}_{ji}^{\mathrm{migr}} = n_j \dot{v}_{ji}^{\mathrm{migr}} \qquad [59]$$

An examination of Eqs. [57] and [59] shows that all interactions conserve volume as required, despite the more complex scheme.

2. *Interactions between grains of the same MSU*

Interactions between grains of the same MSU involve envelope–envelope interactions only. They produce no change in the total volume of the MSU, but generate an increase in the volume and size of grains. Hence, the equations are similar to those obtained for the necklace-only topology. The intermediate rate of change of the grain dimensions is almost unchanged:

$$\dot{D}_{ii}^{\mathrm{migr}} = \frac{\left(1 + \frac{1}{\alpha_{xy\,i}} + \frac{1}{\alpha_{xz\,i}}\right)^2}{1 + \frac{1}{\alpha_{xy\,i}^2} + \frac{1}{\alpha_{xz\,i}^2}}\, q_{eeii}\, \dot{u}_{ii} \qquad [60]$$

Converted to the corresponding volume variations, the following expressions are obtained:

$$\frac{\dot{v}_{e\,ii}^{\mathrm{migr}\,+}}{v_{ei}} = S_{vei}\, \dot{D}_{ii}^{\mathrm{migr}} \qquad [61]$$

$$\dot{v}_{ii}^{\mathrm{migr}\,+} = (1 - X_{bi})\, \dot{v}_{e\,ii}^{\mathrm{migr}\,+} \qquad [62]$$

3. *Effects of nucleation*

Two different nucleation rates are needed, depending on the location of the nucleation sites. Such sites can lie at (1) the periphery of grains, in which case the volume enclosed in their envelope is affected, or (2) the interfaces of intragranular recrystallized zones of ingot grains (initiated through PSN), which do not affect their envelope. The notations for the nucleation rates at the periphery of grains and at the interfaces of intragranular recrystallized zones are $\dot{n}_{ei}^{\mathrm{nucl}}$ and $\dot{n}_{bi}^{\mathrm{nucl}}$, respectively. Their sum is $\dot{n}_i^{\mathrm{nucl}}$. The nucleus volume v^{nucl} is unchanged. The rates of change of the volume of MSU i and its grains due to the generation of nuclei are

$$\dot{v}_{ei}^{\mathrm{nucl}\,-} = \dot{n}_{ei}^{\mathrm{nucl}}\, v^{\mathrm{nucl}} \qquad [63]$$

$$\dot{v}_i^{\mathrm{nucl}\,-} = \left(\dot{n}_{ei}^{\mathrm{nucl}} + \dot{n}_{bi}^{\mathrm{nucl}}\right)\, v^{\mathrm{nucl}} = \dot{n}_i^{\mathrm{nucl}}\, v^{\mathrm{nucl}} \qquad [64]$$

$$\dot{V}_i^{\mathrm{nucl}\,-} = n_i \dot{v}_i^{\mathrm{nucl}\,-} \qquad [65]$$

Expressions for the incorporation of generated nuclei by the MSU of the highest index obtained in Section III for the necklace-only topology are still applicable because this MSU does not allow PSN. The only modification is that the total nucleation rate $\dot{n}_{\mathrm{total}}^{\mathrm{nucl}}$ designates the sum for all MSUs of their two nucleation rates, *i.e.*, not only peripheral, but also intragranular:

$$\dot{V}_{N_{\mathrm{MSU}}}^{\mathrm{nucl}\,+} = \sum_{k=1}^{N_{\mathrm{MSU}}} \dot{V}_i^{\mathrm{nucl}\,-} = \dot{n}_{\mathrm{total}}^{\mathrm{nucl}}\, v^{\mathrm{nucl}} \qquad [66]$$

$$\frac{\dot{v}_{e\,N_{\mathrm{MSU}}}^{\mathrm{nucl}}}{v_{e\,N_{\mathrm{MSU}}}} = \frac{\dot{v}_{N_{\mathrm{MSU}}}^{\mathrm{nucl}}}{v_{N_{\mathrm{MSU}}}} = -\, \frac{\dot{n}_{\mathrm{total}}^{\mathrm{nucl}}}{n_{N_{\mathrm{MSU}}}} \left(1 \;-\; \frac{v^{\mathrm{nucl}}}{v_{e\,N_{\mathrm{MSU}}}}\right) \qquad [67]$$

Here again, the framework provides a tendency to reach a steady state when only the MSU that receives nuclei remains through an equilibrium between Eqs. [61] and [67].

C. *Evolution of Topologies*

One of the objectives of mesoscale models of recrystallization is the prediction of so-called ALA (as large as) grains, some of which may be remnants of the initial ingot grains. When such remnants persist, they may appear to be isolated due to the percolation of intragranular areas, resulting in continuous networks of recrystallized grains. These remnants may resemble the unrecrystallized initial grains of wrought microstructures, except for the fact that adjacent ALA grains may exhibit similar crystallographic orientations. Thus, partially wrought ingot microstructures may be better represented by a necklace-only topology once intragranular areas have reached a substantial fraction. This approach may be especially useful for quantifying the subsequent evolution of the isolated remnants of the coarse initial ingot grains.

To convert from one topological description to the other, the envelope density of isolated remnants, S_{ei}^{new}, is set equal to the sum of the preconversion envelope and the density of intragranular interfaces in order that the interaction surfaces remain identical:

$$S_{ei}^{\mathrm{new}} = S_{ei} + S_{bi} = S_{bi}\left(1 + \frac{S_{ei}}{S_{bi}}\right) \qquad [68]$$

Equation [68] ensures that all mechanisms that depend on grain-boundary densities (grain growth, nucleation, *etc.*) are continuous. As a consequence, not only are the recrystallized fraction and grain size continuous, but their slope before and after the conversion is the same. Considering that each isolated remnant is surrounded by N_{surround} intragranular recrystallized zones, each of which separates two remnants, the expression for the new grain density can be obtained:

$$n_i^{\mathrm{new}} \frac{N_{\mathrm{surround}}}{2} = n_{bi}\,(n_i v_{ei}) \qquad [69]$$

$$n_i^{\mathrm{new}} = \frac{2\, n_{bi}\, n_i\, v_{ei}}{N_{\mathrm{surround}}} \qquad [70]$$

The average diameter of these isolated remnants, D_i^{new}, can then be evaluated by equating the volume of MSU i before and after conversion and incorporating the result into Eq. [70]:

$$n_i^{\mathrm{new}} \frac{\pi}{6} D_i^{\mathrm{new}\,3} = n_i\, v_i = n_i\, v_{ei}(1 - X_{bi}) \qquad [71]$$

$$D_i^{\mathrm{new}} = \left(\frac{3\, N_{\mathrm{surround}}}{\pi\, n_{bi}}(1 - X_{bi})\right)^{1/3} \qquad [72]$$

The condition of surface density equality before and after conversion expressed in Eq. [68] can be expanded as

$$n_i^{\mathrm{new}}\, \pi\, D_i^{\mathrm{new}\,2} = n_{bi}\,(n_i\, v_{ei}\,(1 - X_{bi}))\, \pi\, D_{bi}^2 \left(1 + \frac{S_{ei}}{S_{bi}}\right) \qquad [73]$$

When combined with Eqs. [70], [72], and [41], this condition becomes

$$f(X_{bi}) \equiv N_{\mathrm{surround}} \left(1 + \frac{S_{ei}}{S_{bi}}\right)^3 X_{bi}^2\, (1 - X_{bi}) = 2 \qquad [74]$$

If the function f reaches a value of 2, it is possible to convert the initial ingot grains interspersed with intragranular grains into an equivalent set of necklace-only wrought-like grains. This function attains its maximum value when the fraction of intragranular zones reaches 2/3. The condition expressed in Eq. [74] then becomes

$$N_{\mathrm{surround}} \left(1 + \frac{s_{ei}}{s_{bi}}\right)^3 = \frac{27}{2} \qquad [75]$$

When the surface area of initial boundaries is negligible compared to that of the intragranular areas, the latter equation gives $N \sim 13.5$, a number that lies in the range of the number of faces of typical space-filling polyhedra that resemble grains, *e.g.*, the dodecahedron (12 faces) or tetrakaidecahedron (14 faces). The topological conversion is straightforward inasmuch as the volume of the whole MSU remains unchanged:

$$V_i^{\mathrm{new}} = n_i^{\mathrm{new}} v_{ei}^{\mathrm{new}} = V_i = n_i\, v_i \qquad [76]$$

$$v_{ei}^{\mathrm{new}} = \frac{n_i}{n_i^{\mathrm{new}}} v_{ei}(1 - X_{bi}) = \frac{N_{\mathrm{surround}}}{2 n_{bi} n_i v_{ei}} n_i\, v_{ei}\left(1 - \frac{2}{3}\right) = \frac{N_{\mathrm{surround}}}{6 n_{bi}} \qquad [77]$$

Including the clustering effect (Eq. [40]), the following relation is obtained:

$$v_{ei}^{\mathrm{new}} = \frac{N_{\mathrm{surround}}}{6\, n_{bi}} = \frac{N_{\mathrm{surround}}}{6} \frac{N_{\mathrm{cluster}}(\nu_{\mathrm{PSN}i})}{n_{\mathrm{PSN}}} \qquad [78]$$

Equation [78] indicates that the spatial distribution/clustering of PSN sites has a dramatic influence on the size of the remnants of initial grains, as might be expected. To improve the precision of the estimate, multiple levels of clustering could be defined instead of only one in order to represent the spatial ordering of PSN sites that may occur at different scales.

D. *Tests of the Geometric Framework Using Simple Input*

The behavior of the complete geometric framework for the necklace-and-intragranular topology was evaluated using several hypothetical cases in which constant rates of nucleation and grain-boundary migration were chosen based on the order of magnitude of those observed in practice for Waspaloy ingots.[14] The framework was tested using a two-MSU microstructure initialized with coarse anisotropic ingot grains measuring $2300 \times 2300 \times 23{,}000$ μm, *i.e.*, a volume equivalent to that of a 5000-μm sphere but with an aspect ratio of 10. A constant boundary velocity of 10 μm per unit strain and a nucleation rate of 1 nucleus per 100 μm^2 of grain-boundary per unit strain were assumed. The density of PSN sites was taken to be 0, 1, 10, 100, and 1000 per mm^3. An acceleration of recrystallization induced by an increase in the density of PSN sites was clearly observed (Figure 9). It was accompanied by an increase in the Avrami exponent (Figure 10). Both results are well supported by experimental data[14] as well as by other modeling methods.[16]

Last, the full geometric framework was applied to describe the recrystallization of an ingot microstructure assuming 1000 PSN sites per mm^3. First, the behavior observed for randomly dispersed PSN particles was compared to that obtained with groups of ten particles clustered in spheres of approximately 200 μm. Model results revealed that clustering reduces the enhanced recrystallization effect of PSN (Figure 11). A modeling approach based on converting initial ingot grains to a wrought-like microstructure when the fraction of intragranular zones reached 2/3 was also tested; the subsequent evolution of the recrystallized fraction was almost identical to that without conversion (Figure 11). Furthermore, the beneficial effect of such an approach was made clear in a comparison of the size of the remnants of the initial grains (Figure 12). For the case in which the initial ingot grains are retained in the model until full recrystallization is achieved, the evolution of their size (defined by their envelope) is of little interest, especially during the final stage before they are totally consumed, because most of their recrystallization is actually intragranular. In the corresponding curve of remnant size *vs* strain (Figure 12), the initial ingot grains thus seemed to disappear suddenly. Hence, this approach in general fails to provide significant information about the zones in which evolution occurs. On the other hand, valuable information about the size of the remnants of the initial grains is obtained from the modeling approach involving the topological conversion. At the moment when the initial ingot grains were converted into wrought-like grains, the curve describing the size of the remnants exhibited a sudden change because the information it provided was no longer based on the initial envelope of the ingot grains (Figure 12); it then related to the volume enclosed in the envelopes of the new wrought-like grains. Due to Eq. [68], the envelopes of these grains are mostly inherited from the interfaces of the percolating intragranular zones in which most of the evolution occurs. They are the true remnants of initial grains that are to be dealt with as single entities instead of as a group enclosed in the initial envelope. As a result, the curve that follows the conversion provides the needed information. For the present example, it exhibited a smooth decrease until recrystallization was complete.

V. SUMMARY AND CONCLUSIONS

The geometric framework needed as a prerequisite for the development of a mesoscale-mechanism-based model of recrystallization was formulated. It can represent the geometric evolution of a wide variety of microstructures ranging from columnar-grain ingot materials with PSN to wrought alloys and responds to two kinds of

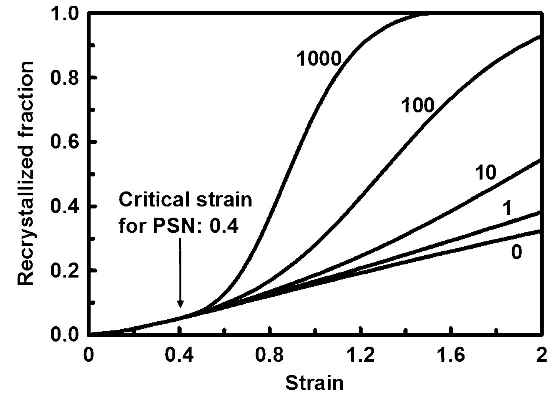

Fig. 9—Model results for the recrystallized fraction during the two-MSU simulation of the dynamic recrystallization of coarse ingot grains for various PSN-site densities per mm^3. The nucleation rate was 1 nucleus per 100 μm^2 of boundary and per unit strain, the grain-boundary velocity was 10 μm per unit strain, and v^{nucl} = 1000 μm^3.

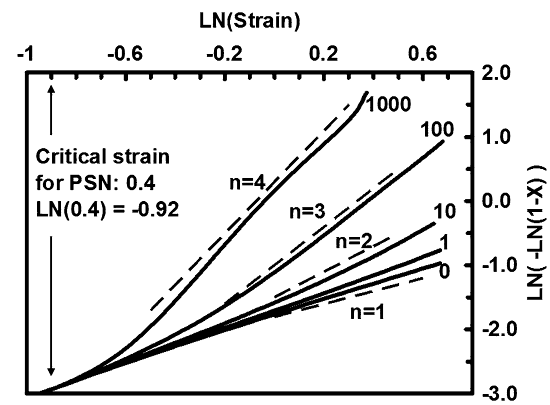

Fig. 10—Avrami analysis of the recrystallized-fraction curves in Fig. 9. X denotes the recrystallized fraction; the slope of the curves is the Avrami exponent n.

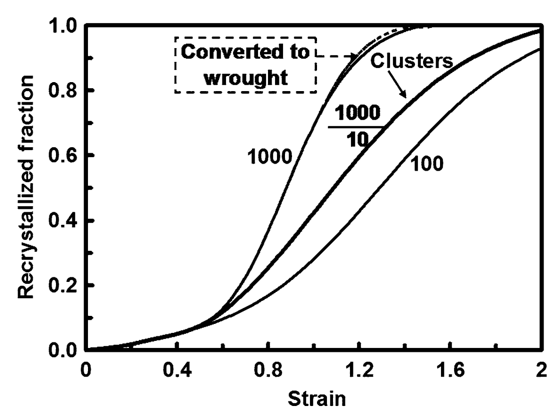

Fig. 11—Model results for the recrystallized fraction during two-MSU simulations of dynamic recrystallization assuming 100 or 1000 PSN sites per mm^3. For the 1000 PSN-site-density case, clustering of groups of 10 PSN particles in 200-μm spheres was evaluated, and conversion of initial ingot grains into wrought-like microstructures at an intragranular recrystallized fraction of 2/3 was performed. The nucleation rate was 1 nucleus per 100 μm^2 of boundary and per unit strain, the grain-boundary velocity was 10 μm per unit strain, and v^{nucl} = 1000 μm^3.

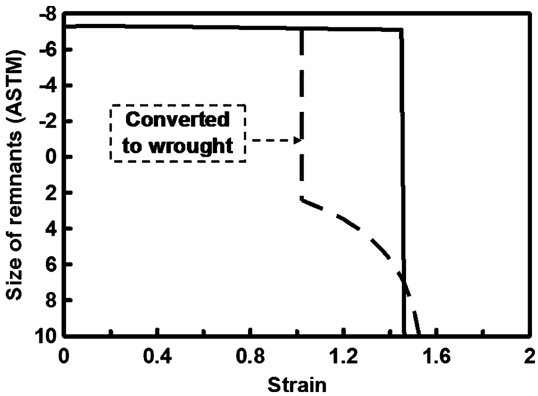

Fig. 12—Model results for the size of the remnants of initial ingot grains developed during two-MSU simulations of dynamic recrystallization, assuming 1000 PSN sites per mm^3. In the first case, ingot grains were kept until full recrystallization using intragranular topology, and in the second case (dashed line) initial ingot grains were converted into wrought-like grains when the fraction of intragranular zones reached 2/3 to allow the prediction of ALAs. The nucleation rate was 1 nucleus per 100 μm^2 of boundary and per unit strain, the grain-boundary velocity was 10 μm per unit strain, and $v^{\text{nucl}} = 1000\ \mu\text{m}^3$.

inputs: nucleation rates and grain-boundary velocities. Based on grain aggregates of similar properties or histories referred to as MSUs, the framework offers the flexibility to adapt the microstructure description to the context in which the mesoscale model will be applied. For instance, the number of MSUs can be chosen per the various grain generations that industrial applications may require in order to follow a specific process, while simultaneously requiring only a limited number of variables (five per MSU) to be stored during modeling runs. Such a design opens the possibility of using mechanism-based models of recrystallization even in the context of large FEM simulations. Tested using simple inputs such as constant grain-boundary velocities and nucleation rates, the geometric framework demonstrated its ability to respond in very realistic ways, thus offering great promise for simulations incorporating more physically representative inputs.

VI. NOMENCLATURE

A. *General Rules Regarding Notations*

For any variable, index "i" relates to the MSU to which it belongs. The additional index "j" denotes the MSU with which MSU i is interacting. Indices "e" and "b" refer to grain envelope and intragranular zones properties, respectively. Variation rates with respect to time are denoted with a dot above the variable. For volume variation rates, the superscripts "migr" and "nucl" denote grain-boundary migration and nucleation effects, respectively, and the additional superscript "+" or "-" denotes the sign with which such values contribute to the total variation rate of the considered volume.

Eq. [#] indicates the equation number in which the considered variable is defined.

*Indicates primary variables
**Indicates input variables

List of the main notations for each MSU i

$*v_{ei}$	volume enclosed in the envelope of a grain
$*v_i$	volume of a grain; equals v_{ei} for necklace-only topology
$*V_i$	volume of the MSU
$*\alpha_{xyi}$, α_{xyi}	anisotropy parameters
n_i	volume density of grains (Eq. [2])
D_{eqi}	diameter of a grain of the same volume as that of a grain of MSU i (Eq. [12])
D_i	grain diameter when grains are isotropic; then equals D_{eqi}
D_{xi}, D_{yi}, D_{zi}	principal grain dimensions (Eqs. [13] through [15])

Notations involved in necklace-only interaction probabilities

s_{ei}	surface area of the envelope of an isotropic grain of MSU i (Eq. [6]) surface area of the envelope of an anisotropic grain of MSU i (Eq. [9])
S_{ei}	surface area density of envelopes of MSU i grains in the structure (Eq. [10])
S_{vei}	surface area density of grain boundaries inside MSU i (Eq. [11])
S_{total}	total density of grain envelopes in the structure (Eq. [23])
q_j	probability that a grain boundary is an interface with an MSU j grain (Eq. [23])

Notations involved in necklace-and-intragranular interaction probabilities

X_{bi}	fraction of intragranular areas (Eq. [37])
$**n_{\text{PSN}}$	volume density of PSN sites
$v_{\text{PSN}\,i}v_{\text{PSN}i}$	volume of intragranular zones per PSN particle (Eq. [39])
n_{bi}	volume density of intragranular zones (Eq. [40])
D_{bi}	diameter of intragranular zones (Eq. [41])
s_{bi}	surface area of intragranular boundaries in a grain of MSU i (Eq. [42])
S_{bi}	surface-area density of intragranular boundaries of grains of MSU i (Eq. [43])
$S_{b\,\text{total}}$	total density of intragranular-zone interfaces in the structure (Eq. [44])
$S_{e\,\text{total}}$	total density of envelope grain boundaries in the structure (Eq. [45])
$S_{ebc\,\text{total}}$	total density of envelope grain boundaries in the structure that can also be intragranular boundaries (Eq. [46])
q_{bei}	fraction of the envelope of a grain of MSU i that is in contact with the intragranular interface of other grains (Eq. [48])
q_{eei}	fraction of the envelope of a grain of MSU i that is in contact with the envelope of other grains (Eq. [49])
q_{eeij}	fraction of the envelope of a grain of MSU i that is in contact with the envelope of grains of MSU j (Eq. [50])
q_{beij}	fraction of the envelope of a grain of MSU i that is in contact with the intragranular interfaces of MSU j (Eq. [51]) fraction of the intragranular interface of a grain of MSU i that is in contact with grain envelopes of MSU j (Eq. [52])

Notations for nucleation

$^{**}\dot{n}_{ei}^{\mathrm{nucl}}$	nucleation rate at the periphery of each grain of MSU i
$^{**}\dot{n}_{bi}^{\mathrm{nucl}}$	nucleation rate at the interface of intragranular zones for each grain of MSU i
$\dot{n}_{i}^{\mathrm{nucl}}$	total nucleation rate for grains of MSU i; equals $\dot{n}_{ei}^{\mathrm{nucl}}$ in the case of necklace-only topology (Eq. [64])
$^{**}v^{\mathrm{nucl}}$	volume of a nucleus

Notation for grain-boundary velocity

$^{**}\dot{u}_{ij}$	velocity of a grain i–grain j boundary

ACKNOWLEDGMENTS

This work was conducted as part of the in-house research activities of the Metals Processing Group of the United States Air Force Research Laboratory's Materials and Manufacturing Directorate. The support and encouragement of the Laboratory management and the Air Force Office of Scientific Research (Dr. J.S. Tiley, program manager) are gratefully acknowledged. One of the authors (JPT) was supported through Air Force Contract No. F33615-03-D-5801.

REFERENCES

1. D. Zhao, C. Cheng, R. Anbajagane, H. Dong, and F.S. Suarez: in *Superalloys 718, 625, 706, and Various Derivatives*, E.A. Loria, ed., TMS, Warrendale, PA, 1997, pp. 163–72.
2. J.T. Yeom, C.S. Lee, J.H. Kim, and N.K. Park: *Mater. Sci. Eng. A*, 2007, vols. A449–A451, pp. 722–26.
3. H.S. Zurob, C.R. Hutchinson, Y. Brechet, and G. Purdy: *Acta Mater*, 2002, vol. 50, pp. 3075–92.
4. G. Shen, S.L. Semiatin, and R. Shivpuri: *Metall. Mater. Trans. A*, 1995, vol. 26A, pp. 1795–1803.
5. J.P. Thomas, E. Bauchet, C. Dumont, and F. Montheillet: in *Superalloys 2004*, K.A. Green, T.M. Pollock, H. Harada, T.E. Howson, R.C. Reed, J.J. Schirra, and S. Walston, eds., TMS, Warrendale, PA, 2004, pp. 959–68.
6. A.D. Rollett, M.J. Luton, and D.J. Srolovitz: *Acta Metall*, 1992, vol. 40, pp. 43–55.
7. R.L. Goetz and V. Seetharaman: *Scripta Mater*, 1998, vol. 38, pp. 405–13.
8. X. Song and M. Rettenmayr: *Comput. Mater. Sci.*, 2007, in press.
9. B. Marty, J.Y. Guedou, P. Gergaud, and J.L. Lebrun: in *Superalloys 718, 625, 706, and Various Derivatives*, E.A. Loria, ed., TMS, Warrendale, PA, 1997, pp. 331–42.
10. C. Sommitsch, V. Wieser, and S. Kleber: *J. Mater. Process. Technol.*, 2002, vols. 125–126, pp. 130–37.
11. P. Poelt, C. Sommitsch, S. Mitsche, and M. Walter: *Mater. Sci. Eng. A*, 2006, vol. A420, pp. 306–14.
12. F. Montheillet: *Proc. 4th Int. Conf. on Recrystallization and Related Phenomena (Rex'99)*, T. Sakai and H.G. Suzuki, eds., Japan Institute of Metals, Sendai, Japan, 1999, pp. 651–58.
13. A. Di Shino and G. Abbruzese: *Proc. 1st Joint Int. Conf. on Recrystallization and Grain Growth*, G. Gottstein and D.A. Molodov, eds., Springer Verlag, Berlin, 2001, pp. 1021–26.
14. S.L. Semiatin, D.S. Weaver, P.N. Fagin, M.G. Glavicic, R.L. Goetz, N.D. Frey, R.C. Kramb, and M.M. Anthony: *Metall. Mater. Trans. A*, 2004, vol. 35A, pp. 679–93.
15. F.J. Humphreys: *Scripta Mater*, 2000, vol. 43, pp. 591–96.
16. R.L. Goetz: *Scripta Mater*, 2005, vol. 52, pp. 851–56.